DESY 94-051
March 1994

Standard-Model Predictions for W-Pair Production in Electron-Positron Collisions

Wim Beenakker

Theory Division, DESY, Hamburg, Germany

Ansgar Denner

Physikalisches Institut, University of Würzburg, Germany

Abstract:

We review the status of the theoretical predictions for W-pair production in e^+e^- collisions within the electroweak standard model (SM). We first consider for on-shell W-bosons the lowest-order cross-section within the SM, the general effects of anomalous couplings, the radiative corrections within the SM, and approximations for them. Then we discuss the inclusion of finite-width effects in lowest order and the existing results for radiative corrections to off-shell W-pair production, and we outline the general strategy to calculate radiative corrections within the pole scheme. We summarize the theoretical predictions for the total and partial W-boson widths including radiative corrections and discuss the quality of an improved Born approximation. Finally we provide a general discussion of the structure-function method to calculate large logarithmic higher-order corrections associated with collinear photon radiation.

DESY 94-051
March 1994

1 Introduction

All known phenomena of electroweak origin are up to now well described[1–4] by the Standard Model of the electroweak interaction (SM)[5], which has even passed high-precision tests performed at LEP1 and the SLC. These experiments as well as the ones at low energies are, however, only sensitive to the mass parameters of the gauge bosons and the gauge-boson–fermion couplings.

The mechanism of mass generation and the non-Abelian couplings between the gauge bosons still await experimental confirmation. These aspects can be ideally studied in gauge-boson production processes, the most prominent being W-pair production. It is the simplest SM e^+e^--annihilation process that contains non-Abelian couplings in lowest order. Moreover it has a large cross-section, i.e. 18 pb at $\sqrt{s} = 200\,\mathrm{GeV}$ and 7 pb at $\sqrt{s} = 500\,\mathrm{GeV}$.

One of the primary aims of LEP200 is a precise direct measurement of the W-boson mass. Presently it is measured at hadron colliders[1,6] yielding $M_\mathrm{W} = 80.22 \pm 0.26\,\mathrm{GeV}$. A global analysis[4] of the electroweak precision data within the SM restricts the W mass to $M_\mathrm{W} = 80.24 \pm 0.09^{+0.01}_{-0.02}$ GeV and provides an indirect determination of the top-quark mass: $m_\mathrm{t} = 164^{+16+18}_{-17-21}$ GeV. In the latter the first errors correspond to M_H=300 GeV and the second to a variation of the unknown Higgs mass in the interval $60\,\mathrm{GeV} < \mathrm{M_H} < 1\,\mathrm{TeV}$. A more precise value of the W mass obtained at LEP200 will give rise to an improved bound on m_t. If in addition the top quark should be discovered at the hadron colliders this will allow to obtain indirect limits[7] on M_H.

For measuring M_W at LEP200 three methods have been thoroughly investigated[7,8], assuming an integrated luminosity of $500\,\mathrm{pb}^{-1}$. The first one makes natural use of the excitation curve of W-pair production near threshold. This amounts essentially to measuring the kinematic increase in phase space near threshold, which depends strongly on M_W. It allows for a statistical accuracy of at most 100 MeV (at $\sqrt{s} = 164\,\mathrm{GeV}$). This requires a precise knowledge about finite-width effects and radiative corrections, in particular initial-state radiation (ISR), which changes the shape of the excitation curve. Unfortunately this method is only sensitive to M_W close to the W-pair production threshold. This of course limits other studies which require high energies exactly to overcome the phase-space suppression.

The second method makes use of the energy spectrum of the leptons from the W decay in leptonic–hadronic events. Neglecting radiative corrections the endpoints of this spectrum depend on M_W as: $[\,E_\mathrm{beam} \pm \sqrt{E^2_\mathrm{beam} - M^2_\mathrm{W}}\,]/2$. Because of contamination from τ events only the higher endpoint is chosen for the analysis. This method favours low energies, hence leading to the same drawbacks as above. Moreover, the statistics is reduced because only leptonic–hadronic events can be used. Thus one arrives at a statistical accuracy for M_W of 150 MeV at best. As this method uses the beam energy it is very sensitive to ISR carrying away energy.

The at present most-favoured method is the direct reconstruction of the W bosons involving hadronic–hadronic and hadronic–leptonic events. This amounts to determining the four-momenta of all final-state fermions. The neutrino momentum and the poorly measured jet energies are determined from a constraint fit using energy–momentum conservation, thereby assuming that no energy or momentum is carried away by additional

photons (beam-energy constraint). Because this method has no strong energy dependence it does not limit other studies. It allows to achieve a statistical error of 55 (65) MeV at $\sqrt{s} = 176$ (190) GeV. Since it involves a beam-energy constraint, the presence of ISR leads to a shift in the reconstructed W-boson mass of roughly $\Delta M_{\mathrm{W}} = \langle E_\gamma \rangle M_{\mathrm{W}}/\sqrt{s}$, where $\langle E_\gamma \rangle$ is the average photon energy. Therefore the precise kowledge of the ISR-photon-energy spectrum is crucial. Not only ISR but anything that introduces a noticeable energy dependence contributes to $\langle E_\gamma \rangle$ and has to be taken into account properly. This concerns in particular finite-width effects and all kinds of radiative corrections.

Consequently one could achieve a statistical accuracy for the W-mass measurement around 60 MeV for each experiment. The total experimental systematic error, which is at present dominated by the uncertainty in the beam-energy determination, amounts to 24 MeV.

Another important feature of W-pair production is the possibility to investigate the triple gauge couplings. At LEP200 their presence can be directly verified for the first time. The present direct limits on anomalous triple gauge couplings from hadron colliders and indirect ones, i.e. via loop effects, from precision measurements still allow for large $\mathcal{O}(1)$ deviations from the SM values. Moreover, indirect determinations can only provide estimates of orders of magnitude as a result of the fact that the leading contributions from loop effects are related to a renormalization of the anomalous bi-linear (propagator) contributions that are already present at tree level. Lacking a model that describes how the new physics will alter the propagators, no rigorous bounds are possible. Concerning these precision measurements, like at LEP1 and SLC, it should be noted that the $\mathcal{O}(1)$ limits do not apply to all tri-linear couplings. Assuming $SU(2)\times U(1)$ gauge invariance, i.e. in an effective-field-theory approach, certain tri-linear couplings are severely constrained by the absence of observed bi-linear effects at LEP1/SLC, as they correspond to anomalous operators that yield bi-linear as well as tri-linear couplings. At LEP200 one hopes[9,10] to improve the limits to the level of 10%. This, however, depends crucially on the energy available, as the contributions from triple gauge couplings are in general suppressed by at least a factor $\sqrt{1-4M_{\mathrm{W}}^2/s}$ in the threshold region. It should be noted that the limits obtained from a simultaneous fit for all anomalous triple gauge couplings are worse by an order of magnitude. It requires additional theoretical constraints, relating various couplings, in order to achieve limits at the 10% level. At a high-energy linear $\mathrm{e^+e^-}$ collider with $\sqrt{s} \geq 500$ GeV (NLC) one expects to achieve limits at the per-cent level or even better[11]. This is due to the fact that already small anomalous couplings upset the intricate gauge cancellations for longitudinal W bosons and lead to a sizeable enhancement of the SM cross-section.

In view of the expected level of accuracy radiative corrections are again indispensable. Moreover, the observable effects of the anomalous couplings are not expected to be larger than the ones caused by the radiative corrections. First of all, assuming the validity of $SU(2)\times U(1)$ gauge invariance, the anomalous tri-linear couplings can only be due to loop effects originating from heavy new-physics particles. Taking the SM Higgs mechanism not to be responsible for the generation of the masses of these heavy particles, gauge invariance entails their decoupling from the Goldstone bosons[12] and no large mass factors can enhance their loop effects. So, enhancement with respect to the SM can only come from the coupling strength of the new-physics particles or from the number of different

flavours. Secondly the absence of observed anomalous bi-linear effects at LEP1/SLC already has large repercussions on the tri-linear couplings as mentioned above. At least no models have been constructed so far that yield small bi-linear effects but large tri-linear ones.

If the Higgs boson is heavy, $M_{\mathrm{H}} \gtrsim 800\,\mathrm{GeV}$, or if there is no Higgs at all, the lack of perturbative gauge cancellations will cause the occurrence of strong interactions between longitudinal gauge bosons at energies in the TeV range, where the physics associated with the symmetry-breaking mechanism must emerge. At low energies this can be parametrized in a model-independent way by an effective field theory (chiral perturbation theory), leading to the aforementioned anomalous gauge-boson couplings in a no-Higgs scenario. If substantial imaginary parts show up in these couplings, this will be a sign of strong interactions in the gauge-boson sector. At high energies a signature of a strongly-interacting symmetry breaking sector is the occurrence of large form factors resulting from final-state interactions between produced longitudinal W bosons (rescattering). In order to preserve partial-wave unitarity at these energies, a unitarization scheme has to be adopted. This leads to various models for the strongly-interacting symmetry breaking sector, involving either scalar or vector resonances, or no resonances at all.

In high-energy W-pair production at $\mathrm{e^+e^-}$ colliders among these resonances only the $J = 1$ vector resonances can be studied[a] through rescattering effects of longitudinal W bosons[b]. Assuming moderate luminosities, the corresponding phase-shift effects show up significantly in T-odd observables, i.e. observables that change sign under reflection of the spins and three-momenta of the particles, only at energies close to the mass of the vector resonance[14]. The SM background from the absorptive parts of the $\mathcal{O}(\alpha)$ corrections are fairly small[15], hardly reaching a 1σ significance. By studying backward-scattered W bosons the signal from the longitudinal W-pair events can be improved and the absolute size of the rescattering form factors can be accessed. This allows vector resonances with mass below 1.5 TeV to be traced with a 3σ significance at a 500 GeV linear collider with $10\,\mathrm{fb}^{-1}$ of integrated luminosity[14]. It would require a 1.5 TeV linear collider and $500\,\mathrm{fb}^{-1}$ of integrated luminosity to clearly see techni-rho-like vector resonances and possibly even distinguish between the weakly-interacting SM and a strongly-interacting scenario without resonances[13].

Low- and high-energy W-pair production provides an ideal laboratory for studying CP breaking in the gauge-boson sector. This can be directly tested in tailored CP-odd observables[16,17], for which the SM contributions are negligibly small. The analysis of T-odd observables, which receive contributions from CP-violating interactions and from absorptive parts, will allow a study of CP-violating triple gauge-boson couplings at roughly the same level as the CP-conserving ones[15].

W-pair production furthermore enables the investigation of the total and partial widths of the W boson. At LEP200 one expects an error on the total width[18] of about 150 MeV, i.e. 7%. By measuring the branching ratios one can test lepton universality and derive

[a] In $\mathrm{e^+e^-} \to \mathrm{W^+W^-}$ the spin-state $J = 0$ is forbidden by initial-state fermion-helicity conservation.

[b] As a result of the great variety of partons inside the proton, many different (iso)spin- and charge-states are open simultaneously in longitudinal gauge-boson scattering at the LHC. Some of these channels are also accessible at high-energy $\mathrm{e^+e^-}$ colliders in fusion processes like $\mathrm{e^+e^-} \to \nu_\mathrm{e}\bar{\nu}_\mathrm{e}\mathrm{W_L^+W_L^-}$. Here also some inelastic channels involving pseudo-Goldstone bosons could be studied in hadronic final states[13].

information on the quark-mixing matrix elements. This might lead in particular to an improved determination[19] of V_{cs}.

In the hadronic–hadronic decays of the W bosons, moreover, interesting novel reconnection effects[20] in the hadronization process of the quark partons can eventually be studied experimentally. This is due to the fact that there are in the clean e^+e^--annihilation environment two hadronically-decaying particles in the final state, the decay of which is very well understood in the absence of QCD interference phenomena. The latter lead to reconnection effects between the original colour singlets originating from different W bosons. The perturbative effects are small[21], being of the order of α_s^2 with an additional colour suppression factor $1/(N_C^2-1)$. Several models of non-perturbative reconnection mechanisms have been investigated in detail in Ref. 21. As the most striking result the QCD interference effects lead to a bias in the W-mass determination of about 40 MeV, caused by the fact that the W mass is not conserved in the fragmentation.

In order to enable the above-mentioned experimental studies at the indicated level of accuracy one needs appropriate theoretical predictions. To this end an accuracy for the W-pair-production cross-section at the level of 1% is required, necessitating the proper inclusion of finite-width effects and radiative corrections.

A theoretical summary of the lowest-order aspects of W-pair production including an exhaustive list of references has been given in Ref. 16. The purpose of this review is to update this where necessary and in particular to provide a comprehensive overview on higher-order corrections. A discussion of the experimental aspects can be found in Refs. 22–27.

This paper is organized as follows: In Sec. 2 we discuss on-shell W-pair production, which already exhibits the general features very well. This involves a discussion of the lowest-order cross-section within the SM, the general effects of anomalous couplings, radiative corrections within the SM, and approximations for them. In Sec. 3 we deal with the off-shell case. We discuss the inclusion of finite-width effects in lowest order, the existing results for radiative corrections to off-shell W-pair production, and we outline the general strategy to calculate radiative corrections within the pole scheme. The theoretical predictions for the total and partial W widths including radiative corrections and an improved Born approximation are given in Sec. 4. A general discussion of the structure-function method, which can be used to calculate the large logarithmic higher-order corrections associated with collinear photon radiation, is given in Sec. 5. Finally we collect some useful formulae in the appendices.

2 On-Shell W-Pair Production

2.1 Notation and conventions

We use the Bjørken–Drell metric $g_{\mu\nu} = \mathrm{diag}(+1,-1,-1,-1)$ and fix the totally antisymmetric tensor by $\epsilon^{0123} = +1$. The matrix γ_5 is defined as $\gamma_5 = i\gamma^0\gamma^1\gamma^2\gamma^3$ and the helicity projectors $\omega_\pm$, which are used to project on right- and left-handed massless fermions, as

$$\omega_\pm = \frac{1}{2}(1 \pm \gamma_5). \tag{2.1}$$

First we set the conventions for the process

$$\mathrm{e}^+(p_+,\kappa_+)+\mathrm{e}^-(p_-,\kappa_-)\to \mathrm{W}^+(k_+,\lambda_+)+\mathrm{W}^-(k_-,\lambda_-), \tag{2.2}$$

where the arguments indicate the momenta and helicities of the incoming fermions and outgoing bosons ($\kappa_i=\pm\frac{1}{2}$, $\lambda_i=1,0,-1$). Note that we sometimes use the shorthand version $\kappa_i=\pm$ in certain sub- and superscripts. In the centre-of-mass (CM) system of the $\mathrm{e}^+\mathrm{e}^-$ pair, which we will refer to as the laboratory (LAB) system in the following, the momenta read

$$p_\pm^\mu = E(1,0,0,\mp 1), \qquad k_\pm^\mu = E(1,\mp\beta\sin\theta,0,\mp\beta\cos\theta), \tag{2.3}$$

with E denoting the beam energy, θ the scattering angle between the e^+ and the W^+, and $\beta=\sqrt{1-M_\mathrm{W}^2/E^2}$ the velocity of the W bosons. The Mandelstam variables used in the following are given by

$$\begin{aligned} s &= (p_+ + p_-)^2 = (k_+ + k_-)^2 = 4E^2, \\ t &= (p_+ - k_+)^2 = (p_- - k_-)^2 = -E^2(1+\beta^2-2\beta\cos\theta), \\ u &= (p_+ - k_-)^2 = (p_- - k_+)^2 = -E^2(1+\beta^2+2\beta\cos\theta). \end{aligned} \tag{2.4}$$

In order to define helicity amplitudes we need to introduce the corresponding polarization vectors for the W^+ and W^- boson[c]

$$\begin{aligned} \varepsilon_\pm^{*\mu}(k_\pm,+1) &= \frac{1}{\sqrt{2}}(0,\mp\cos\theta,-i,\pm\sin\theta), \\ \varepsilon_\pm^{*\mu}(k_\pm,-1) &= \frac{1}{\sqrt{2}}(0,\mp\cos\theta,+i,\pm\sin\theta), \\ \varepsilon_\pm^{*\mu}(k_\pm,\ \ 0) &= \frac{E}{M_\mathrm{W}}(\beta,\mp\sin\theta,0,\mp\cos\theta). \end{aligned} \tag{2.5}$$

Because we are neglecting the electron mass, the helicity of the positron is opposite to the helicity of the electron

$$\kappa_- = -\kappa_+ = \kappa. \tag{2.6}$$

Henceforth we refer to the helicity amplitudes as $\mathcal{M}(\kappa,\lambda_+,\lambda_-,s,t)$. CP invariance implies the relation:

$$\mathcal{M}(\kappa,\lambda_+,\lambda_-,s,t) = \mathcal{M}(\kappa,-\lambda_-,-\lambda_+,s,t). \tag{2.7}$$

This holds in the SM if we neglect the CP-violating phase in the quark-mixing matrix. Even in the presence of this CP-violating phase, the CP breaking occurring in SM W-pair production at the one-loop level involves at most terms of $\mathcal{O}(\alpha m_\mathrm{b}^2/[\pi M_\mathrm{W}^2])$ and is additionally suppressed by the smallness of the mixing angles between the quarks. Consequently there are only 12 independent helicity-matrix elements instead of 36.

[c] Note that the helicity of the massive W bosons is not Lorentz invariant. We define it in the LAB system.

The general helicity amplitude can be decomposed into basic matrix elements and invariant functions:

$$\mathcal{M}(\kappa,\lambda_+,\lambda_-,s,t) = \sum_i \mathcal{M}_i^\kappa F_i^\kappa(s,t). \tag{2.8}$$

The basic matrix elements are simple, purely kinematical objects and contain the complete dependence on the W polarization. The invariant functions contain the whole dynamical information, i.e. the model dependence, but are independent of the W polarizations. We introduce the following set of CP-invariant basic matrix elements:

$$\begin{aligned}
\mathcal{M}_1^\kappa &= \bar v(p_+)\not\varepsilon_+^*(\not k_+ - \not p_+)\not\varepsilon_-^*\omega_\kappa u(p_-),\\
\mathcal{M}_2^\kappa &= \bar v(p_+)\frac{\not k_+ - \not k_-}{2}(\varepsilon_+^*\cdot\varepsilon_-^*)\omega_\kappa u(p_-),\\
\mathcal{M}_3^\kappa &= \bar v(p_+)[\not\varepsilon_+^*(\varepsilon_-^*\cdot k_+) - \not\varepsilon_-^*(\varepsilon_+^*\cdot k_-)]\omega_\kappa u(p_-),\\
\mathcal{M}_4^\kappa &= \bar v(p_+)[\not\varepsilon_+^*(\varepsilon_-^*\cdot p_-) - \not\varepsilon_-^*(\varepsilon_+^*\cdot p_+)]\omega_\kappa u(p_-),\\
\mathcal{M}_5^\kappa &= \bar v(p_+)\frac{\not k_+ - \not k_-}{2}\omega_\kappa u(p_-)(\varepsilon_+^*\cdot k_-)(\varepsilon_-^*\cdot k_+),\\
\mathcal{M}_6^\kappa &= \bar v(p_+)\frac{\not k_+ - \not k_-}{2}\omega_\kappa u(p_-)(\varepsilon_+^*\cdot p_+)(\varepsilon_-^*\cdot p_-),\\
\mathcal{M}_7^\kappa &= \bar v(p_+)\frac{\not k_+ - \not k_-}{2}\omega_\kappa u(p_-)[(\varepsilon_+^*\cdot k_-)(\varepsilon_-^*\cdot p_-) + (\varepsilon_+^*\cdot p_+)(\varepsilon_-^*\cdot k_+)].
\end{aligned} \tag{2.9}$$

Corresponding to the twelve independent CP-conserving helicity amplitudes only twelve of those basic matrix elements are linear-independent. The last pair, which has been kept for convenience, can be expressed by the others as follows:

$$\mathcal{M}_7^\kappa = -\frac{s}{2}(\mathcal{M}_1^\kappa + \mathcal{M}_2^\kappa) + \frac{M_\mathrm{W}^2 - t}{2}\mathcal{M}_3^\kappa + \frac{s}{2}\mathcal{M}_4^\kappa + \mathcal{M}_5^\kappa. \tag{2.10}$$

In the presence of CP violation one has to introduce six further basic matrix elements, as there are now 18 independent helicity amplitudes. These can be obtained from $\mathcal{M}_3^\kappa$, $\mathcal{M}_4^\kappa$ and $\mathcal{M}_7^\kappa$ by reversing the relative sign between the two summands:

$$\begin{aligned}
\widetilde{\mathcal{M}}_3^\kappa &= \bar v(p_+)[\not\varepsilon_+^*(\varepsilon_-^*\cdot k_+) + \not\varepsilon_-^*(\varepsilon_+^*\cdot k_-)]\omega_\kappa u(p_-),\\
\widetilde{\mathcal{M}}_4^\kappa &= \bar v(p_+)[\not\varepsilon_+^*(\varepsilon_-^*\cdot p_-) + \not\varepsilon_-^*(\varepsilon_+^*\cdot p_+)]\omega_\kappa u(p_-),\\
\widetilde{\mathcal{M}}_7^\kappa &= \bar v(p_+)\frac{\not k_+ - \not k_-}{2}\omega_\kappa u(p_-)[(\varepsilon_+^*\cdot p_+)(\varepsilon_-^*\cdot k_+) - (\varepsilon_+^*\cdot k_-)(\varepsilon_-^*\cdot p_-)].
\end{aligned} \tag{2.11}$$

In appendix A we list the explicit expressions for all non-vanishing basic matrix elements in terms of E, θ and β.

The differential cross-sections for fixed electron polarization, with matching positron polarization, and for transverse (T), mixed (M), longitudinal (L), and unpolarized (U) W bosons are given by

$$\left(\frac{\mathrm{d}\sigma}{\mathrm{d}\Omega}\right)_{\pm,\mathrm{T}} = \frac{\beta}{64\pi^2 s}\sum_{\lambda_+,\lambda_-=\pm1}|\mathcal{M}(\pm\tfrac{1}{2},\lambda_+,\lambda_-,s,t)|^2,$$

$$\left(\frac{\mathrm{d}\sigma}{\mathrm{d}\Omega}\right)_{\pm,\mathrm{M}} = \frac{\beta}{64\pi^2 s}\left\{\sum_{\lambda_+=\pm1}|\mathcal{M}(\pm\frac{1}{2},\lambda_+,0,s,t)|^2 + \sum_{\lambda_-=\pm1}|\mathcal{M}(\pm\frac{1}{2},0,\lambda_-,s,t)|^2\right\},$$
$$\left(\frac{\mathrm{d}\sigma}{\mathrm{d}\Omega}\right)_{\pm,\mathrm{L}} = \frac{\beta}{64\pi^2 s}|\mathcal{M}(\pm\frac{1}{2},0,0,s,t)|^2,$$
$$\left(\frac{\mathrm{d}\sigma}{\mathrm{d}\Omega}\right)_{\pm,\mathrm{U}} = \frac{\beta}{64\pi^2 s}\sum_{\lambda_+,\lambda_-}|\mathcal{M}(\pm\frac{1}{2},\lambda_+,\lambda_-,s,t)|^2. \tag{2.12}$$

For definite degrees of polarization $P^{\pm}$ of the leptons ($P^- = \pm$ corresponds to purely right- and left-handed electrons, respectively) and unpolarized W bosons the differential cross-section reads

$$\left(\frac{\mathrm{d}\sigma}{\mathrm{d}\Omega}\right) = \frac{\beta}{64\pi^2 s}\sum_{\kappa,\lambda_+,\lambda_-}\frac{1}{4}(1-2\kappa P^+)(1+2\kappa P^-)\,|\mathcal{M}(\kappa,\lambda_+,\lambda_-,s,t)|^2\,. \tag{2.13}$$

The helicity amplitudes for the process

$$\mathrm{e}^+(p_+,\kappa_+)+\mathrm{e}^-(p_-,\kappa_-)\to\mathrm{W}^+(k_+,\lambda_+)+\mathrm{W}^-(k_-,\lambda_-)+\gamma(k,\lambda) \tag{2.14}$$

will be referred to as $\mathcal{M}_{1\gamma}(p_+,\kappa_+,p_-,\kappa_-,k_+,\lambda_+,k_-,\lambda_-,k,\lambda)$ in the following. Here the helicities of the outgoing particles are again defined in the LAB system. CP invariance implies the relation:

$$\begin{aligned}&\mathcal{M}_{1\gamma}(p_+,\kappa_+,p_-,\kappa_-,k_+,\lambda_+,k_-,\lambda_-,k,\lambda)\\ &\qquad=\mathcal{M}_{1\gamma}(\bar{p}_-,-\kappa_-,\bar{p}_+,-\kappa_+,\bar{k}_-,-\lambda_-,\bar{k}_+,-\lambda_+,\bar{k},-\lambda),\end{aligned} \tag{2.15}$$

which reduces the number of independent helicity amplitudes from 72 to 36. Here $\bar{p}$ stands for the momentum p after parity transformation: $\bar{p}^\mu = (p_0,-\vec{p})$. In the case of massless electrons and positrons we would have been able to relate their helicities according to $\kappa_+ = -\kappa_-$. For finite m_e, however, collinear photon radiation allows the spin of the $\mathrm{e}^\pm$ to change sign (spin-flip), provided the helicity of the photon and the one of the $\mathrm{e}^\pm$ before radiation have the same sign.

Finally the sine and cosine of the weak mixing angle are defined by

$$c_\mathrm{W} = \frac{M_\mathrm{W}}{M_\mathrm{Z}}, \qquad s_\mathrm{W} = \sqrt{1-c_\mathrm{W}^2}. \tag{2.16}$$

For the numerical evaluations we used the following set of parameters[1,4,3]:

$$\begin{aligned}
&\alpha = 1/137.0359895, && G_\mu = 1.16639\times10^{-5}\,\mathrm{GeV}^{-2},\\
&M_\mathrm{Z} = 91.187\,\mathrm{GeV}, && M_\mathrm{H} = 250\,\mathrm{GeV},\\
&m_\mathrm{e} = 0.51099906\,\mathrm{MeV}, && m_\mu = 105.65839\,\mathrm{MeV}, && m_\tau = 1.777\,\mathrm{GeV},\\
&m_\mathrm{u} = 46.0\,\mathrm{MeV}, && m_\mathrm{c} = 1.50\,\mathrm{GeV}, && m_\mathrm{t} = 165\,\mathrm{GeV},\\
&m_\mathrm{d} = 46.0\,\mathrm{MeV}, && m_\mathrm{s} = 150\,\mathrm{MeV}, && m_\mathrm{b} = 4.50\,\mathrm{GeV}.
\end{aligned}$$

The masses of the light quarks are adjusted in such a way that the experimentally measured hadronic vacuum polarization is reproduced[28]. The strong coupling constant is

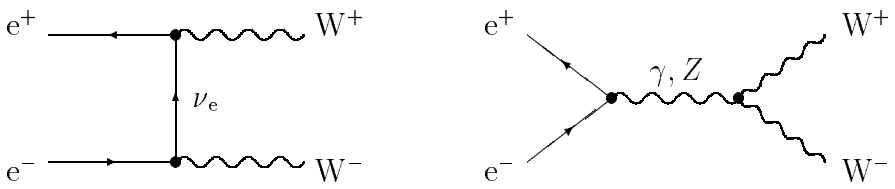

Fig. 1: Lowest-order diagrams for $e^+e^- \to W^+W^-$.

calculated according to the parametrization of Ref. 29, using $\alpha_s(M_Z^2) = 0.12$ as input. As the Fermi constant G_μ is empirically much better known than the W mass, we calculate M_W from all the other parameters using the muon decay width including radiative corrections [see (2.56) and (2.57) for more details]. The above set of parameters yields

$$M_W = 80.299\,\mathrm{GeV}.$$

2.2 Lowest order

2.2.1 Standard Model

In the SM there are three lowest-order diagrams (Fig. 1), if we omit a Higgs-exchange diagram which is suppressed by a factor m_e/M_W and thus completely negligible. The t-channel diagram involving the ν_e exchange only contributes for left-handed electrons. The s-channel diagrams, containing the non-Abelian triple gauge couplings, contribute for both helicities of the electron. The corresponding analytical expressions read

$$\mathcal{M}_{\mathrm{Born}}(\kappa,\lambda_+,\lambda_-,s,t) = \frac{e^2}{2s_W^2}\frac{1}{t}\mathcal{M}_1^\kappa\delta_{\kappa-} + e^2\left[\frac{1}{s} - \frac{c_W}{s_W}g_{eeZ}^\kappa\frac{1}{s-M_Z^2}\right]2(\mathcal{M}_3^\kappa - \mathcal{M}_2^\kappa), \quad (2.17)$$

with $\delta_{\kappa-} = 1$ for left-handed electrons and $\delta_{\kappa-} = 0$ for right-handed electrons. After inserting the explicit form of the Z-boson–fermion couplings

$$g_{eeZ}^\kappa = \frac{s_W}{c_W} - \delta_{\kappa-}\frac{1}{2s_Wc_W}, \quad (2.18)$$

we can organize the lowest-order amplitude into two gauge-invariant subsets:

$$\mathcal{M}_{\mathrm{Born}}(\kappa,\lambda_+,\lambda_-,s,t) = \frac{e^2}{2s_W^2}\mathcal{M}_I(\kappa,\lambda_+,\lambda_-,s,t)\delta_{\kappa-} + e^2\mathcal{M}_Q(\kappa,\lambda_+,\lambda_-,s,t), \quad (2.19)$$

where

$$\begin{aligned}\mathcal{M}_I(\kappa,\lambda_+,\lambda_-,s,t) &= \frac{1}{t}\mathcal{M}_1^\kappa + \frac{1}{s-M_Z^2}2(\mathcal{M}_3^\kappa - \mathcal{M}_2^\kappa),\\ \mathcal{M}_Q(\kappa,\lambda_+,\lambda_-,s,t) &= \left[\frac{1}{s} - \frac{1}{s-M_Z^2}\right]2(\mathcal{M}_3^\kappa - \mathcal{M}_2^\kappa). \end{aligned} \quad (2.20)$$

The gauge invariance of the two contributions $\mathcal{M}_I$ and $\mathcal{M}_Q$ can be simply inferred from the fact that they are accompanied by different coupling constants, one of which involving the electromagnetic coupling constant e, the other the charged-current coupling

constant $e/(\sqrt{2}s_{\rm W})$. Whereas $\mathcal{M}_I$ corresponds to the pure $SU(2)$ contribution, the parity-conserving contribution $\mathcal{M}_Q$ is a result of the symmetry-breaking mechanism.

Using $\hat{t} = 2t/s$, $\gamma = \sqrt{s}/(2M_{\rm W})$ and $z = M_{\rm Z}^2/s$ the expressions for the independent matrix elements read

$$
\begin{aligned}
\mathcal{M}_I(\kappa,\pm,\mp,s,t) &= -2\frac{\cos\theta \mp 2\kappa}{1-2\beta\cos\theta+\beta^2}\sin\theta = \frac{\cos\theta\mp 2\kappa}{\hat{t}}\sin\theta,\\
\mathcal{M}_Q(\kappa,\pm,\mp,s,t) &= 0,\\
\mathcal{M}_I(\kappa,+,+,s,t) &= -(1-\beta^2)\left[\frac{2\cos\theta-\beta}{1-2\beta\cos\theta+\beta^2}+\frac{\beta}{4c_{\rm W}^2-1+\beta^2}\right]\sin\theta\\
&= \frac{1}{\gamma^2}\left[\frac{1}{\beta}-\frac{1}{4c_{\rm W}^2}\frac{\beta}{1-z}+\frac{1}{2\beta\hat{t}}\right]\sin\theta,\\
\mathcal{M}_Q(\kappa,+,+,s,t) &= \frac{1}{\gamma^2}\frac{1}{4c_{\rm W}^2}\frac{\beta}{1-z}\sin\theta,\\
\mathcal{M}_I(\kappa,0,\mp,s,t) &= \sqrt{2(1-\beta^2)}\left[\frac{2\cos\theta-\beta\pm 2\kappa}{1-2\beta\cos\theta+\beta^2}+\frac{\beta}{4c_{\rm W}^2-1+\beta^2}\right](\cos\theta\mp 2\kappa)\\
&= -\frac{\sqrt{2}}{\gamma}\left[\frac{1}{\beta}-\frac{1}{4c_{\rm W}^2}\frac{\beta}{1-z}+\frac{1\pm 2\kappa\beta}{2\beta\hat{t}}\right](\cos\theta\mp 2\kappa),\\
\mathcal{M}_Q(\kappa,0,\mp,s,t) &= -\frac{\sqrt{2}}{\gamma}\frac{1}{4c_{\rm W}^2}\frac{\beta}{1-z}(\cos\theta\mp 2\kappa),\\
\mathcal{M}_I(\kappa,0,0,s,t) &= \left[4\frac{\cos\theta-\beta}{1-2\beta\cos\theta+\beta^2}+\beta+\frac{\beta(3-\beta^2)}{4c_{\rm W}^2-1+\beta^2}\right]\sin\theta\\
&= -\left[\frac{2}{\beta}-\beta-\frac{1}{2c_{\rm W}^2}\frac{\beta}{1-z}(1+\frac{1}{2\gamma^2})+\frac{1}{\gamma^2\beta\hat{t}}\right]\sin\theta,\\
\mathcal{M}_Q(\kappa,0,0,s,t) &= -\frac{1}{2c_{\rm W}^2}\frac{\beta}{1-z}(1+\frac{1}{2\gamma^2})\sin\theta.
\end{aligned}
\tag{2.21}
$$

The others follow from the symmetry relations (2.7). Note that all matrix elements vanish in the forward and backward direction except those for one longitudinal and one transverse W boson. This is a direct consequence of angular-momentum conservation: because of electron-helicity conservation the angular momentum in the direction of the incoming $\rm e^-$ is $J_3 = 2\kappa$. If the $\rm W^-$ boson goes into the same/opposite direction, the difference of the helicities of the two W bosons $\lambda_- - \lambda_+$ has to be equal/opposite to J_3. Thus only the two helicity configurations $(\lambda_+,\lambda_-) = (-/+2\kappa, 0), (0, +/-2\kappa)$ are allowed.

The lowest-order cross-section determines the essential features of W-pair production. The threshold behaviour is important for the determination of the W mass[30,31] in a threshold scan. For small β the matrix elements behave as

$$
\mathcal{M}_2^\kappa, \mathcal{M}_3^\kappa \propto \beta, \qquad \mathcal{M}_1^\kappa \propto 1 \tag{2.22}
$$

for fixed scattering angles. Consequently the s-channel matrix elements vanish at threshold[d] and the t-channel graph dominates in the threshold region. For $\beta \ll 1$ the differential cross-section for unpolarized beams and W bosons is given by

$$\left(\frac{\mathrm{d}\sigma}{\mathrm{d}\Omega}\right)_{\mathrm{Born}} \approx \frac{\alpha^2}{s}\frac{1}{4s_{\mathrm{W}}^4}\beta\left[1 + 4\beta\cos\theta\,\frac{3c_{\mathrm{W}}^2 - 1}{4c_{\mathrm{W}}^2 - 1} + \mathcal{O}(\beta^2)\right], \tag{2.23}$$

where the leading term $\propto \beta$ originates from the t-channel diagram only. Note that the leading term is angular-independent. In the total cross-section

$$\sigma_{\mathrm{Born}} \approx \frac{\pi\alpha^2}{s}\frac{1}{4s_{\mathrm{W}}^4}4\beta + \mathcal{O}(\beta^3), \tag{2.24}$$

all terms $\propto \beta^2$ drop out and the s-channel and the s–t-interference contribution are proportional to β^3. This can be explained as follows: at threshold the orbital angular momentum in the final state vanishes and the total angular momentum J is equal to the total spin of the two W bosons, which can take the values $0, 1, 2$. Fermion-helicity conservation in the initial state implies $J \geq 1$ and CP conservation forbids $J = 1$. Therefore only $J = 2$ is possible. As the s-channel spin-1 exchanges are restricted to $J \leq 1$ they have to vanish at threshold, i.e. in a partial-wave expansion they do not contain an S-wave contribution. When integrating over all scattering angles, the orthogonality of the different partial waves prevents the s-channel from interfering with the t-channel S-wave contributions. Thus the s–t-interference contribution to the total cross-section does not involve S-wave terms and, since all other contributions are proportional to β on the matrix-element level, their contribution to the total cross-section is at least of order β^3 (including one β from phase space). This conclusion still holds for any symmetric integration range, as the interference between the S- and P-waves still vanishes due to their different symmetry properties and the higher partial waves are proportional to β^2 at least. Hence in the threshold region the t-channel is dominant and the cross-section for $\mathrm{e^+e^-} \to \mathrm{W^+W^-}$ is not very sensitive to the triple gauge couplings.

In the SM the coefficient of the β^3 term in (2.24) is roughly equal to the coefficient of the leading β term. Consequently the shape of the total cross-section close to threshold is completely governed by the linear rise in β and hence by kinematics alone. This is even true after the inclusion of finite-width effects because the next-to-leading β^3 term becomes only sizeable several Γ_{W} above threshold. This fact allows for a model-independent determination of the W mass from the W-pair production threshold[30].

At high energies there are strong unitarity (gauge) cancellations between the various diagrams. For $s \gg M_{\mathrm{W}}^2$ and longitudinal gauge bosons the contributions of individual Feynman diagrams behave as

$$\frac{\mathcal{M}_1^\kappa}{t} \sim 2\frac{\mathcal{M}_2^\kappa - \mathcal{M}_3^\kappa}{s} \sim -\frac{s}{2M_{\mathrm{W}}^2}\sin\theta, \tag{2.25}$$

but the Born matrix element and its gauge-invariant subsets $\mathcal{M}_I$, $\mathcal{M}_Q$ exhibit a decent high-energy behaviour, which can be directly read off from (2.21) by putting $\beta = 1$, $z = 0$ and $1/\gamma^2 = 0$. The gauge cancellations are illustrated in Fig. 2 for the total cross-section.

[d] This holds for arbitrary CP-conserving s-channel contributions in the limit of vanishing electron mass[16].

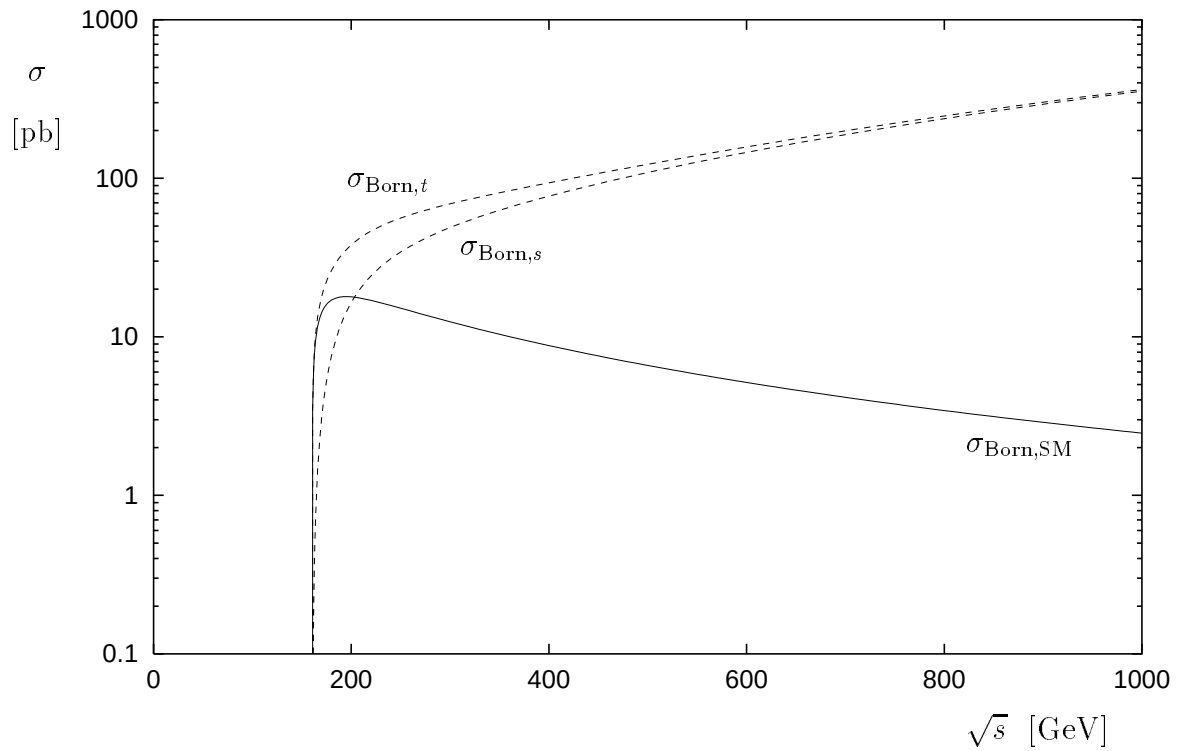

Fig. 2: Gauge cancellations in the total cross-section for W-pair production. The individual curves correspond to the Born cross-sections arising from the s-channel ($\sigma_{\mathrm{Born},s}$) and t-channel ($\sigma_{\mathrm{Born},t}$) diagrams alone, and to the complete SM cross-section ($\sigma_{\mathrm{Born,SM}}$).

They reach one order of magnitude at 400 GeV and two orders at 1 TeV.

As a consequence of the unitarity cancellations the matrix elements corresponding to equal transverse polarizations are suppressed by a factor M_{W}^2/s, the ones for one transverse and one longitudinal W boson (M) by a factor $M_{\mathrm{W}}/\sqrt{s}$ and the ones for two longitudinal bosons (L) are of order one. The matrix elements for opposite W polarizations are not suppressed owing to the absence of the s-channel exchange which cannot contribute to the $|\lambda_+ - \lambda_-| = \Delta\lambda = 2$ final state. Thus three helicity amplitudes survive at high energies and finite scattering angles. Note, however, that in the backward and in the extreme forward direction the matrix elements corresponding to M dominate because all others go to zero as discussed above.

After the gauge cancellations the t-channel contributions dominate again the SM cross-section. As far as the three unsuppressed amplitudes are concerned the t-channel pole is cancelled by a kinematical zero in the matrix element $\mathcal{M}(-,-,+,s,t)$ and suppressed by a factor M_{W}^2/s for the L amplitude. Moreover the latter is at least by a factor of four smaller than the unsuppressed amplitudes for transverse W bosons (T) at all scattering angles. Consequently the cross-section in the forward direction and also the total cross-section are dominated by $\mathcal{M}(-,+,-,s,t)$, i.e. by purely transverse W bosons. Note that this helicity amplitude originates from the t-channel diagram only. Hence there is no interference between the s-channel diagrams (involving the triple gauge couplings) and the unsuppressed t-channel-pole contribution. For right-handed electrons there is

no t-channel contribution and the cross-section is completely dominated by longitudinal W bosons.

The lowest-order differential cross-sections for definite transverse and/or longitudinal W bosons read in the high-energy limit:

$$\begin{aligned}
\left(\frac{\mathrm{d}\sigma}{\mathrm{d}\Omega}\right)^{\mathrm{Born}}_{-,\mathrm{L}} &= \frac{\alpha^2}{4s}\frac{1}{16s_{\mathrm{W}}^4c_{\mathrm{W}}^4}\sin^2\theta, & \left(\frac{\mathrm{d}\sigma}{\mathrm{d}\Omega}\right)^{\mathrm{Born}}_{+,\mathrm{L}} &= \frac{\alpha^2}{4s}\frac{1}{4c_{\mathrm{W}}^4}\sin^2\theta,\\
\left(\frac{\mathrm{d}\sigma}{\mathrm{d}\Omega}\right)^{\mathrm{Born}}_{-,\mathrm{T}} &= \frac{\alpha^2}{4s}\frac{1}{4s_{\mathrm{W}}^4}\frac{u^2+t^2}{t^2}\sin^2\theta, & \left(\frac{\mathrm{d}\sigma}{\mathrm{d}\Omega}\right)^{\mathrm{Born}}_{+,\mathrm{T}} &= \frac{\alpha^2}{4s}\frac{2}{c_{\mathrm{W}}^4}\frac{M_{\mathrm{W}}^4}{s^2}\sin^2\theta,\\
\left(\frac{\mathrm{d}\sigma}{\mathrm{d}\Omega}\right)^{\mathrm{Born}}_{-,\mathrm{M}} &= \frac{\alpha^2}{4s}\frac{1}{s_{\mathrm{W}}^4c_{\mathrm{W}}^4}\frac{M_{\mathrm{W}}^2}{s}\frac{u^2+t^2+4c_{\mathrm{W}}^2u(u-t)+8c_{\mathrm{W}}^4u^2}{s^2},\\
\left(\frac{\mathrm{d}\sigma}{\mathrm{d}\Omega}\right)^{\mathrm{Born}}_{+,\mathrm{M}} &= \frac{\alpha^2}{4s}\frac{4}{c_{\mathrm{W}}^4}\frac{M_{\mathrm{W}}^2}{s}\frac{u^2+t^2}{s^2},
\end{aligned} \tag{2.26}$$

The corresponding total cross-sections are given by

$$\begin{aligned}
\sigma^{\mathrm{Born}}_{-,\mathrm{L}} &= \frac{\pi\alpha^2}{s}\frac{1}{24s_{\mathrm{W}}^4c_{\mathrm{W}}^4}, & \sigma^{\mathrm{Born}}_{+,\mathrm{L}} &= \frac{\pi\alpha^2}{s}\frac{1}{6c_{\mathrm{W}}^4},\\
\sigma^{\mathrm{Born}}_{-,\mathrm{T}} &= \frac{\pi\alpha^2}{s}\frac{1}{3s_{\mathrm{W}}^4}\left[6\log\left(\frac{s}{M_{\mathrm{W}}^2}\right)-8\right], & \sigma^{\mathrm{Born}}_{+,\mathrm{T}} &= \frac{\pi\alpha^2}{s}\frac{4}{3c_{\mathrm{W}}^4}\frac{M_{\mathrm{W}}^4}{s^2},\\
\sigma^{\mathrm{Born}}_{-,\mathrm{M}} &= \frac{\pi\alpha^2}{s}\frac{2}{3s_{\mathrm{W}}^4c_{\mathrm{W}}^4}\frac{M_{\mathrm{W}}^2}{s}[1+c_{\mathrm{W}}^2+10c_{\mathrm{W}}^4], & \sigma^{\mathrm{Born}}_{+,\mathrm{M}} &= \frac{\pi\alpha^2}{s}\frac{8}{3c_{\mathrm{W}}^4}\frac{M_{\mathrm{W}}^2}{s},
\end{aligned} \tag{2.27}$$

resulting in the total unpolarized cross-section:

$$\sigma_{\mathrm{Born}} \approx \frac{\pi\alpha^2}{s}\frac{1}{4s_{\mathrm{W}}^4}\left[2\log\left(\frac{s}{M_{\mathrm{W}}^2}\right)-\frac{5}{2}-\frac{1}{3c_{\mathrm{W}}^2}+\frac{5}{24c_{\mathrm{W}}^4}\right]. \tag{2.28}$$

Compared to $\sigma^{\mathrm{Born}}_{-,\mathrm{T}}$, which involves the only unsuppressed t-channel-pole contribution, all other polarized cross-sections are suppressed by at least $30\log(s/M_{\mathrm{W}}^2)$.

We now consider the complete Born results for the W-pair production cross-section. In Figs. 3 and 4 we show the differential cross-section for different polarizations of the W bosons and electrons for $\sqrt{s} = 190$ and 500 GeV, respectively. The positrons are assumed to be unpolarized. The minima near 70° or 30° in the cross-sections for longitudinal W bosons would be zeros for purely left-handed electrons. The small finite contribution is caused by the right-handed electrons. The curves for 500 GeV exhibit the features of the high-energy limit discussed above. Already at 190 GeV the T contributions dominate the cross-section.

In Tab. 1 we give the integrated cross-section for different centre-of-mass energies and different polarizations of the electrons (+,−) and W bosons (T,L,M). Positrons are again assumed to be unpolarized. Using right-handed electrons one could study a pure triple-gauge-coupling process, but this would require longitudinally polarized electron beams. Furthermore, for all energies the cross-section for right-handed electrons is suppressed by two orders of magnitude compared with the dominant left-handed mode, mainly because

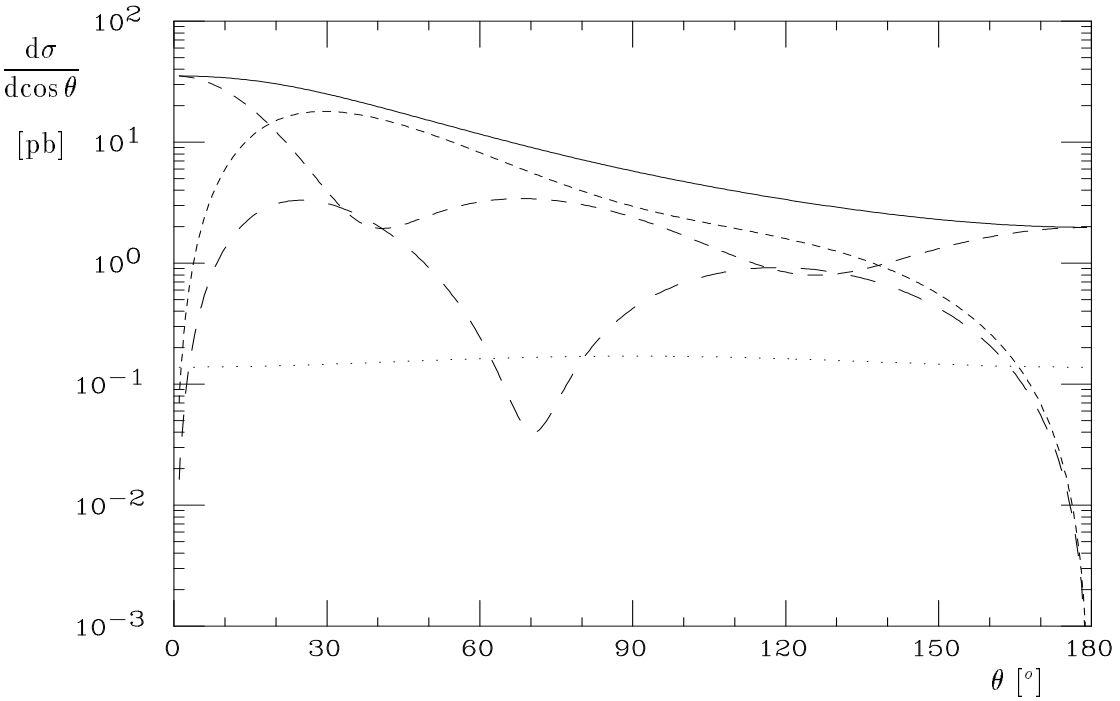

Fig. 3: Lowest-order differential cross-section at $\sqrt{s} = 190\,\mathrm{GeV}$. The solid curve corresponds to unpolarized W bosons and unpolarized electrons, the dotted one to unpolarized W bosons and right-handed electrons. The dashed curves represent unpolarized electrons and in order of increasing dash length the W-boson polarization states T, M and L, respectively.

$\sqrt{s}$ [GeV]	σ^{Born}	σ_-^{Born}	σ_+^{Born}	$\sigma_{\mathrm{T}}^{\mathrm{Born}}$	$\sigma_{\mathrm{L}}^{\mathrm{Born}}$	$\sigma_{\mathrm{M}}^{\mathrm{Born}}$
165.0	10.712	21.372	0.053	5.223	1.346	4.143
176.0	16.285	32.358	0.212	8.751	1.769	5.765
190.0	17.863	35.408	0.319	10.625	1.625	5.613
250.0	15.154	30.032	0.276	11.592	0.738	2.824
500.0	6.599	13.149	0.050	6.239	0.114	0.247
1000.0	2.465	4.920	0.010	2.421	0.027	0.017

Tab. 1: Integrated lowest-order cross-section in pb for different polarizations and different centre-of-mass energies.

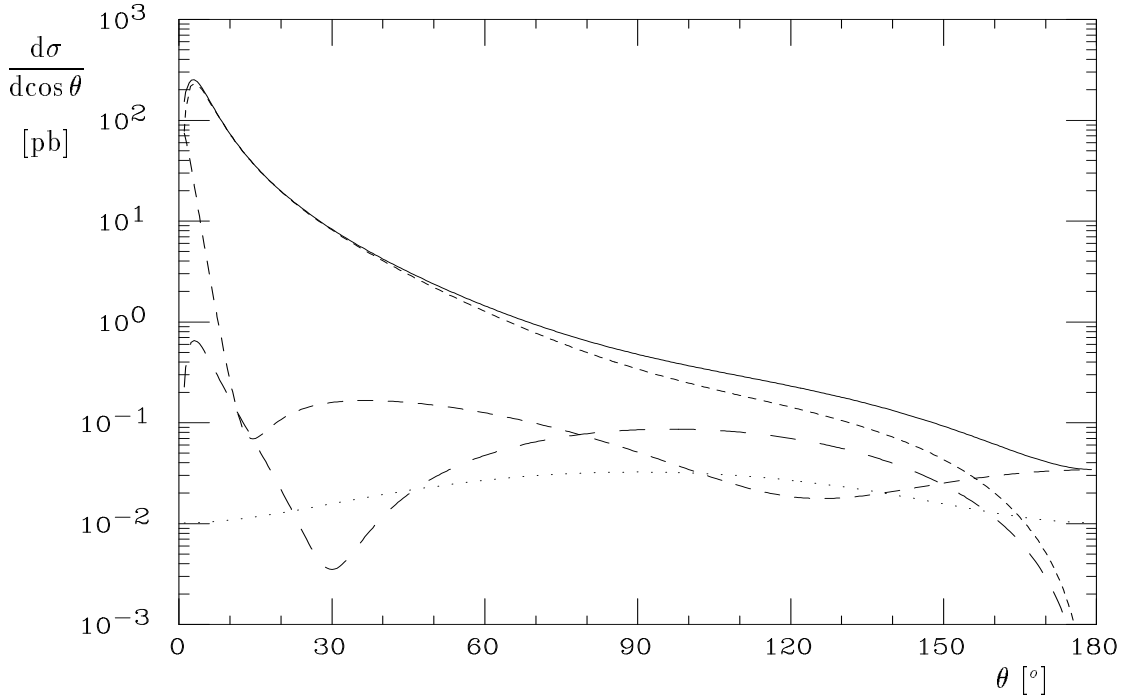

Fig. 4: Lowest-order differential cross-section at $\sqrt{s} = 500\,\mathrm{GeV}$. Same signature as adopted in Fig. 3.

there is no t-channel contribution. Therefore essentially only the latter can be investigated at LEP. With transverse beam polarization, however, one could obtain information on the right-handed matrix element via its interference with the left-handed one.

As stated in Sec. 2.1, for on-shell W-pair production and unpolarized electrons and positrons there are nine independent helicity-matrix elements or six if CP is conserved. These yield nine or six independent observables. Taking into account the decay of the W bosons there are much more observables: 81 or, if CP is conserved, 36 products of the various helicity-matrix elements[16]. Because the $V-A$ structure of the W decays is well established, these observables can in principle be extracted in a model-independent way from the data for the five-fold differential cross-section $\mathrm{d}\sigma/(\mathrm{d}\cos\theta\,\mathrm{d}\cos\theta_1\,\mathrm{d}\phi_1\,\mathrm{d}\cos\theta_2\,\mathrm{d}\phi_2)$ where $\theta_{1,2}$ and $\phi_{1,2}$ represent the decay angles of the two W bosons. However, because of limited statistics the five-fold differential distribution cannot be analyzed and one has to resort to more inclusive distributions. Using the three-fold differential distributions $\mathrm{d}\sigma/(\mathrm{d}\cos\theta\,\mathrm{d}\cos\theta_1\,\mathrm{d}\phi_1)$, $\mathrm{d}\sigma/(\mathrm{d}\cos\theta\,\mathrm{d}\cos\theta_2\,\mathrm{d}\phi_2)$ and $\mathrm{d}\sigma/(\mathrm{d}\cos\theta\,\mathrm{d}\cos\theta_1\,\mathrm{d}\cos\theta_2)$, and disregarding any CP violation, one ends up with eight independent observables[10] which can be measured at LEP200 and the NLC. Five of them do not rely on charge identification of the final-state fermions, the remaining three require only the identification of the charge of one of those fermions. This is at least possible for hadronic–leptonic or leptonic–leptonic events.

Note that without any charge identification one would not only lose three observables, but also the information on the sign of $\cos\theta$, the determination of which needs at least the identification of the charge of one of the decaying W bosons. As a consequence only

production-forward–backward-symmetric observables would be left. As argued above, in those observables for instance the s-channel contribution is suppressed by β^2 in the threshold region. Moreover, high-energy rescattering and triple-gauge-boson-coupling studies would suffer severely, because the backward hemisphere could not be isolated any more. Consequently, if one cannot identify the jet charges the purely hadronic events will not be of much use for these studies at LEP200 and the NLC. Of course this does not concern the W-mass determination as it does not rely on s-channel contributions.

2.2.2 Anomalous triple gauge-boson couplings

As already mentioned previously the study of the process $e^+e^- \to W^+W^-$ at LEP200 allows the first direct test of the non-Abelian nature of the SM, or more precisely of the triple gauge couplings between the W and the neutral gauge bosons $V = \gamma$, Z.

The most general phenomenological parametrization of the WWV vertex has been given in Ref. 16. Taking into account that our definition of the epsilon tensor differs by a minus sign from the one in Ref. 16 the corresponding effective Lagrangian reads:

$$\begin{aligned}
\mathcal{L}_{\mathrm{WWV}}/(-e g_{\mathrm{WWV}}) = {} & i g_1^V (W^\dagger_{\mu\nu} W^\mu V^\nu - W^{\mu\nu} W^\dagger_\mu V_\nu) + i\kappa^V W^\dagger_\mu W_\nu V^{\mu\nu} \\
& + i\frac{\lambda^V}{M_{\mathrm{W}}^2} W^\dagger_{\rho\mu} W^\mu{}_\nu V^{\nu\rho} - g_4^V W^\dagger_\mu W_\nu (\partial^\mu V^\nu + \partial^\nu V^\mu) \\
& - g_5^V \epsilon^{\mu\nu\rho\sigma} (W^\dagger_\mu \partial_\rho W_\nu - W_\nu \partial_\rho W^\dagger_\mu) V_\sigma - \frac{i}{2}\tilde{\kappa}^V \epsilon^{\mu\nu\rho\sigma} W^\dagger_\mu W_\nu V_{\rho\sigma} \\
& - \frac{i}{2}\frac{\tilde{\lambda}^V}{M_{\mathrm{W}}^2} \epsilon^{\mu\nu\rho\sigma} W^\dagger_{\nu\lambda} W^\lambda{}_\mu V_{\rho\sigma}. \qquad (2.29)
\end{aligned}$$

Here V^μ stands for either the photon or the Z-boson field, W^μ is the W^--boson field, $W_{\mu\nu} = \partial_\mu W_\nu - \partial_\nu W_\mu$, and $V_{\mu\nu} = \partial_\mu V_\nu - \partial_\nu V_\mu$. The operators in (2.29) exhaust all possible Lorentz structures which do not involve the scalar components of any of the three vector bosons:

$$\partial_\mu V^\mu = 0, \qquad \partial_\mu W^\mu = 0. \qquad (2.30)$$

These conditions are fulfilled for the on-shell W bosons and for $V = \gamma$, being coupled to a conserved current, and hold for $V = \mathrm{Z}$ in W-pair production up to terms proportional to the electron mass. This follows directly from the fact that in the limit of zero electron mass also the Z bosons couple to a conserved current. The general parametrization (2.29) violates electromagnetic gauge invariance, a concept that is too well established to tamper with. As we will discuss below this can be cured by considering appropriate higher-dimensional operators. All higher-dimensional operators for on-shell W bosons can be obtained from the ones in (2.29) by replacing V_μ by $\Box^n V_\mu = (\partial^2)^n V_\mu$.

In momentum space these give rise to an energy dependence of the various form factors and the WWV vertex can be expressed as follows:

$$\begin{aligned}
\Gamma_V^{\sigma\rho\mu}(k_-, k_+, P) = {} & -ie g_{\mathrm{WWV}} \Big[f_1^V(P^2)(k_- - k_+)^\mu g^{\sigma\rho} - \frac{f_2^V(P^2)}{M_{\mathrm{W}}^2}(k_- - k_+)^\mu P^\sigma P^\rho \\
& + f_3^V(P^2)(P^\sigma g^{\mu\rho} - P^\rho g^{\mu\sigma}) + i f_4^V(P^2)(P^\sigma g^{\mu\rho} + P^\rho g^{\mu\sigma}) \\
& - i f_5^V(P^2)\epsilon^{\mu\sigma\rho\alpha}(k_- - k_+)_\alpha + f_6^V(P^2)\epsilon^{\mu\sigma\rho\alpha} P_\alpha
\end{aligned}$$

$$+\frac{f_7^V(P^2)}{M_{\rm W}^2}(k_- - k_+)^\mu \epsilon^{\sigma\rho\alpha\beta} P_\alpha (k_- - k_+)_\beta \Big]. \tag{2.31}$$

Here $k_\pm$ denote, as usual, the momenta of the outgoing $\mathrm{W}^\pm$ bosons and $P = k_+ + k_-$ the incoming momentum of the boson V. The overall coupling constants g_{WWV} are fixed to their SM values

$$g_{\mathrm{WW}\gamma} = 1, \qquad g_{\mathrm{WWZ}} = -\frac{c_{\rm W}}{s_{\rm W}}. \tag{2.32}$$

The dimensionless form factors f_i^V are related to the coefficients of the operators appearing in the Lagrangian (2.29) as follows:

$$\begin{aligned} f_1^V &= g_1^V + \frac{P^2}{2M_{\rm W}^2}\lambda^V, \qquad f_2^V = \lambda^V, \qquad f_3^V = g_1^V + \kappa^V + \lambda^V, \\ f_4^V &= g_4^V, \qquad f_5^V = g_5^V, \qquad f_6^V = \tilde\kappa^V - \tilde\lambda^V, \qquad f_7^V = -\frac{1}{2}\tilde\lambda^V. \end{aligned} \tag{2.33}$$

While the couplings $f_{1,2,3}^V$ conserve C and P separately, f_5^V conserves only CP, the remaining ones are CP-violating.

Because the charge of the W is fixed we have

$$g_1^\gamma(P^2 = 0) = 1. \tag{2.34}$$

$U(1)_{\rm em}$ gauge invariance relates g_1^γ to the W-boson two-point function. Consequently a non-standard value of g_1^γ leads to anomalous contributions to the W-boson two-point function. In view of the precise data from LEP1/SLC, which restrict the two-point functions close to their standard values, this means that (2.34) holds to a very good approximation for all P^2 that are accessible to LEP1/SLC. Therefore one usually assumes (2.34) to hold for all P^2. Another restriction follows from the fact that the terms containing g_4^V and g_5^V in (2.29) break electromagnetic gauge invariance. This can be restored by replacing $g_{4,5}^V V^\mu$ by $-g_{4,5}'^V \partial_\lambda V^{\lambda\mu}/M_{\rm W}^2$ for $V = \gamma$ in those terms. In momentum space this leads to the effective replacement $g_{4,5}^V \to g_{4,5}'^V P^2/M_{\rm W}^2$. Consequently those couplings have to vanish for $P^2 = 0$:

$$g_4^\gamma(P^2 = 0) = 0, \qquad g_5^\gamma(P^2 = 0) = 0. \tag{2.35}$$

Assuming in addition CP and C invariance for the electromagnetic interaction of the W boson one is left with two free couplings in the WWγ case, f_2^γ and f_3^γ. These are related to the magnetic dipole moment $\mu_{\rm W}$ and the electric quadrupole moment $Q_{\rm W}$ of the W boson via

$$\begin{aligned} \mu_{\rm W} &= \frac{e}{2M_{\rm W}}[1 + \kappa^\gamma(0) + \lambda^\gamma(0)] = \frac{e}{2M_{\rm W}} f_3^\gamma(0), \\ Q_{\rm W} &= -\frac{e}{M_{\rm W}^2}[\kappa^\gamma(0) - \lambda^\gamma(0)] = -\frac{e}{M_{\rm W}^2}\left[f_3^\gamma(0) - f_1^\gamma(0) - 2f_2^\gamma(0)\right]. \end{aligned} \tag{2.36}$$

Note that (2.34) and (2.36) are strictly speaking only valid for $P^2 = 0$. Moreover, owing to the P^2 dependence of the form factors, experimental limits or theoretical predictions obtained for certain values of P^2 (e.g. at low energies) need not be appropriate for other values of P^2 (e.g. high energies).

In the SM the non-Abelian gauge symmetry implies

$$f_1^V = 1, \qquad f_3^V = 2, \qquad f_i^V = 0, \quad i \neq 1,3 \tag{2.37}$$

or

$$g_1^V = \kappa^V = 1, \qquad \lambda^V = g_4^V = g_5^V = \tilde{\kappa}^V = \tilde{\lambda}^V = 0 \tag{2.38}$$

for both $V = \gamma, \mathrm{Z}$, up to radiative corrections (see below).

The parametrization (2.31) should be viewed as appropriate for the tree-level process $\mathrm{e^+e^-} \to \mathrm{W^+W^-}$. As it stands it is not invariant under the $SU(2) \times U(1)$ gauge transformations. Gauge invariance can however be achieved[32] by embedding the terms appearing in (2.29) into local gauge-invariant operators based on covariant derivatives and field strengths. These operators give rise to related anomalous contributions to other couplings, e.g. to the bi-linear couplings, the quartic gauge couplings, or the Higgs–gauge-boson couplings. The gauge-invariant operators of dimension four, i.e. the renormalizable ones, correspond to those appearing already in the SM. The anomalous couplings are related to operators of higher dimensions. In this respect it should be noted that owing to the requirement of gauge invariance the effective dimensions of these anomalous operators are higher than one would naïvely expect from derivative counting in (2.29). Thus in a gauge-invariant formulation the anomalous couplings correspond to gauge-invariant but non-renormalizable operators.

If one assumes that the new-physics effects are $SU(2) \times U(1)$ gauge-invariant and that the SM Higgs mechanism is not responsible for the mass generation of the new-physics particles, they decouple at low energies and the corresponding higher-dimensional operators are inverse proportional to the scale of new physics Λ. Consequently they are small at low energies ($E \ll \Lambda$). More precisely they are suppressed by a factor $(E/\Lambda)^{n-4}$ where n is the dimension of the operator and E the energy scale of the experiment. This corresponds to an effective-field-theory approach, parametrizing new physics well below the scale where its structure will show up by local operators:

$$\mathcal{L} = \mathcal{L}_{\mathrm{SM}} + \mathcal{L}_{\mathrm{eff}}, \qquad \mathcal{L}_{\mathrm{eff}} = \sum_{n=1}^{\infty} \sum_i \frac{c_i^{(n)}}{\Lambda^n} O_i^{(n+4)}, \tag{2.39}$$

where $O_i^{(n+4)}$ stands for all possible local operators with dimension $(n+4)$. This naturally introduces a hierarchy of the couplings based on the dimension of the corresponding operators[32,33]. The smaller the dimension of such an operator the more likely the corresponding coupling might be seen in the 'low-energy' experiments in the 200–1000 GeV range. If one assumes lepton- and baryon-number conservation one cannot construct dimension-five operators from the fields present in the SM[34]. Thus the most important anomalous couplings, i.e. the ones which most likely influence the results of future experiments, are those related to dimension-six operators. Inserting dimension-six operators in loops gives rise to contributions of the form $(E^2/\Lambda^2)\log(\Lambda)$, whereas all higher-dimensional operators yield only terms of the form (E^2/Λ^2). Since all higher-dimensional operators contribute to those terms they cannot be predicted in a model-independent way and only the $(E^2/\Lambda^2)\log(\Lambda)$ terms are known. Moreover, these logarithmic one-loop contributions can be viewed as a renormalization of new-physics couplings contributing to the same quantity at tree level. They correspond to an operator mixing due to the renormalization-group evolution between the scale of new physics, Λ, and the gauge-boson

mass scale. Thus the contributions of anomalous gauge couplings to the precision observables at LEP1/SLC are predominantly related to the new-physics contributions to the gauge-boson propagators. Therefore rigorous indirect bounds on the triple gauge-boson couplings at LEP1/SLC cannot be obtained without making assumptions about how the new physics will enter the propagators[35]. As a consequence the anomalous WWV couplings arising from operators that only contribute to four-fermion amplitudes at one-loop level are only very weakly constrained by the present precision experiments at and below the Z-mass scale.

In a non-linear scenario, i.e. in a scenario without Higgs boson, a new-physics scale does not necessarily appear; then the hierarchy is based on an expansion in powers of $P^2/(16\pi^2 v^2)$, where $v \approx 246\,\mathrm{GeV}$ is the electroweak scale. The lowest-dimensional operator of order P^2 is universal, being fixed by the low-energy theorems for symmetry breaking[36]. Higher-dimensional operators provide information on the specific symmetry-breaking dynamics.

Note that for $E = \mathcal{O}(\Lambda)$ the above-discussed hierarchy is ineffective and the anomalous couplings cannot be ordered on the basis of simple dimensionality arguments. In that case, however, the effects of new physics should be seen directly.

An additional hierarchy is based on global symmetry requirements. For instance, based on presently known experimental facts, CP-violating couplings are considered to be less likely than the CP-conserving ones. The same holds for C-violating WWγ couplings. A further classification[37,10] can be based on the amount of intrinsic global custodial $SU(2)_c$ symmetry breaking beyond the one present in the SM. Thereby intrinsic $SU(2)_c$ violation is the one not caused by the mixing between the $\mathrm{W}^\pm$ and B fields. An argument in favour of assuming the intrinsic $SU(2)_c$ breaking beyond the SM to be small is the fact that if it is zero, the CP-violating Z interactions are only allowed if there is also electromagnetic CP violation. In addition this assumption can be motivated by the extrapolation of present empirical evidence on the electroweak interaction, in particular on the ratio of the W and Z masses and the fact that the ρ parameter is close to one. Combining gauge invariance and the absence of intrinsic $SU(2)_c$ global symmetry breaking beyond the SM, and keeping only the dimension-six operators does not give any C or P violation.

In addition there are experimental restrictions. In a general parametrization there are operators that contribute to both the triple gauge couplings and the gauge-boson self-energies. Their direct contribution to the two-boson interactions is strongly constrained by precision tests at LEP1/SLC[38,35,32]. As a consequence these operators have to be so strongly suppressed that the observation of their three-gauge-boson parts at LEP200 is precluded. Therefore only the others might yield interesting effects.

Based on all those restrictions one arrives at the 'most likely' WWV couplings. These involve three CP-conserving dimension-six operators which contribute with well-defined ratios to the general C- and P-conserving form factors. For a further discussion of this subject we refer to the literature[33,10].

Given the general parametrization of the WWV couplings, it is easy to calculate the contributions of the anomalous couplings to $\mathrm{e}^+\mathrm{e}^- \to \mathrm{W}^+\mathrm{W}^-$ in terms of the basic matrix elements defined in Sec. 2.1:

$$\delta\mathcal{M}_{\mathrm{anom}}(\kappa,\lambda_+,\lambda_-,s,t) = e^2 \sum_V g_{\mathrm{WWV}}\, g^\kappa_{\mathrm{eeV}} \frac{1}{s-M_V^2}\Big[[f_3^V(s)-2]\mathcal{M}_3^\kappa - 2[f_1^V(s)-1]\mathcal{M}_2^\kappa$$

$$+ 2\frac{f_2^V(s)}{M_{\rm W}^2}\mathcal{M}_5^\kappa - f_5^V(s)\mathcal{M}_8^\kappa$$
$$+ if_4^V(s)\widetilde{\mathcal{M}}_3^\kappa + if_6^V(s)\widetilde{\mathcal{M}}_8^\kappa + 2i\frac{f_7^V(s)}{M_{\rm W}^2}\widetilde{\mathcal{M}}_9^\kappa\Big], \tag{2.40}$$

with

$$\begin{aligned}
\mathcal{M}_8^\kappa &= 2\kappa[2(\mathcal{M}_1^\kappa + \mathcal{M}_2^\kappa - \mathcal{M}_4^\kappa) - \mathcal{M}_3^\kappa], \\
\widetilde{\mathcal{M}}_8^\kappa &= 2\kappa[2\widetilde{\mathcal{M}}_4^\kappa - \widetilde{\mathcal{M}}_3^\kappa], \\
\widetilde{\mathcal{M}}_9^\kappa &= 2\kappa[2\widetilde{\mathcal{M}}_7^\kappa + (s - 4M_{\rm W}^2)\widetilde{\mathcal{M}}_4^\kappa + (t + M_{\rm W}^2)\widetilde{\mathcal{M}}_3^\kappa].
\end{aligned} \tag{2.41}$$

Note that we have subtracted the SM contribution.

An often asked question is how much the radiative corrections contribute to the anomalous couplings. In the context of $e^+e^- \to W^+W^-$ this amounts to relating the invariant functions F_i^κ to the anomalous couplings f_i^V. The contributions of the f_i^V to the F_i^κ can be directly read off from (2.40). However, since there are 18 (12) independent invariant functions but only 14 (8) coupling parameters assuming (no) CP violation[e], one cannot express the invariant functions in terms of the anomalous couplings without introducing four additional anomalous coupling parameters related to the t channel. The outcome will depend on the definition of the t-channel parameters. But even worse, as the box diagrams contribute to all invariant functions it is likely that in any definition one ends up with t-channel contributions to the anomalous triple gauge-boson couplings, which by definition should only depend on s. Therefore one should not consider the SM radiative corrections to the process $e^+e^- \to W^+W^-$ as contributions to the anomalous triple gauge-boson couplings, but rather view the anomalous couplings as well as the radiative corrections as contributions to the invariant functions $F_i^\kappa(s,t)$. These invariant functions comprise an effective parametrization for the process $e^+e^- \to W^+W^-$ itself, rather than just for the WWV vertex.

The fact that the parametrization in terms of the $F_i^\kappa(s,t)$ allows to combine radiative corrections and anomalous couplings is very important. Leaving the anomalous contributions aside one can of course check the SM. However, in case of deviations from the SM it is very useful to compare these with an effective theory in order to identify the physics behind these deviations. In the absence of departures from the SM the same approach can be adopted to put limits on new physics. To this end one has to introduce the anomalous couplings. Determining on the other hand the anomalous couplings by using only the lowest-order SM prediction does not give the correct deviation from the SM, as the radiative corrections have been neglected. Therefore, for a complete analysis of the data one needs predictions, i.e. Monte-Carlo routines, that include simultaneously the radiative corrections and the anomalous couplings. One might ask how one can combine these two in a sensible way as the anomalous operators give rise to a non-renormalizable theory. At least for small contributions of the anomalous operators, which are expected at energies that are small with respect to the new-physics scale, there is a simple recipe. One just takes the $\mathcal{O}(\alpha)$-corrected SM cross-section and adds the anomalous contributions that are

[e] This is reflected by the fact that in (2.40) $\mathcal{M}_6^\kappa$ does not occur and $\mathcal{M}_1^\kappa$ and $\mathcal{M}_4^\kappa$ appear only in one linear combination.

linear in the couplings. This corresponds to a simultaneous expansion in α and in the anomalous couplings. All terms that contain the squares of anomalous couplings or the product of anomalous couplings with $\mathcal{O}(\alpha)$ corrections are considered to be negligible.

Just as the SM s-channel contributions, almost all anomalous-coupling contributions to the matrix elements for $e^+e^- \to W^+W^-$ are suppressed by a factor β close to threshold. The only exception is the CP-violating coupling f_6^V which, being CP-breaking, is rather low in the hierarchy mentioned above. The leading contributions of $f_{5,7}^V$ are even suppressed by β^2 and the one of f_2^V by β^3. Moreover the leading contributions of $f_{1,2,7}^V$ are asymmetric in $\cos\theta$ and thus even suppressed by an additional factor β in symmetric quantities such as the total cross-section. If one cannot separate the helicities $+1$ and -1 of the W bosons, this applies also to the leading contributions of $f_{3,4}^V$ and the contribution of f_7^V vanishes altogether. Without identification of the charges of the W bosons only forward–backward-symmetric observables are accessible and in addition to the leading contributions of $f_{1,2,7}^V$ also the ones of $f_{3,6}^V$ drop out.

On the other hand the gauge cancellations for longitudinal gauge bosons depend crucially on the values of the SM couplings. Any deviations from these values can lead to sizeable effects at higher energies. Typically the contributions of anomalous couplings are enhanced by a factor s/M_W^2. Note that in a gauge-invariant scenario the factors $1/M_W^2$ associated with λ^V, $\tilde{\lambda}^V$ or f_2^V, f_7^V will effectively be replaced by $1/\Lambda^2$ and will not give rise to a further enhancement. Of course any sensible anomalous couplings have to yield a unitary cross-section, which can be guaranteed by an appropriate high-energy behaviour of the corresponding form factors. Nevertheless the cross-section for $e^+e^- \to W^+W^-$ becomes very sensitive to anomalous couplings at high energies because the SM prediction is far below the unitarity limit.

A rough estimate for the sensitivity to anomalous couplings is given by: $\beta t^2/s^2 \times s/M_W^2$. Here the first factor originates from the suppression of the s-channel diagrams in the threshold region and in the forward direction at high energies, the second factor is due to the enhancement in the absence of unitarity cancellations. Accordingly one should go to high energies and in this regime consider observables that are not dominated by the t-channel pole. This requires the study of angular distributions of the W bosons and their decay products. For LEP200 these angular distributions are even more important as the anomalous couplings are suppressed by β^2 in the total cross-section as well as in any other forward–backward-symmetric observable. At any rate the highest possible energy should be aimed at in order to overcome this suppression.

The contributions of the various anomalous couplings can be disentangled by studying observables that are constructed from products of the various helicity-matrix elements. For instance the T matrix elements get only contributions from $f_{1,6,7}^V$, the L matrix element only from $f_{1,2,3}^V$ and the M matrix elements only from $f_{3,4,5,6}^V$. In the case of T polarization the anomalous couplings contribute only if the helicities of the W bosons are equal. To discriminate between anomalous WWZ and WWγ couplings one needs measurable information on the contributions for left- and right-handed electrons. This requires initial-state transverse polarization.

The CP-odd matrix elements are purely imaginary, except in the presence of absorptive parts, like the ones related to W-rescattering effects. Consequently their effects hardly show up in the on-shell differential distributions, because in the on-shell SM amplitudes

there is no large imaginary part to interfere with. In order to study the CP-violating couplings one needs to consider observables that involve interferences of the CP-violating contributions with relative phases between different helicity amplitudes, i.e. T-odd and CP-odd observables[15,17].

2.3 Radiative corrections

As has been argued above, the SM theoretical predictions for W-pair production should have an uncertainty below 1% in order to obtain reasonable limits on the structure of the gauge-boson self-couplings at LEP200 and the NLC, and to determine the W-boson mass at LEP200 with the envisaged precision of roughly 60 MeV. In this context radiative corrections are indispensable.

Much effort has been made in recent years to obtain such precise theoretical predictions for W-pair production. In the following we review and update the existing results for the virtual and real electroweak corrections in the on-shell case. In addition we discuss approximate formulae for the W-pair production cross-section at LEP200 and NLC energies.

The $\mathcal{O}(\alpha)$ radiative corrections can be naturally divided into three classes, the virtual, soft-photonic, and hard-photonic contributions. Since the process $e^+e^- \to W^+W^-$ involves the charged current in lowest order, the corresponding radiative corrections cannot be separated on the basis of Feynman diagrams into electromagnetic and weak contributions in a gauge-invariant way.

2.3.1 Virtual and soft-photonic $\mathcal{O}(\alpha)$ corrections

The virtual electroweak and soft-photonic $\mathcal{O}(\alpha)$ corrections were calculated by several authors[39–42]. The complete analytical results for arbitrary polarizations of the external particles were published in Ref. 41. For the unpolarized case they numerically agree with those of Ref. 42 to better than 0.1%. While Ref. 39 is in reasonable agreement with Refs. 41 and 42 apart from the backward direction at high energies, the results of Ref. 40 disagree with the others.

The virtual corrections get contributions from the ν_e, γ and Z self-energies, from the γ–Z mixing-energy, from the vertex corrections to the eeγ, eeZ, eν_eW, WWγ and WWZ vertices, and from box diagrams. The necessary counterterms involve in addition the e and W self-energies. Altogether one has to calculate about 200 individual diagrams. By using Dirac algebra, Lorentz covariance, the mass-shell conditions for the external particles, and momentum conservation, these one-loop diagrams can be reduced to the basic matrix elements defined in (2.9). We thus arrive at an expression for the virtual $\mathcal{O}(\alpha)$ corrections of the form

$$\delta\mathcal{M}_1^{\mathrm{V}}(\kappa,\lambda_+,\lambda_-,s,t) = \sum_{i=1}^{7} \mathcal{M}_i^{\kappa}\,\delta F_i^{\kappa}. \tag{2.42}$$

Here the basic matrix elements $\mathcal{M}_i^{\kappa}$ contain the full Dirac and Lorentz structure of the one-loop diagrams and the invariant functions δF_i^{κ} comprise linear combinations of the one-loop integrals. Analytical results for the invariant functions are listed in Ref. 41.

The virtual corrections contain IR divergences, which result from virtual photons exchanged between external charged particles. In order to compensate these divergences one has to add the cross-section for the process $e^+e^- \to W^+W^-\gamma$. If the energy of the emitted photon is small compared with the detector resolution, this process cannot be distinguished experimentally from the non-radiative W-pair production process.

In order to obtain IR-finite results it is sufficient to add the cross-section for $e^+e^- \to W^+W^-\gamma$ in the soft-photon approximation, i.e. in the limit where the energy k_0 of the emitted photon is small compared with the beam energy: $k_0 < \Delta E \ll E$. Here $\Delta E \equiv \varepsilon E$ is the soft-photon cut-off energy. In the soft-photon approximation the real-photonic corrections yield a simple correction factor $\delta_{\rm soft}$ to the lowest-order cross-section.

When adding the soft-photon cross-section to the contribution of the virtual corrections, not only the IR singularities but also the large Sudakov double logarithms $\log^2(m_e^2/s)$ drop out. The cross-section including virtual and soft-photonic $\mathcal{O}(\alpha)$ corrections reads

$$\left(\frac{d\sigma}{d\Omega}\right)_{V+S} = \frac{\beta}{64\pi^2 s} \sum_{\kappa,\lambda_+,\lambda_-} \frac{1}{4}(1-2\kappa P^+)(1+2\kappa P^-)\left[|\mathcal{M}_{\rm Born}|^2(1+\delta_{\rm soft}) + 2{\rm Re}\left(\mathcal{M}^*_{\rm Born}\delta\mathcal{M}_1^V\right)\right]. \tag{2.43}$$

There are various sources of potentially large virtual and soft-photonic $\mathcal{O}(\alpha)$ corrections at LEP200 and NLC energies. Besides the obviously large $\log(\varepsilon)$ terms, which will be cancelled when hard-photon radiation is taken into account, there are large QED corrections of the form $(\alpha/\pi)\log(Q^2/m_e^2)$ with $Q^2 \gg m_e^2$, originating from collinear photon radiation from the electron or positron. They amount to 6–7% for $Q^2 = (200\,{\rm GeV})^2 - (1\,{\rm TeV})^2$, not taking into account possible enhancements from the corresponding coefficients. These large collinear corrections also show up in the radiation of hard photons and will be discussed in detail in Sec. 5. For the virtual and soft-photonic $\mathcal{O}(\alpha)$ corrections these large logarithmic QED corrections take on the form of a correction factor

$$\delta^{\rm LL}_{V+S} = \frac{\alpha}{\pi}\left\{\frac{3}{2}\log\left(\frac{s}{m_e^2}\right) + 2\log(\varepsilon)\left[\log\left(\frac{s}{m_e^2}\right) + \frac{s-2M_W^2}{s\beta}\log\left(\frac{1+\beta}{1-\beta}\right) + 2\log\left(\frac{M_W^2-t}{M_W^2-u}\right) - 2\right]\right\} \tag{2.44}$$

to the lowest-order cross-section.

From the renormalization two sets of potentially large fermionic corrections arise. The first set is associated with the charge renormalization at zero momentum transfer, where the relevant scale is set by the fermion masses entering the vacuum polarization. In high-energy experiments, however, the running charge should be evaluated at scales much larger than the masses of the light fermions $f_\ell = \{e, \mu, \tau, u, d, c, s, b\}$. This leads to large logarithmic ('mass singular') contributions of the form $(\alpha/\pi)\log(Q^2/m_{f_\ell}^2)$ with $Q^2 \gg m_{f_\ell}^2$, which can amount to a shift in α of 8–9% for $Q^2 = (200\,{\rm GeV})^2 - (1\,{\rm TeV})^2$. If the top quark is heavy, corrections $\propto m_t^2/M_W^2$ will occur. They show up as universal corrections via the renormalization of the W and Z masses (or equivalently s_W^2) if the corresponding renormalization scales are small compared with the mass splitting in the (t, b) isospin doublet, or as process-dependent corrections either via the Yukawa couplings of the physical and unphysical Higgs bosons or at high energies as a remnant after unitarity

cancellations (see Sec. 2.4.2). For W-pair production only the first and last mechanisms are relevant.

At LEP200 energies the long-range electromagnetic interaction between the slowly moving W bosons leads to the so-called Coulomb singularity[43]. This singularity yields an $\mathcal{O}(\alpha)$ correction factor $\alpha\pi/(2\beta)$, resulting in an $\mathcal{O}(\alpha)$-corrected cross-section that does not vanish at threshold for left-handed electrons. The right-handed cross-section remains suppressed by at least β^2. This correction factor exhibits the fact that the free particle approximation is inadequate near the W-pair production threshold in the presence of the long-range Coulomb interaction. We want to stress here that the Coulomb singularity is changed substantially by effects that effectively truncate the range of the interaction, like the off-shellness and the decay of the W bosons. This will be treated in Sec. 3.2.1 and will lead to the conclusion that higher-order Coulombic corrections are not important.

At high energies there are two mechanisms for large corrections. First of all the unitarity cancellations are not yet complete when the energy is of the order of the masses of heavy particles, like the top quark and the Higgs boson, appearing in loop corrections[44]. This just means that terms $\propto M^2/s$, which for light particles cancel the growth with energy of the polarization vectors for longitudinal W bosons, are of $\mathcal{O}(1)$ and spoil the cancellations. This leads to large corrections $\propto s/M_{\mathrm{W}}^2$ known as delayed unitarity effects. The second mechanism is an analogon of the above-mentioned collinear QED logarithms. At very high energies the masses of the heavy SM particles $\{\mathrm{W},\mathrm{Z},\mathrm{H},\mathrm{t}\}$ become small compared with the energy. This leads to large logarithmic corrections[45] of the form $(\alpha/\pi)\log^i(s/M^2)$ with i=1,2, where M stands for the mass of an arbitrary heavy SM particle. At $\sqrt{s} = 1\,\mathrm{TeV}$ a correction of the form $(\alpha/\pi)\log^2(s/M_{\mathrm{W}}^2)$ amounts to roughly 6%, not taking into account possible enhancements resulting from prefactors (see Sec. 2.4.2).

We now present some numerical results for the radiative corrections in the soft-photon approximation. The soft-photon cut-off is chosen to be $\varepsilon = 0.1$. Different choices of ε shift the absolute value of the corrections in a roughly uniform way, but do not influence the general features very much. It should be noted that whenever this choice of the soft-photon cut-off leads to a maximum photon energy that exceeds the amount of available energy, it is automatically reset to $\varepsilon = 2 - 4M_{\mathrm{W}}/\sqrt{s}$. Fig. 5 shows the relative correction factor $\delta_{\mathrm{V+S}}$, defined through

$$\left(\frac{\mathrm{d}\sigma}{\mathrm{d}\Omega}\right)_{\mathrm{V+S}} = \left(\frac{\mathrm{d}\sigma}{\mathrm{d}\Omega}\right)_{\mathrm{Born}} (1 + \delta_{\mathrm{V+S}}), \tag{2.45}$$

for the unpolarized case. While the variation with the scattering angle is relatively flat for LEP200 energies it becomes stronger with increasing energy. In the forward direction, where the Born cross-section is dominated by the t-channel pole, the energy dependence is very weak. This is due to the fact that there only the diagrams that involve a t-channel pole contribute, i.e. the t-channel self-energy, vertex, and bremsstrahlung diagrams, and that the corresponding residues of the t-channel pole in the correction factors do not depend on the energy, being related to the limit that the neutrino becomes quasi-real. Moreover, in that limit the resulting correction factor becomes W-polarization independent. For increasing scattering angle the percentage correction changes rapidly with energy and reaches large negative values up to -50% at 1 TeV in the backward direction. This is the combined result of large weak logarithmic corrections proportional to $\log^2(s/M_{\mathrm{W}}^2)$,

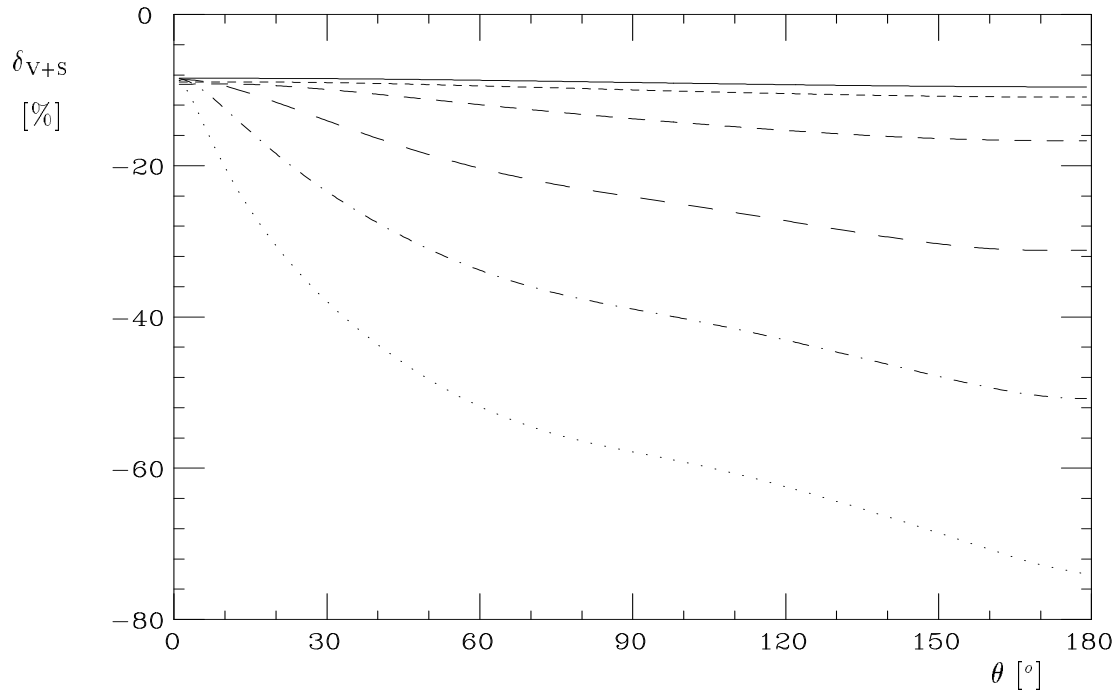

Fig. 5: Virtual and soft-photonic $\mathcal{O}(\alpha)$ correction factor $\delta_{\mathrm{V+S}}$ for the unpolarized differential cross-section $\mathrm{d}\sigma/(\mathrm{d}\cos\theta)$. The upper (solid) curve corresponds to $\sqrt{s} = 176\,\mathrm{GeV}$ followed by $\sqrt{s} = 190$, 250, 500, 1000 and 2000 GeV in consecutive vertical order.

$\log(s/M_{\mathrm{W}}^2)\log(-t/s)$, $\log(s/M_{\mathrm{W}}^2)\log(-u/s)$, etc. (see Sec. 2.4.2). However, the absolute cross-section is small for large scattering angles (see Fig. 4). Consequently, the relative corrections to the integrated cross-section stay below 20% up to 1 TeV. Note that the one-loop corrections are large in the very region where the sensitivity to new physics is highest.

The behaviour of the corrections for purely transverse W bosons is similar to the unpolarized case. In contrast to this the corrections for purely longitudinal bosons (Fig. 6) exhibit a strong angular dependence arising from the minima in the lowest-order cross-section (Figs. 3 and 4). The features of the corrections in the forward and backward directions are, however, roughly the same as for purely transverse W bosons.

The sensitivity of the total unpolarized cross-section to the unknown masses of the Higgs boson and top quark is illustrated in Tab. 2. A change of m_{t} from 120 to 210 GeV affects the cross-section by less than 2% apart from the region very close to threshold. The large effect close to threshold is due to the variation of M_{W}, and thus the variation of the threshold itself, with m_{t}. A variation of M_{H} between 60 and 1000 GeV influences the total cross-section by less than 0.5%, again with the exception of the threshold region. Note that this is valid for constant α, G_μ and M_{Z}. Fixing M_{W} instead of G_μ, the dependence on m_{t} is much weaker. This allows to determine M_{W} from the cross-section practically independently on m_{t} and M_{H} as pointed out by Jegerlehner[46]. These results for the top- and Higgs-mass dependence will remain more or less the same if we include hard-photonic corrections.

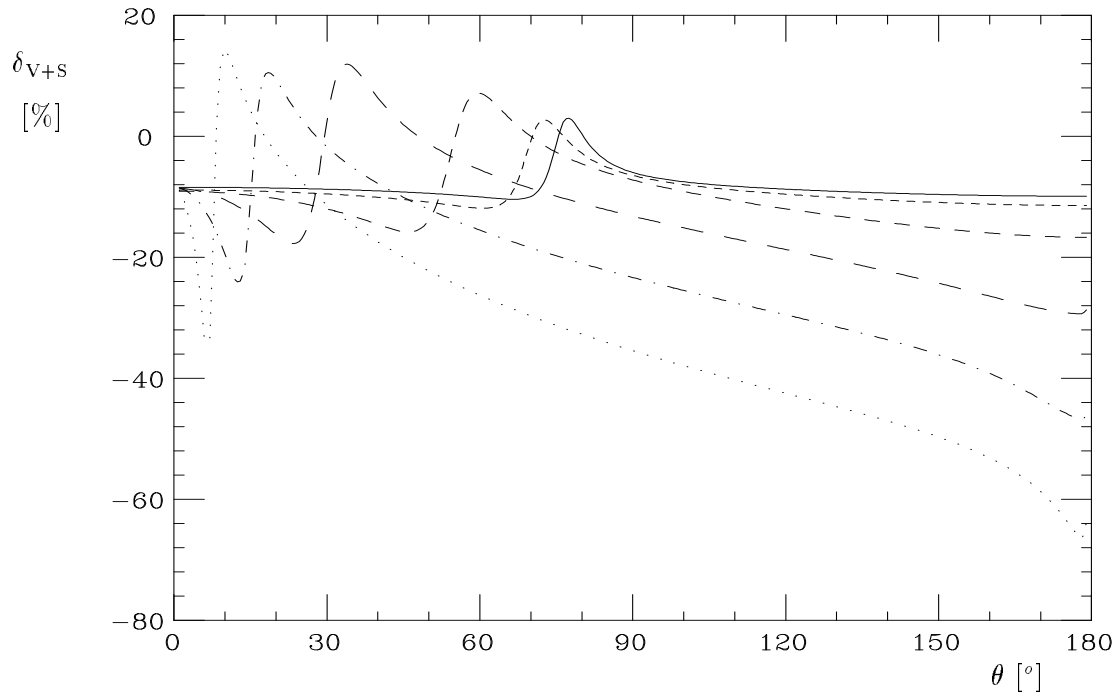

Fig. 6: The same signature as adopted in Fig. 5, but now for purely longitudinal W bosons.

$M_{\rm H}$ [GeV] =	250	250	250	60	250	1000
$m_{\rm t}$ [GeV] =	120	165	210	165	165	165
$M_{\rm W}$ [GeV] =	80.034	80.299	80.620	80.383	80.299	80.192
$\sqrt{s}$ [GeV]	σ [pb]					
165.0	9.810	9.261	8.475	9.149	9.261	9.477
176.0	14.924	14.851	14.674	14.876	14.851	14.866
190.0	16.139	16.168	16.110	16.187	16.168	16.145
250.0	13.429	13.498	13.499	13.490	13.498	13.473
500.0	5.732	5.758	5.758	5.761	5.758	5.750
1000.0	2.079	2.086	2.081	2.087	2.086	2.083

Tab. 2: Integrated unpolarized cross-section including virtual and soft-photonic $\mathcal{O}(\alpha)$ corrections for different top-quark and Higgs-boson masses at various centre-of-mass energies.

More details concerning the structure of the virtual and soft-photonic $\mathcal{O}(\alpha)$ corrections and the corresponding numerical results will be given in Sec. 2.4 as part of the discussion of approximations in the LEP200 and NLC energy ranges.

2.3.2 $\mathcal{O}(\alpha)$ hard-photon bremsstrahlung

In practical experiments the soft-photon approximation is in general not sufficient and one has to include the radiation of hard photons, too. The amplitudes for the process $e^+e^- \to W^+W^-\gamma$ were calculated in Refs. 47–51 using three different methods. The first one, described in detail in Refs. 47 and 49, uses the Weyl representation for Dirac matrices and spinors, and results in expressions for the amplitudes in terms of the components of momentum and polarization vectors in the centre-of-mass frame of the incoming leptons. In Ref. 51 a variation of this spinor-product technique has been used. The second method used in Ref. 48 is based on the Weyl–van der Waerden formalism, yielding concise and manifestly Lorentz-invariant analytical formulae for the amplitude. The relative numerical difference between the results of Refs. 48 and 49 was found to be less than 10^{-6} for the amplitude squared. In Ref. 50, finally, the amplitudes were calculated numerically, using a definite representation for the Dirac matrices and spinors.

From the amplitudes $\mathcal{M}_{1\gamma}$ the total unpolarized cross-section is obtained as

$$\begin{aligned}\sigma_{\mathrm{H}}(s) &= \frac{1}{(2\pi)^5}\frac{1}{2s}\int \frac{\mathrm{d}^3k_+}{2k_{+0}}\frac{\mathrm{d}^3k_-}{2k_{-0}}\frac{\mathrm{d}^3k}{2k_0}\sum_{\mathrm{pol}}|\mathcal{M}_{1\gamma}|^2\delta^{(4)}(p_+ + p_- - k_+ - k_- - k) \\ &= \frac{1}{2s}\frac{1}{8(2\pi)^4}\int \mathrm{d}\cos\theta_+\,\mathrm{d}\cos\theta_\gamma\,\mathrm{d}\phi_\gamma\,\mathrm{d}k_0 \left|\frac{k_0|\vec{k}_+|^2}{|\vec{k}_+|(\sqrt{s}-k_0)+k_0k_{+0}c_{+\gamma}}\right| \sum_{\mathrm{pol}}|\mathcal{M}_{1\gamma}|^2\,,\end{aligned} \tag{2.46}$$

where θ_+, θ_γ are the polar angles of the W^+ boson and the photon with respect to the incoming positron, ϕ_γ is the azimuthal angle of the photon, and

$$c_{+\gamma} = \sin\theta_+\sin\theta_\gamma\cos\phi_\gamma + \cos\theta_+\cos\theta_\gamma. \tag{2.47}$$

For convenience we have introduced here the shorthand notation

$$\sum_{\mathrm{pol}} = \sum_{\kappa,\lambda_+,\lambda_-,\lambda}\frac{1}{4}(1-2\kappa P^+)(1+2\kappa P^-). \tag{2.48}$$

In the second line of (2.46) we have made use of the rotational invariance of $\mathcal{M}_{1\gamma}$ and have put the azimuthal angle of the W^+ boson equal to zero. The integrand of (2.46) should be interpreted as being summed over the physical (i.e. real and non-negative) solutions for $|\vec{k}_+|$. The nontrivial phase-space integrations are performed using Monte-Carlo routines. Thus experimental cuts can be easily implemented. The calculations of Refs. 48 and 49 have been combined with the virtual corrections and agree with each other within 1%. The difference can be attributed to the numerical uncertainties of the Monte-Carlo integration over the photon phase space.

Equation (2.46) contains the soft-photon poles. These are eliminated by a cut $k_0 > \Delta E$ on the photon energy. After combining soft- and hard-photonic corrections the cut dependence drops out.

As indicated in the last subsection, the dominant hard-photon corrections originate from the collinear regime and are of the form $(\alpha/\pi)\log(Q^2/m_{\rm e}^2)$ with $Q^2 \gg m_{\rm e}^2$. In the limit of collinear hard-photon radiation in the direction of the incoming e^+, for instance, $|\mathcal{M}_{1\gamma}|^2$ can be approximated by

$$\begin{aligned}|\mathcal{M}_{1\gamma}(p_+,\kappa_+,p_-,\kappa_-,k_+,\lambda_+,k_-,\lambda_-,k,\lambda)|^2_{\rm coll}& \\ = e^2 f_{\rm coll}^{(\kappa_-)}(p_+,\kappa_+,k,\lambda)\,|\mathcal{M}_{\rm Born}(x_+p_+,-\kappa_-,p_-,\kappa_-,k_+,\lambda_+,k_-,\lambda_-)|^2,& \quad (2.49)\end{aligned}$$

with $x_+ = 1 - 2k_0/\sqrt{s}$ in the initial-state CM system. Here the collinear factors $f_{\rm coll}$, which are of $\mathcal{O}(m_{\rm e}^{-2})$ in the collinear limit, are given by:

$$\begin{aligned}f_{\rm coll}^{(\kappa_-)}(p_+,\kappa_+,k,\lambda) = \delta^{\kappa_-}_{-\kappa_+}[\delta^{\lambda}_{2\kappa_+} + x_+^2\delta^{\lambda}_{-2\kappa_+}]\left\{\frac{1}{x_+(1-x_+)}\,\frac{1}{(p_+\cdot k)} - \frac{1}{2x_+}\,\frac{m_{\rm e}^2}{(p_+\cdot k)^2}\right\}& \\ + \delta^{\kappa_-}_{\kappa_+}\delta^{\lambda}_{2\kappa_+}\,\frac{(1-x_+)^2}{2x_+}\,\frac{m_{\rm e}^2}{(p_+\cdot k)^2},& \quad (2.50)\end{aligned}$$

where δ^i_j is the standard Kronecker delta. Collinear hard-photon radiation in the direction of the incoming e^- yields the same collinear factor with the role of e^+ and e^- interchanged. Note that summation over the helicities κ_+ and λ in (2.49) eliminates the helicity dependence of the collinear factors and leads to the well known helicity-independent result

$$\sum_{\kappa_+,\lambda} f_{\rm coll}^{(\kappa_-)}(p_+,\kappa_+,k,\lambda) = \frac{1+x_+^2}{x_+(1-x_+)}\,\frac{1}{(p_+\cdot k)} - \frac{m_{\rm e}^2}{(p_+\cdot k)^2}. \quad (2.51)$$

This is however not the case when keeping the positron helicity fixed and summing over κ_- and λ, because the collinear factor for flipped positron helicity multiplies in that case a different helicity amplitude than the one without spin-flip.

After integration over the photon angles the terms $\propto 1/(p_+\cdot k)$ yield contributions of the large-logarithmic type and the terms $\propto m_{\rm e}^2/(p_+\cdot k)^2$ give rise to additional $\mathcal{O}(1)$ contributions:

$$\begin{aligned}\int \mathrm{d}\Omega_k e^2 f_{\rm coll}^{(\kappa_-)}(p_+,\kappa_+,k,\lambda) = \frac{64\pi^3}{s x_+(1-x_+)}\left\{\delta^{\kappa_-}_{-\kappa_+}[\delta^{\lambda}_{2\kappa_+} + x_+^2\delta^{\lambda}_{-2\kappa_+}]\,\frac{\alpha}{2\pi}\,\frac{\log(s/m_{\rm e}^2)-1}{1-x_+}\right.& \\ \left. + \delta^{\kappa_-}_{\kappa_+}\delta^{\lambda}_{2\kappa_+}\,\frac{\alpha}{2\pi}\,(1-x_+)\right\}.& \quad (2.52)\end{aligned}$$

More details about the large logarithms and their evaluation beyond $\mathcal{O}(\alpha)$ are given in the following subsection and in Sec. 5.

In Fig. 7 and Tab. 3 we display the influence of the full $\mathcal{O}(\alpha)$ corrections on the total unpolarized cross-section near the W-pair production threshold. In the calculation of the hard-photon corrections the soft-photon cut-off has been set to $\varepsilon = 0.5\times10^{-3}$, unless reset by the lack of available energy to $\varepsilon = (2-4M_{\rm W}/\sqrt{s})/200$ for $2-4M_{\rm W}/\sqrt{s} < 0.1$. In order to have a cleaner look at the QED corrections we present in addition to the Born cross-section also the lowest-order cross-section in the so-called G_μ representation, i.e. the Born cross-section with α replaced by $\sqrt{2}G_\mu M_{\rm W}^2 s_{\rm W}^2/\pi$, which already contains an important part of the leading low-energy weak normalization effects. We will refer to

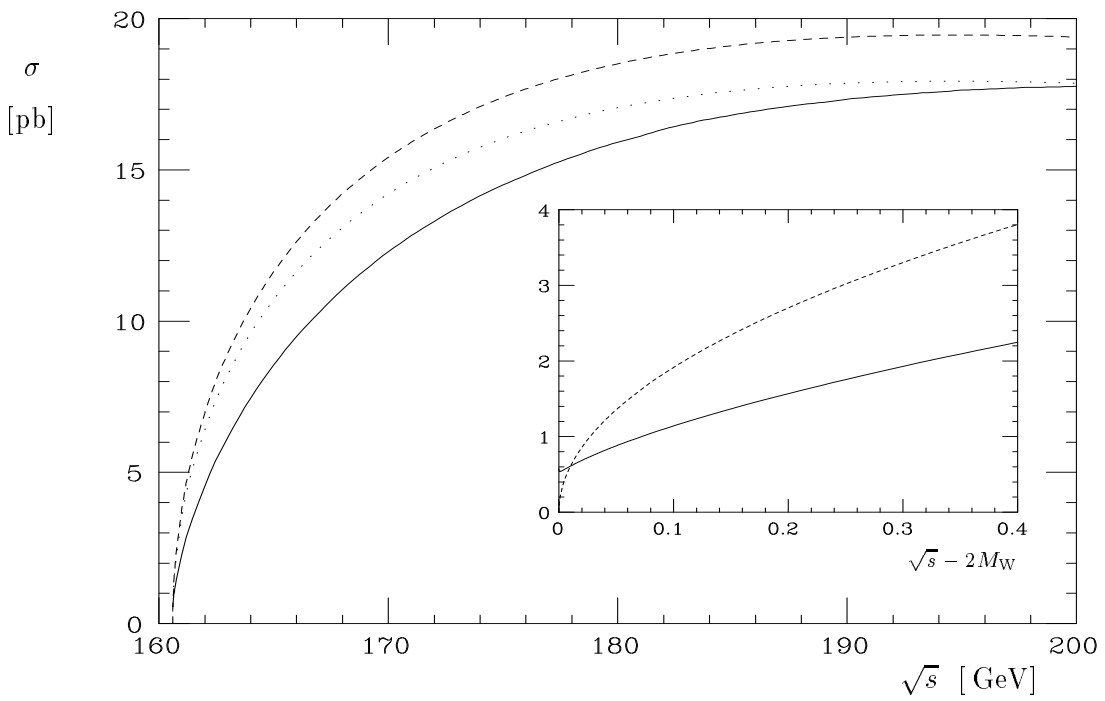

Fig. 7: Unpolarized total cross-section in the threshold region. The dotted curve corresponds to Born, the dashed one to G_μ-Born, and the solid one to the results including full $\mathcal{O}(\alpha)$ corrections.

$\sqrt{s}$ [GeV]	Born	G_μ-Born	Born + $\mathcal{O}(\alpha)$ V+S	Born + full $\mathcal{O}(\alpha)$
165.0	10.712	11.626	9.261	8.539 ± 0.003
176.0	16.285	17.673	14.851	14.839 ± 0.005
190.0	17.863	19.386	16.168	17.334 ± 0.006
250.0	15.154	16.446	13.498	15.939 ± 0.006
500.0	6.599	7.162	5.758	7.381 ± 0.005
1000.0	2.465	2.675	2.086	2.832 ± 0.003

Tab. 3: Unpolarized total cross-section in various approximations given in pb.

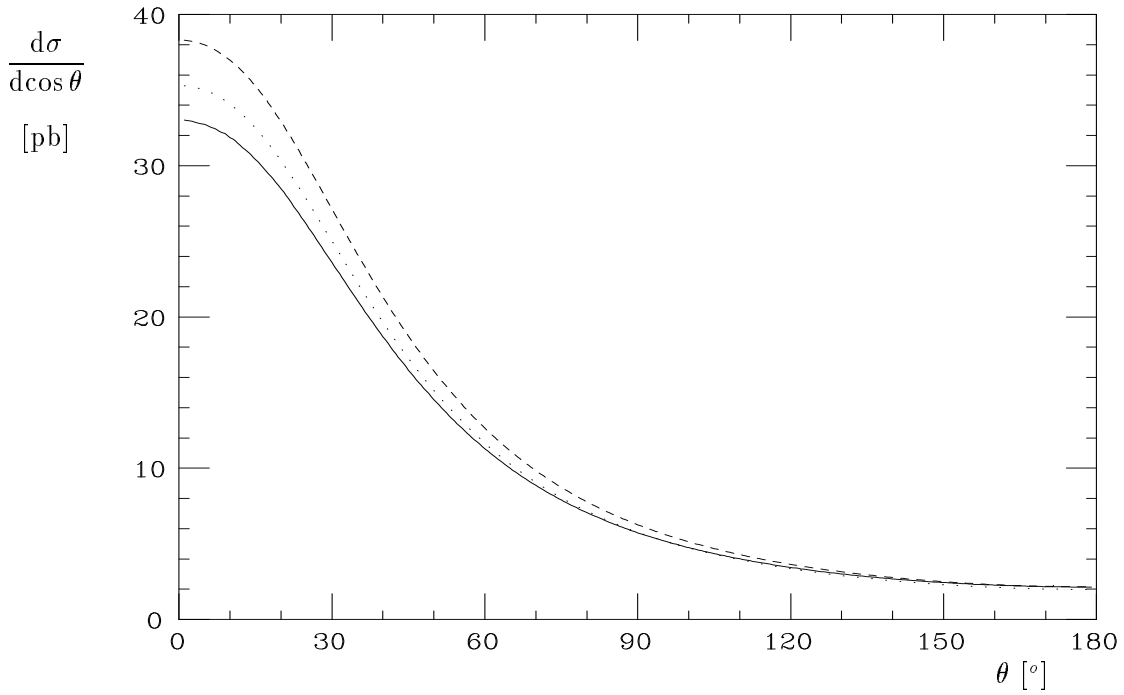

Fig. 8: Unpolarized differential cross-section $d\sigma/(d\cos\theta_+)$ at $\sqrt{s} = 190\,\mathrm{GeV}$. The same signature as adopted in Fig. 7.

this cross-section as G_μ-Born. As a result of the steep drop with decreasing centre-of-mass energy of the W-pair cross-section close to threshold, large and predominantly soft QED effects can be observed. Compared with G_μ-Born the $\mathcal{O}(\alpha)$ corrections amount to more than -25% in the direct vicinity of the threshold ($\sqrt{s} < 165\,\mathrm{GeV}$), apart from the region very close to threshold where the positive Coulomb-singularity contribution takes over (see close-up in Fig. 7), and still -11% at $\sqrt{s} = 190\,\mathrm{GeV}$. The size of these effects necessitates the inclusion of higher-order QED corrections in order to end up with an acceptable theoretical uncertainty. A discussion of these higher-order QED corrections can be found in the next subsection. It should be noted that the use of the soft-photon approximation close to threshold is restricted by the requirement that the cross-section should be almost insensitive to the energy shift ΔE. This means that we have to take $\varepsilon \ll \beta^2$.

In Fig. 8 the effect of the $\mathcal{O}(\alpha)$ corrections on the unpolarized differential cross-section $d\sigma/(d\cos\theta_+)$ is shown for $\sqrt{s} = 190\,\mathrm{GeV}$. Apart from the expected normalization effects that are already observed in the total cross-section, also a distortion of the distribution occurs. As this is exactly the type of signature one might expect from anomalous gauge-boson couplings, this underlines again the importance of having a profound knowledge of the SM radiative corrections. The origin of the distortion can be traced back to hard initial-state photonic corrections. Hard-photon emissions boost the CM system of the W bosons, causing a migration of events to take place from regions with large cross-section in the CM system (e.g. forward direction) to regions with small cross-section in the laboratory (LAB) system (e.g. backward direction).

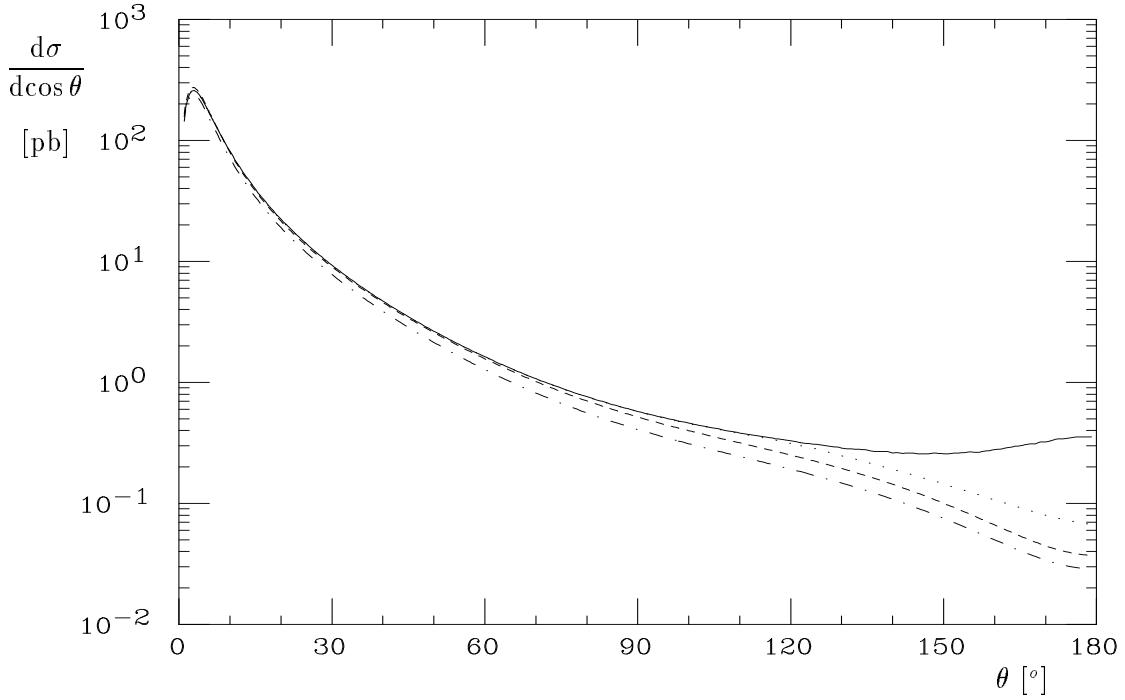

Fig. 9: Unpolarized differential cross-section $d\sigma/(d\cos\theta_+)$ at $\sqrt{s} = 500\,\text{GeV}$. The dashed curve corresponds to G_μ-Born and the solid, dotted, and dash-dotted ones to the results including full $\mathcal{O}(\alpha)$ corrections without cuts, with $\angle(\text{W}^+,\text{W}^-) > 70°$, or with $k_{+0} + k_{-0} > 0.9\sqrt{s}$, respectively.

As in the threshold region the distributions are rather flat for fixed CM energy and the cross-sections for different W polarizations are roughly comparable, the observed migration effects are moderate. At high energies, however, the distributions are varying strongly and the cross-sections for the individual W polarizations differ substantially, as we have seen in Sec. 2.2. Consequently the migration effects can take on huge proportions[52,53]. This is exemplified in Fig. 9 for the unpolarized differential cross-section $d\sigma/(d\cos\theta_+)$, which gets enhanced tremendously in the backward direction. The effect of migration of transverse W bosons in their CM system to longitudinal ones in the LAB system can be observed in Tab. 4. The extreme size of all these boost phenomena jeopardizes the quest of constructing theoretical SM predictions with the required accuracy. Fortunately they can (and will) be removed by experimental cuts that strongly reduce the hard-photon phase space. This involves selecting events in which not much CM energy has been lost or in which the W bosons are produced almost back-to-back. The impact of such types of cuts is displayed in Fig. 9. There a cut is imposed on the acollinearity of the W bosons, in order to reduce the migration from the forward to the backward hemisphere in the $\cos\theta_+$ distribution[54], or on the energy of the W bosons. The remaining $\mathcal{O}(\alpha)$ corrections indeed indicate that the large boost effects can be brought back to a manageable level, only necessitating the evaluation of the standard leading higher-order corrections. Another way to eliminate the large boost effects is to reconstruct the W-boson CM system assuming that a collinear photon has been radiated in the initial state.

	σ_{U}	σ_{+}	σ_{T}	σ_{L}	σ_{M}
Born	6.599	0.050	6.239	0.114	0.247
G_μ-Born	7.162	0.054	6.771	0.123	0.268
Born + $\mathcal{O}(\alpha)$ V+S	5.758	0.051	5.443	0.098	0.216
Born + $\mathcal{O}(\alpha)$ full	7.381	0.083	6.781	0.142	0.451
$k_{+0} + k_{-0} > 0.9\sqrt{s}$	6.224	0.056	5.874	0.109	0.243
$\angle(\mathrm{W}^+, \mathrm{W}^-) > 70°$	7.285	0.079	6.759	0.141	0.385
$\angle(\mathrm{W}^+, \mathrm{W}^-) > 160°$	6.842	0.063	6.437	0.119	0.288

Tab. 4: Total cross-section, given in pb, for different polarizations at $\sqrt{s} = 500\,\mathrm{GeV}$. In the last three lines the $\mathcal{O}(\alpha)$ corrections are restricted by the indicated cuts. The error in the results including full $\mathcal{O}(\alpha)$ corrections is roughly 0.1%.

As can be seen from Tabs. 3 and 4, the QED corrections are moderate where the cross-sections are large. For the unpolarized or transverse cross-section in the forward direction, and the total unpolarized cross-section the full $\mathcal{O}(\alpha)$ corrections with respect to G_μ-Born are less than 6% in the energy range of the NLC.

The strong energy dependence of the $\mathcal{O}(\alpha)$ corrections to the total and differential cross-section close to threshold is primarily due to the Coulomb singularity and soft-photon radiation, because the production threshold acts as natural cut-off of the photon energy spectrum. These effects lead to a divergent correction of the form

$$\left(\frac{\mathrm{d}\sigma}{\mathrm{d}\Omega}\right)_{\mathrm{div}} = \left(\frac{\mathrm{d}\sigma}{\mathrm{d}\Omega}\right)_{\mathrm{Born}} \left\{\frac{\alpha\pi}{2\beta} + \frac{4\alpha}{\pi}\left[\log(s/m_{\mathrm{e}}^2) - 1\right]\log(\beta)\right\}. \tag{2.53}$$

The remaining $\mathcal{O}(\alpha)$ corrections are predominantly the result of virtual contributions, and yield at threshold a W-polarization-independent relative correction factor of about 7.7%. This can be easily understood by realizing that only two of the CP-conserving standard matrix elements, $\mathcal{M}_1$ and $\mathcal{M}_4$, survive at threshold (see appendix A). As these two matrix elements become equal for vanishing β, the matrix element including virtual $\mathcal{O}(\alpha)$ corrections is given by

$$\mathcal{M}(\kappa, \lambda_+, \lambda_-, s, t) \sim \mathcal{M}_1^{\kappa}(\lambda_+, \lambda_-)\,\left[F_1^{\kappa}(s,t) + F_4^{\kappa}(s,t)\right], \qquad \beta \to 0. \tag{2.54}$$

For unpolarized $\mathrm{e}^{\pm}$ the on-threshold relative correction factor is hence determined by $F_1^-(s,t) + F_4^-(s,t)$, which is independent of the W polarization.

2.3.3 Higher-order corrections

In Secs. 2.3.1 and 2.3.2 we have encountered large $\mathcal{O}(\alpha)$ corrections. A short description of the way to include the corresponding higher-order corrections is hence in place.

The higher-order large logarithmic contributions associated with the running of α can be obtained using the renormalization group. Like at LEP1/SLC they are properly taken into account by replacing $\alpha \equiv \alpha(0)$ by

$$\alpha(s) = \frac{\alpha}{1 + \Sigma_\gamma^{\mathrm{f}\neq\mathrm{t}}(s)/s} \tag{2.55}$$

in the $\mathcal{M}_Q$ part of (2.19), where $\Sigma_\gamma^{\mathrm{f}\neq\mathrm{t}}(s)$ is the renormalized $\mathcal{O}(\alpha)$ transverse photon self-energy originating from fermion loops, excluding top-quark loops.

The $\mathcal{O}(\alpha)$ corrections $\propto m_\mathrm{t}^2/M_\mathrm{W}^2$ in W-pair production near threshold are of the same nature as the ones observed at LEP1/SLC. In particular the corrections associated with the top-loop contribution to the non-Abelian triple gauge-boson vertices are not enhanced by factors $m_\mathrm{t}^2/M_\mathrm{W}^2$, but only by logarithms. At high energies, however, additional large top-mass corrections appear in the cross-sections for longitudinal W bosons (see Sec. 2.4.2), either as a remnant of unitarity cancellations [terms $\propto m_\mathrm{t}^2/M_\mathrm{W}^2 \log(m_\mathrm{t}^2/s)$] or from the absence thereof (delayed unitarity terms). Except for these additional large top-mass effects the corresponding higher-order corrections can be implemented following the methods used at LEP1/SLC[55,56]. This involves the QCD corrections to the top-loop contributions to the gauge-boson self-energies, which are of $\mathcal{O}(\alpha\alpha_s m_\mathrm{t}^2/M_\mathrm{W}^2)$, and the terms $\propto \alpha^2 m_\mathrm{t}^4/M_\mathrm{W}^4$. This can be accounted for by replacing $\pi\alpha/(\sqrt{2}s_\mathrm{W}^2)$ by

$$M_\mathrm{W}^2 G_\mu \equiv \frac{\pi\alpha}{\sqrt{2}s_\mathrm{W}^2}\frac{1}{1-\Delta r} = \frac{\pi\alpha}{\sqrt{2}s_\mathrm{W}^2}\frac{1}{(1-\Delta\alpha)(1+\frac{c_\mathrm{W}^2}{s_\mathrm{W}^2}\Delta\bar{\rho}) - \Delta r_\mathrm{rem}} \tag{2.56}$$

in the $\mathcal{M}_I$ part of (2.19), with

$$\begin{aligned}
&\Delta r_\mathrm{rem} = \Delta r^{\text{1-loop}} - \Delta\alpha + \frac{c_\mathrm{W}^2}{s_\mathrm{W}^2}\Delta\rho,\\
&\Delta\rho = \frac{3\alpha m_\mathrm{t}^2}{16\pi s_\mathrm{W}^2 M_\mathrm{W}^2}, \qquad \Delta\bar{\rho} = \frac{3G_\mu m_\mathrm{t}^2}{8\sqrt{2}\pi^2}\left[1 + \frac{G_\mu m_\mathrm{t}^2}{8\sqrt{2}\pi^2}(19-2\pi^2) - \frac{2}{3}\left(1+\frac{\pi^2}{3}\right)\frac{\alpha_s(m_\mathrm{t}^2)}{\pi}\right],\\
&\Delta\alpha = 1 - \frac{\alpha}{\alpha(M_\mathrm{W}^2)},
\end{aligned} \tag{2.57}$$

and $\Delta r^{\text{1-loop}}$ can be found in Ref. 57. Note that in this way also the running of α is included. For a treatment that also takes into account the terms $\propto \log(s)$ in the running of α and s_W^2 without breaking the unitarity cancellations at high energies, we refer to Ref. 58. The higher-order corrections corresponding to the additional large top-mass effects at high energies mentioned above are not yet known.

The complete $\mathcal{O}(\alpha\alpha_s)$ corrections to the gauge-boson self-energies can be found in Ref. 56, whereas the effects resulting from the $\mathrm{t\bar{t}}$ threshold were summarized in Ref. 59 using dispersion integrals. The QCD corrections associated with the gauge-boson vertex corrections have, to our knowledge, not been calculated yet.

As pointed out in the previous subsections, the virtual and real corrections reveal the presence of large logarithmic QED effects of the form $\alpha L/\pi \equiv (\alpha/\pi)\log(Q^2/m_\mathrm{e}^2)$ with $Q^2 \gg m_\mathrm{e}^2$. They arise when photons or light fermions are radiated off in the direction of incoming or outgoing light particles. In the case of W-pair production the only terms

of this sort originate from initial-state photon emission. Radiation of photons from the final-state W bosons can only lead to sizeable corrections if the energy of the W bosons is much larger than their mass (see Sec. 2.4.2). The leading large logarithmic corrections can be calculated by using the so-called structure-function method[60] in leading-log (LL) approximation, i.e. only taking along the terms $\propto (\alpha L/\pi)^n$. This procedure also allows the inclusion of soft-photon effects to all orders by means of exponentiation.

The leading logarithmic QED corrections to the W-pair production (differential) cross-section were calculated in Refs. 61 and 62. The resulting total cross-section is given by

$$\sigma_{\mathrm{LL,exp}}(s,Q^2) = \int_{4M_{\mathrm{W}}^2/s}^1 \mathrm{d}z\, \phi(2\alpha,z,Q^2)\, \hat{\sigma}_0(zs), \tag{2.58}$$

where $\hat{\sigma}_0(zs)$ denotes the (possibly improved) Born cross-section at the reduced CM energy squared zs. The flux function ϕ is defined in (5.9). There also the assumptions are given that go into its derivation. The appropriate choice for the scale Q^2, which is a free parameter, will be discussed below.

In Ref. 48 the integral in (2.58) was performed numerically. Neglecting the $O(\alpha^2)$ leading logarithms and the non-logarithmic terms it has been evaluated analytically in Ref. 63 as part of an $\mathcal{O}(\alpha)$ approximation in the LEP200 energy range (see Sec. 2.4.1). As an example we give the result for photon radiation very close to threshold taking into account the effect of the phase-space reduction factor β:

$$\sigma_{\mathrm{LL,exp}}^{\mathrm{thr}}(s,Q^2) \approx (\beta)^{4\zeta_\alpha}\, \frac{\exp[-2\zeta_\alpha\gamma_E + 3\alpha L/(2\pi)]\,\Gamma(3/2)}{\Gamma(3/2+2\zeta_\alpha)}\, \sigma_{\mathrm{Born}}(s), \tag{2.59}$$

with ζ_α as defined in (5.10). In this regime a proper scale choice is given by $Q^2 = s$, as can be read off from (2.53). For the motivation of scale choices in general we refer to Sec. 5.

In Tab. 5 the effects related to the higher-order leading-log contributions are displayed. The improved-Born entry contains the lowest-order cross-section and the $\mathcal{O}(\alpha)$ corrections associated with $\Delta r^{\text{1-loop}}$ and the Coulomb singularity: $\sigma_{\mathrm{Born}}[1+\alpha\pi(1-\beta^2)^2/(2\beta) + 2\Delta r^{\text{1-loop}}]$. In the next two columns the $\mathcal{O}(\alpha)$ LL corrections are added using $\hat{\sigma}_0 = \sigma_{\mathrm{Born}}$ in the convolution (2.58). The two separate columns correspond to two different scale choices:

$$\begin{aligned} Q^2 &= s, \\ Q^2 &= s\,\frac{1-\beta}{1+\beta}. \end{aligned} \tag{2.60}$$

The first scale choice is motivated by the near threshold behaviour of the total cross-section, see (2.53). The second one is motivated by the fact that the relative virtual and soft correction factor for the differential cross-section at $\theta = 0^\circ$ goes to an energy-independent constant at high energies. As the major part of the total unpolarized cross-section at high energies comes from the forward region, a scale choice that is constant at $\theta = 0^\circ$ is favoured. So, a reasonable scale at high energies might be $Q^2 = s(t - M_{\mathrm{W}}^2)/(u - M_{\mathrm{W}}^2)$, which equals the first scale at threshold and goes to M_{W}^2 at $\theta = 0^\circ$. For convenience we have taken this scale at $\theta = 0^\circ$. If hard-photon effects are removed by experimental cuts, this scale gets further motivation by the fact that the resulting $\log(\varepsilon)$ terms at $\theta = 0^\circ$ approximate the exact ones well [see (2.44)]. As we can see from

$\sqrt{s}$ [GeV]	improved Born	+ $\mathcal{O}(\alpha)$ LL		Born + full $\mathcal{O}(\alpha)$	+ h.o.t. for $Q^2 = s\frac{1-\beta}{1+\beta}$	
		$Q^2 = s$	$Q^2 = s\frac{1-\beta}{1+\beta}$		$\mathcal{O}(\alpha^2)$ LL	full LL
161.0	4.334	2.298	2.310	2.251 ± 0.001	2.869	2.435
165.0	11.979	8.644	8.708	8.539 ± 0.003	9.026	8.761
170.0	15.640	12.404	12.495	12.282 ± 0.004	12.583	12.445
175.0	17.536	14.618	14.720	14.501 ± 0.004	14.681	14.628
180.0	18.578	16.010	16.114	15.909 ± 0.005	16.007	16.016
190.0	19.370	17.434	17.529	17.334 ± 0.006	17.336	17.425
200.0	19.321	17.887	17.969	17.745 ± 0.006	17.701	17.836
250.0	16.305	16.134	16.149	15.939 ± 0.006	15.864	16.056
300.0	13.375	13.614	13.591	13.415 ± 0.007	13.360	13.541
500.0	7.085	7.567	7.500	7.381 ± 0.005	7.368	7.484
1000.0	2.646	2.970	2.910	2.832 ± 0.003	2.835	2.890

Tab. 5: Unpolarized total cross-section, given in pb, including $\mathcal{O}(\alpha)$ corrections and higher-order leading-log corrections (see text).

Tab. 5 the difference between the $\mathcal{O}(\alpha)$ LL results for these two scale choices is small near threshold, but roughly 2% at 1 TeV. Comparing the LL results with the full $\mathcal{O}(\alpha)$ results confirms the appropriateness of the chosen scales in the threshold region. Note that we have used an improved Born including some of the dominant non-LL corrections in order to make this comparison meaningful. At high energies there is a preference for the second scale choice, but a substantial difference remains. This is caused by large logarithmic corrections that are residing in the weak sector and that are not associated with photonic corrections (see Sec. 2.4.2). So we can conclude that the difference in the higher-order leading-log corrections related to different (physically motivated) scales is not so important, as these scales are roughly equal in the threshold region, where the $\mathcal{O}(\alpha^2)$ corrections can be large, and because the LL $\mathcal{O}(\alpha^2)$ corrections are relatively small at high energies[f].

The latter is shown in the last two entries of Tab. 5. The $\mathcal{O}(\alpha^2)$ LL entry contains, in addition to the full $\mathcal{O}(\alpha)$ result, the contribution from $\mathcal{O}(\alpha^2)$ LL corrections using $\hat{\sigma}_0 = \sigma_{\rm Born}$ in the convolution (2.58). The full LL entry contains on top of that the exponentiation of soft-photon effects and uses $\hat{\sigma}_0 = \sigma_{\rm Born}[1 + \alpha\pi(1-\beta^2)^2/(2\beta)]/(1-\Delta r)^2$ in the convolution. Compared with the full $\mathcal{O}(\alpha)$ results we observe in the energy range up to 1 TeV large $\mathcal{O}(\alpha^2)$ LL effects near threshold, e.g. 27% at $\sqrt{s} = 161$ GeV, and moderate ones when sufficiently far above threshold, i.e. $< 1\%$ (0.5%) for energies above roughly 175 (180) GeV. Note that finite-W-width effects will smoothen the threshold behaviour

[f] Note that this statement is not valid for observables that are very sensitive to QED (boost) effects. Moreover, for different observables different scale choices might be appropriate.

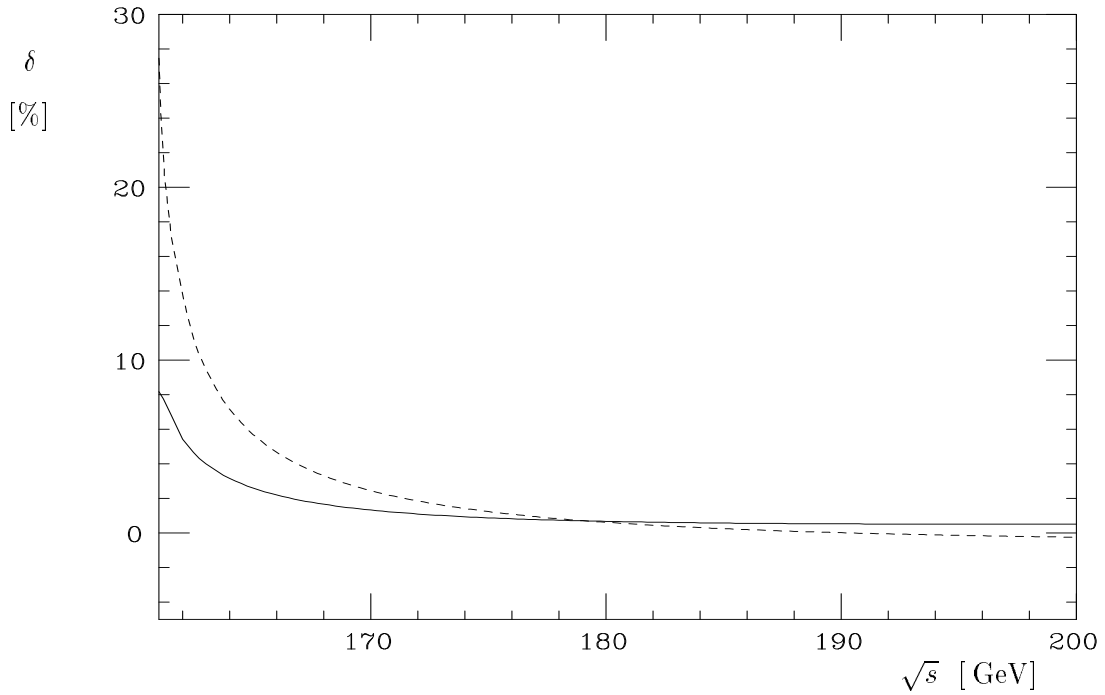

Fig. 10: $\mathcal{O}(\alpha^2)$ leading-log corrections (– – –) and full higher-order leading-log corrections (———) to the total cross-section, given as correction factor δ relative to the full $\mathcal{O}(\alpha)$ results.

and hence reduce the size of the $\mathcal{O}(\alpha^2)$ LL effects, nevertheless they will stay sizeable near threshold. The full higher-order LL corrections turn out to be substantially smaller in the threshold region. A small part of this difference can be attributed to the exponentiation of the soft-photon effects, which are important near threshold, but the bulk is the result of an accidental cancellation between the positive $\mathcal{O}(\alpha^2)$ LL contribution and the negative $\mathcal{O}(\alpha)$ LL corrections to the positive terms that improve the lowest-order cross-section in $\hat{\sigma}_0$. Finite W-width effects will change the lowest-order cross-section and the Coulomb singularity in different ways (see Sec. 3), hence the extent of the cancellation is also expected to differ in that case. At high energies the full higher-order LL corrections become noticeable again, i.e. $> 1\%$ for energies above roughly 300 GeV. The discrepancy between the $\mathcal{O}(\alpha^2)$ LL and full higher-order LL corrections at high energies are the result of equal-sign higher-order terms entering via Δr.

Finally the higher-order corrections to the total cross-section are plotted in Fig. 10 in the LEP200 energy range. Shown are the $\mathcal{O}(\alpha^2)$ LL and full higher-order LL corrections, defined in the same way as described for Tab. 5, relative to the full $\mathcal{O}(\alpha)$ corrected results.

2.4 Approximations for On-Shell W-Pair Production

The complete analytic results for the electroweak corrections are very lengthy and complicated, resulting in huge and rather slow computer programs. Moreover the formu-

lae are completely untransparent. In view of this, simple approximative expressions are desirable. Apart from providing fast computer programs, which are useful for many applications, simple transparent formulae should reveal the physical content and the origin of the dominant radiative corrections.

The construction of simple and sufficiently good approximations is, however, highly non-trivial. The approximation should be valid from threshold to very high energies. Consequently there is no distinguished energy scale as for the Z physics at LEP1, but several different scales are simultaneously present. In additon all one-loop diagrams including the boxes are a priori of the same order of magnitude. There are many sizeable effects originating from different sources and their extraction is obscured by the presence of unitarity cancellations. Apart from the region very close to threshold and in the high-energiy limit there are no obvious expansion parameters.

Consequently so far no reasonably simple approximation has been constructed that reproduces the full $\mathcal{O}(\alpha)$ results sufficiently well for all energies. There exists an improved Born approximation for LEP200 energies[63] and a high-energy approximation with improvements for intermediate energies[45]. These will be described in the following.

2.4.1 Improved Born approximation

Whereas the lowest-order matrix element involves only three, at $\mathcal{O}(\alpha)$ twelve independent tensor structures occur, each of which is associated with an independent invariant function, which can be considered as an s- and t-dependent effective coupling. The dominant radiative corrections, as e.g. those that are related to UV, IR or mass singularities, in general have factorization properties and are at $\mathcal{O}(\alpha)$ restricted to those invariant functions that appear already at lowest order. Therefore the contributions of the other invariant functions should be relatively small. Indeed a numerical analysis reveals that in a suitably chosen representation for the tensor structures[g] only the three Born-like invariant functions and F_I^+ are relevant for a sufficiently good approximation[63,64], resulting in the following approximation for the matrix element:

$$\mathcal{M}^\kappa_{\rm app} = \mathcal{M}^\kappa_I F^\kappa_I + \mathcal{M}^\kappa_Q F^\kappa_Q, \tag{2.61}$$

with $\mathcal{M}_I$ and $\mathcal{M}_Q$ defined in (2.20). The term involving F_I^+ is only needed for the differential cross-section in the threshold region because of contributions $\propto \beta^2 \cos\theta$, originating from the interference of $\mathcal{M}_{\rm Born}$ with $\mathcal{M}_{1,4}$, which are not present at lowest order. These terms are irrelevant for energies above 250 GeV such that for high energies only the three Born-like invariant amplitudes remain. Neglecting the other invariant functions introduces errors below the per-cent level. This is of course only true for observables where $\mathcal{M}^\kappa_{\rm app}$ is not suppressed or absent. All this demonstrates that improved Born approximations are possible.

In order to construct an improved Born approximation one has to specify simple expressions for the invariant functions $F^\kappa_{I,Q}$, which reproduce the corresponding exact ex-

[g] This basis consists of linear combinations of the $\mathcal{M}^\kappa_1, \ldots, \mathcal{M}^\kappa_6$ given in (2.9).

pressions with sufficient accuracy. In the LEP200 energy region the following expressions approximate the full weak corrections reasonably well[63]

$$F_I^\kappa = \left[2\sqrt{2}G_\mu M_{\rm W}^2 + \frac{4\pi\alpha}{2s_{\rm W}^2}\frac{\pi\alpha}{4\beta}(1-\beta^2)^2\right]\delta_{\kappa-} + F_{I,\rm rem}^\kappa,$$
$$F_Q^\kappa = \left[4\pi\alpha(s) + 4\pi\alpha\frac{\pi\alpha}{4\beta}(1-\beta^2)^2\right] + F_{Q,\log}^\kappa + F_{Q,\rm rem}^\kappa. \tag{2.62}$$

The terms containing G_μ and $\alpha(s)$, as defined in Sec. 2.3.3, incorporate all the leading universal corrections associated with the running of α and the corrections $\propto \alpha m_{\rm t}^2/M_{\rm W}^2$. As these are linked to the renormalization of the electric charge at zero momentum transfer and of the weak mixing angle, they only contribute to the structures already present at lowest order. The corresponding leading $\mathcal{O}(\alpha)$ contributions can be recovered from (2.62) by substituting

$$\alpha(s) \to \alpha[1+\Delta\alpha^{\rm LL}(s)], \qquad 2\sqrt{2}G_\mu M_{\rm W}^2 \to \frac{4\pi\alpha}{2s_{\rm W}^2}\left[1+\Delta\alpha^{\rm LL}(M_{\rm W}^2) - \frac{c_{\rm W}^2}{s_{\rm W}^2}\Delta\rho\right], \tag{2.63}$$

with

$$\Delta\alpha^{\rm LL}(s) = \frac{\alpha}{3\pi}\sum_{f\neq {\rm t}} N_{\rm C}^f Q_f^2 \log\left(\frac{s}{m_f^2}\right) \tag{2.64}$$

and $\Delta\rho$ as defined in (2.57).

The $1/\beta$ term describes the effect of the Coulomb singularity, which for $\beta \ll 1$ yields a simple correction factor to the lowest-order cross-section:

$$\delta\sigma_{\rm Coul} = \frac{\pi\alpha}{2\beta}\sigma_{\rm Born}. \tag{2.65}$$

The factor $(1-\beta^2)^2$ is introduced by hand to restrict the $1/\beta$ contribution to the threshold region. Sufficiently far above threshold the Coulomb-singularity contribution can be dropped.

The large logarithms which arise from a heavy top quark or Higgs boson and which are not yet absorbed into G_μ are contained in $F_{Q,\log}^\kappa$:

$$F_{Q,\log}^+ = 4\pi\alpha\frac{\alpha}{24\pi s_{\rm W}^2 c_{\rm W}^2}\frac{s}{M_{\rm Z}^2}\left\{\frac{1}{4}\log\left(\frac{M_{\rm H}^2}{M_{\rm W}^2}\right) - \log\left(\frac{m_{\rm t}^2}{M_{\rm W}^2}\right)\right\},$$
$$F_{Q,\log}^- = 4\pi\alpha\frac{\alpha}{48\pi s_{\rm W}^4 c_{\rm W}^2}\frac{s}{M_{\rm Z}^2}\left\{\frac{1}{4}\log\left(\frac{M_{\rm H}^2}{M_{\rm W}^2}\right) + (3c_{\rm W}^2 - s_{\rm W}^2)\log\left(\frac{m_{\rm t}^2}{M_{\rm W}^2}\right)\right\}. \tag{2.66}$$

The ones that are already absorbed in G_μ are given by

$$F_{I,\log}^- = \frac{4\pi\alpha}{2s_{\rm W}^2}\frac{\alpha}{48\pi s_{\rm W}^4}\left\{11 s_{\rm W}^2\log\left(\frac{M_{\rm H}^2}{M_{\rm W}^2}\right) - 2(3c_{\rm W}^2 - s_{\rm W}^2)\log\left(\frac{m_{\rm t}^2}{M_{\rm W}^2}\right)\right\}. \tag{2.67}$$

Note that these expressions have been derived from the limit $s \ll m_{\rm t}^2, M_{\rm H}^2$. The terms containing the factor $s/M_{\rm Z}^2$ disappear in the unitarity limit $s \gg m_{\rm t}^2, M_{\rm H}^2$. Numerically the contributions of the $\log m_{\rm t}$ and $\log M_{\rm H}$ terms are below 0.02% for unpolarized or

left-handed electrons and below 0.8% for right-handed electrons if $m_t < 200\,\mathrm{GeV}$ and $M_H < 1\,\mathrm{TeV}$.

The remainder $F^{\kappa}_{\{I,Q\},\mathrm{rem}}$ contains the ZZ threshold, which is practically only relevant for right-handed electrons, and some empirical functions given explicitly in Ref. 63. It is necessary to reproduce the angular dependence of the differential cross-section but can be dropped for the total cross-section.

In addition to the contributions described so far, one has to include the LL-QED corrections, which in particular take into account the leading hard-photonic corrections. These can be calculated using the structure-function method as described in Sec. 5. They comprise all contributions $\propto (\alpha/\pi)\log(m_e^2/Q^2)$. Explicit analytical results for the leading logarithmic QED corrections are given in Ref. 63. Appropriate scale choices have been discussed in Sec. 2.3.3. It turns out that $Q^2 = s/4$ and $Q^2 = s(1-\beta)/(1+\beta)$ are suitable for right-handed electrons and left-handed electrons, respectively. These scales have been used for the following numerical analysis.

As we want to compare the approximation with an $\mathcal{O}(\alpha)$ calculation we do not use the square of the matrix element defined in (2.61) and (2.62) for the numerical analysis, but only the square of the terms involving G_μ and $\alpha(s)$ and the interference of these terms with the others. Moreover, in this interference G_μ and $\alpha(s)$ are replaced by the corresponding lowest-order expressions in terms of s_W^2 and $\alpha(0)$. Nevertheless the so-obtained approximation still contains higher-order contributions through the squares of $\alpha(s)$ and G_μ. To allow a meaningful comparison these have been included in the numbers for the exact one-loop results given in Tab. 6 and Fig. 11 in the same way (compare Ref. 63 for more details).

In Tab. 6 we show the lowest-order total cross-section σ_{Born}, the full one-loop corrected cross-section σ including real-photon radiation and the cross-section σ_{app} resulting from the improved Born approximation for right-handed, left-handed and unpolarized electrons. The positrons are assumed to be polarized opposite to the electrons. The uncertainty of σ arises from the Monte-Carlo integration over the photon phase space. In the LEP200 energy region the relative difference $\Delta = (\sigma_{\mathrm{app}} - \sigma)/\sigma_{\mathrm{Born}}$ is below 1% for left-handed or unpolarized electrons and about 2% for right-handed electrons. These errors have to be compared to the expected statistical error of LEP200 which is about 1% for the total unpolarized cross-section and about 10% for the right-handed cross-section. Note that the approximation for the integrated cross-section does not include $F^{\kappa}_{\{I,Q\},\mathrm{rem}}$.

For unpolarized positrons there are additional contributions from equal helicities of electron and positron that are not contained in the approximation. These contributions arise from collinear hard-photonic corrections allowing a spin-flip. They are small for left-handed electrons, being of the order $(\alpha/\pi)\log(s/M_W^2)$ at most. For right-handed electrons they are still small near threshold, i.e. $\propto \beta^4$, because of the lack of phase space and because the spin-flip is a hard-photon effect. At high energies, however, they are large as they originate from a $\mathcal{O}([\alpha/\pi]\log[s/M_W^2]) \times \sigma^-$ correction to the suppressed right-handed cross-section. Consequently for unpolarized positrons the quality of the approximation given in Tab. 6 is essentially unchanged for left-handed electrons in general and right-handed electrons near threshold. For right-handed electrons at high energies the approximation gets much worse. This could be improved by including these helicity-changing contributions in the approximation.

$\sqrt{s}$/ GeV	165	175	200	300	500	1000
$\sigma^+_{\rm Born}/10^{-2}$ pb	10.64	40.00	69.07	36.61	10.00	1.99
$\sigma^+/10^{-2}$ pb	9.02 ±0.002	38.70 ±0.01	75.12 ±0.02	47.06 ±0.02	14.40 ±0.01	3.02 ±0.004
$\sigma^+_{\rm app}/10^{-2}$ pb	8.84	37.85	73.47	45.69	14.01	3.12
$\Delta^+_{\rm app}$	−1.6%	−2.1%	−2.4%	−3.7%	−4.0%	5.3%
$\sigma^-_{\rm Born}$/pb	42.74	63.72	70.77	49.42	26.30	9.84
σ^-/pb	34.62 ±0.01	58.44 ±0.02	71.15 ±0.02	53.77 ±0.03	29.61 ±0.02	11.41 ±0.01
$\sigma^-_{\rm app}$/pb	34.58	58.66	71.75	54.64	30.32	11.81
$\Delta^-_{\rm app}$	−0.1%	0.3%	0.8%	1.7%	2.7%	4.1%
$\sigma_{\rm Born}$/pb	10.71	16.03	17.87	12.45	6.60	2.47
σ/pb	8.68 ±0.003	14.71 ±0.004	17.98 ±0.006	13.58 ±0.007	7.46 ±0.005	2.87 ±0.003
$\sigma_{\rm app}$/pb	8.67	14.76	18.12	13.77	7.62	2.96
$\Delta_{\rm app}$	−0.1%	0.3%	0.8%	1.6%	2.4%	3.7%

Tab. 6: Comparison between the completely corrected total cross-section and the improved Born approximation.

Figure 11 illustrates the quality of the improved Born approximation for the unpolarized differential cross-section in the LEP200 energy range for different scattering angles. Note that the approximation for the differential cross-section is only valid for soft photons. In Fig. 11 a soft-photon cut-off $\Delta E = 0.05E$ has been chosen. The relative error of the approximation is below $\sim 1\%$ for $\sqrt{s} \lesssim 200\,\mathrm{GeV}$. While the error does not depend very much on the energy for small angles, its increase for large angles occurs in a region where it does not harm because of limited statistics.

2.4.2 Approximations at intermediate and high energies

In contrast to the threshold region, the construction of effective approximations in the intermediate- and high-energy range ($\sqrt{s} > 500$ GeV) poses more of a problem. In principle an approximation that neglects, whenever possible, the masses of the SM particles with respect to the energy seems to be the obvious approach. Special care, however, has to be taken with the top-quark and Higgs-boson masses, which are at present still allowed to be of the order of NLC type of energies. Below $\sqrt{s} = 1$ TeV also the gauge-boson masses can still become relevant, especially in combination with large corrections. An additional difficulty is raised by the unitarity cancellations for longitudinal W bosons, which cause the actual role played by the gauge-boson masses to be revealed only after the leading high-energy terms have cancelled.

Based on the existing complete virtual and soft-photonic $\mathcal{O}(\alpha)$ corrections, recently a high-energy approximation has been constructed[45] in the limit $s, |t|, |u| \gg M^2_{\rm W,Z} \gg m^2_{f_\ell}$, keeping $m_{\rm t}$ and $M_{\rm H}$ arbitrary. This involves a systematic expansion of the matrix element

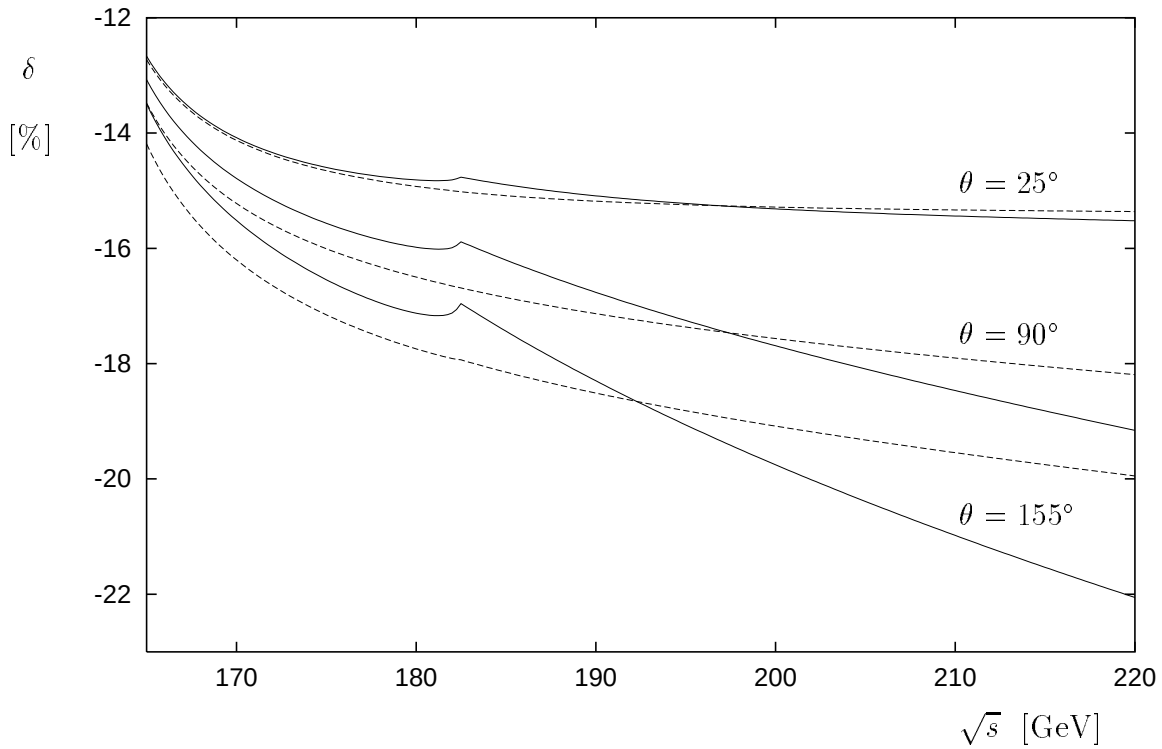

Fig. 11: Relative corrections δ to the unpolarized differential cross-section for the full one-loop result in the soft-photon approximation (———) and in the corresponding improved Born approximation (– – –).

squared, keeping all terms that do not vanish in the indicated limit. Since $M^2_{\mathrm{W,Z}}$ are neglected with respect to the Mandelstam variables s, t and u, the results are not reliable for small energies or in the very forward and backward directions, which will, however, be removed by experimental cuts.

Here we only give those corrections which are associated with the non-suppressed cross-sections (see Sec. 2.2) and which become large at high energies. Presented as correction factors to the high-energy lowest-order cross-sections (2.26) they read:

$$
\begin{aligned}
C^{\mathrm{dom}}_{-,\mathrm{L}} = {} & \Delta_{\mathrm{LL}} + 2\Delta\alpha^{\mathrm{LL}}(M^2_{\mathrm{W}}) - 2(c^2_{\mathrm{W}} - s^2_{\mathrm{W}})\frac{c^2_{\mathrm{W}}}{s^2_{\mathrm{W}}}\Delta\rho \\
& + \frac{\alpha}{2\pi}\Bigg[-\frac{1-2c^2_{\mathrm{W}}+4c^4_{\mathrm{W}}}{2c^2_{\mathrm{W}}s^2_{\mathrm{W}}}L_s^2 + 4\frac{c^2_{\mathrm{W}}}{s^2_{\mathrm{W}}}L_s(L_s-L_t) + \frac{103-158c^2_{\mathrm{W}}+80c^4_{\mathrm{W}}}{12c^2_{\mathrm{W}}s^2_{\mathrm{W}}}L_s \\
& + \frac{(1-2c^2_{\mathrm{W}})^2}{c^2_{\mathrm{W}}s^2_{\mathrm{W}}}[L_sL_{\mathrm{Z}} + (L_u-L_t)(L_s-L_{\mathrm{Z}})] + \frac{(1+4c^4_{\mathrm{W}})s}{4c^2_{\mathrm{W}}s^2_{\mathrm{W}}u}(L_s-L_t)^2 \\
& - \frac{s}{4c^2_{\mathrm{W}}s^2_{\mathrm{W}}t}(L_s-L_u)^2 - 2(L_u-L_t)^2 - 8\,\mathrm{Li}_2\left(-\frac{u}{t}\right) \\
& + \frac{1}{2s^2_{\mathrm{W}}}L^2_{\mathrm{H}} - \frac{M^2_{\mathrm{H}}}{8s^2_{\mathrm{W}}M^2_{\mathrm{W}}} + \frac{3m^2_{\mathrm{t}}}{2s^2_{\mathrm{W}}M^2_{\mathrm{W}}}(L_{\mathrm{top}} - L_s + 2 - c^2_{\mathrm{W}})\Bigg],
\end{aligned}
$$

$$
C^{\mathrm{dom}}_{+,\mathrm{L}} = \Delta_{\mathrm{LL}} + 2\Delta\alpha^{\mathrm{LL}}(M^2_{\mathrm{W}}) + \frac{\alpha}{2\pi}\Bigg[-\frac{5-10c^2_{\mathrm{W}}+8c^4_{\mathrm{W}}}{4c^2_{\mathrm{W}}s^2_{\mathrm{W}}}L_s^2 + \frac{65-65c^2_{\mathrm{W}}+18c^4_{\mathrm{W}}}{6c^2_{\mathrm{W}}s^2_{\mathrm{W}}}L_s
$$

$$
\begin{aligned}
&+\frac{L_s L_{\rm Z}}{2c_{\rm W}^2 s_{\rm W}^2}+\frac{2(1-2c_{\rm W}^2)}{c_{\rm W}^2}[L_s L_{\rm Z}+(L_u-L_t)(L_s-L_{\rm Z})]+\frac{s}{2c_{\rm W}^2 u}(L_s-L_t)^2\\
&-\frac{s}{2c_{\rm W}^2 t}(L_s-L_u)^2-2(L_u-L_t)^2-8\,{\rm Li}_2\left(-\frac{u}{t}\right)+\frac{1}{2s_{\rm W}^2}L_{\rm H}^2-\frac{M_{\rm H}^2}{8s_{\rm W}^2 M_{\rm W}^2}\\
&+\frac{3m_{\rm t}^2}{2s_{\rm W}^2 M_{\rm W}^2}(L_{\rm top}-L_s+2)\Big],
\end{aligned}
$$

$$
\begin{aligned}
C_{-,{\rm T}}^{\rm dom} = {}& \Delta_{\rm LL}+2\Delta\alpha^{\rm LL}(M_{\rm W}^2)-2\frac{c_{\rm W}^2}{s_{\rm W}^2}\Delta\rho+\frac{\alpha}{2\pi}\Big[-\frac{1+2c_{\rm W}^2+8c_{\rm W}^4}{4c_{\rm W}^2 s_{\rm W}^2}L_s^2+\frac{3(1-2c_{\rm W}^2+4c_{\rm W}^4)}{4c_{\rm W}^2 s_{\rm W}^2}L_s\\
&+\frac{L_s L_{\rm Z}}{2c_{\rm W}^2 s_{\rm W}^2}+\frac{4u+2s}{s_{\rm W}^2 u}L_s(L_s-L_t)-\frac{2(1-2c_{\rm W}^2)}{s_{\rm W}^2}[L_s L_{\rm Z}+(L_u-L_t)(L_s-L_{\rm Z})]\\
&-\frac{2s}{s_{\rm W}^2 u}(L_s-L_t)(L_s-L_u)-\Big(\frac{s(s+3t-6c_{\rm W}^2 s)}{4c_{\rm W}^2 s_{\rm W}^2(t^2+u^2)}+\frac{(1-6c_{\rm W}^2)s}{2c_{\rm W}^2 s_{\rm W}^2 u}\Big)(L_s-L_t)^2\\
&-\frac{3st}{2s_{\rm W}^2(t^2+u^2)}(L_s-L_u)^2-2(L_u-L_t)^2-8\,{\rm Li}_2\left(-\frac{u}{t}\right)\\
&-\frac{s[3s+t+6c_{\rm W}^2(s+3t)]}{4c_{\rm W}^2 s_{\rm W}^2(t^2+u^2)}(L_s-L_t)-\frac{(1-6c_{\rm W}^2)su}{4c_{\rm W}^2 s_{\rm W}^2(t^2+u^2)}\Big],
\end{aligned}
\tag{2.68}
$$

where we have introduced the following short-hand notations:

$$
\begin{aligned}
\Delta_{\rm LL} &= \frac{\alpha}{\pi}\Big\{\frac{3}{2}\log\Big(\frac{s}{m_{\rm e}^2}\Big)+2\log(\varepsilon)\Big[\log\Big(\frac{s}{m_{\rm e}^2}\Big)+\log\Big(\frac{s}{M_{\rm W}^2}\Big)+2\log\Big(\frac{t}{u}\Big)-2\Big]\Big\},\\
L_s &= \log\Big(\frac{s}{M_{\rm W}^2}\Big), \qquad L_t=\log\Big(\frac{-t}{M_{\rm W}^2}\Big), \qquad L_u=\log\Big(\frac{-u}{M_{\rm W}^2}\Big),\\
L_{\rm H} &= \log\Big(\frac{M_{\rm H}^2}{M_{\rm W}^2}\Big), \qquad L_{\rm Z}=\log\Big(\frac{M_{\rm Z}^2}{M_{\rm W}^2}\Big), \qquad L_{\rm top}=\log\Big(\frac{m_{\rm t}^2}{M_{\rm W}^2}\Big),
\end{aligned}
\tag{2.69}
$$

and the dilogarithm is defined as

$$
{\rm Li}_2(x)=-\int_0^1\frac{{\rm d}t}{t}\log(1-xt), \qquad |\arg(1-x)|<\pi. \tag{2.70}
$$

The remaining parts of the correction factors, which do not become large at high energies, can be found in Ref. 45. It should be noted that the Mandelstam variables t and u are the ones given in (2.4), hence they have not been expanded.

The dominant contributions given above include all terms containing $\log(s)$, all energy- and angle-dependent terms, and all leading corrections that are of the same kind as at low energies, i.e. the running of α ($\Delta\alpha^{\rm LL}$), the corrections associated with the ρ-parameter ($\Delta\rho$), and the leading collinear and soft QED logarithms ($\Delta_{\rm LL}$), consisting of the terms proportional to $\log(m_{\rm e}^2/s)$ and $\log(\varepsilon)$. Moreover all terms behaving as $m_{\rm t}^2/M_{\rm W}^2$, $M_{\rm H}^2/M_{\rm W}^2$ or $L_{\rm H}^2$ for $s\gg m_{\rm t}^2, M_{\rm H}^2\gg M_{\rm W}^2$ have been kept.

The most important corrections at high energies result from the terms proportional to the high-energy leading logarithms $\log^n(s/M_{\rm W}^2)$ ($n=1,2$) or $\log(s/m_{\rm e}^2)$. While for the polarization $(+,L)$ the angular dependence is small, terms proportional to $\log(s/M_{\rm W}^2)\times\log(-s/t)$ cause a sizeable angular dependence at high energies for $(-,L)$ and $(-,T)$:

roughly 20% at 1 TeV and 40% at 10 TeV. The angular dependence of all the other contributions is weaker. In particular there are no poles $1/t$ or $1/u$, as the corresponding residues vanish in the high-energy limit owing to the relation $s + t + u = 2M_{\mathrm{W}}^2$.

In the high-energy limit the complete Higgs- and top-mass dependence of the correction factors for transverse W bosons is entirely due to renormalization effects and hence intrinsically not different from that at LEP200. On the contrary unitarity cancellations lead to a variety of additional contributions for longitudinal W bosons.

For $s \ll M_{\mathrm{H}}^2, m_{\mathrm{t}}^2$ we obtain the same terms proportional to $m_{\mathrm{t}}^2/M_{\mathrm{W}}^2$, L_{top} and L_{H} as present in the LEP200 approximation described in the last subsection, which was derived exactly in this limit. In particular this involves those terms that are accompanied by a factor s/M_{W}^2. The latter lead to large corrections, known as delayed unitarity effects[44], and result from the fact that the unitarity cancellations are not yet complete in the presence of heavy particles.

In the limit $s \gg m_{\mathrm{t}}^2, M_{\mathrm{H}}^2$, these delayed unitarity terms disappear. On the other hand the terms containing $m_{\mathrm{t}}^2/M_{\mathrm{W}}^2$, L_{top}, L_{H}, or L_{H}^2 deviate from the ones appearing at low energies, and for $M_{\mathrm{W}}^2 \ll M_{\mathrm{H}}^2 \ll s$ screening is not complete, resulting in large corrections proportional to $M_{\mathrm{H}}^2/M_{\mathrm{W}}^2$. In particular large top-mass terms $\propto m_{\mathrm{t}}^2/M_{\mathrm{W}}^2 \log(m_{\mathrm{t}}^2/s)$ appear as a remnant of the unitarity cancellations.

The approximation we have discussed so far has been derived for high energies. However, it turns out that a substantial part of the dominant corrections at high energies are the same as at low energies, i.e. the corrections related to the running of α ($\Delta\alpha^{\mathrm{LL}}$) and those associated with the ρ-parameter ($\Delta\rho$). Moreover these leading low-energy corrections appear as universal factors. Therefore the approximation can be easily improved by using the complete lowest-order cross-section as far as these leading corrections are concerned.

To this end the terms proportional to $\Delta\alpha^{\mathrm{LL}}$ and $\Delta\rho$ are discarded in the high-energy expansion and the exact contribution of these terms is added via the following improved Born matrix elements:

$$\begin{aligned}\mathcal{M}^{\mathrm{impr}}(\kappa,\lambda_+,\lambda_-) = {} & \delta_{\kappa-}\frac{1}{2s_{\mathrm{W}}^2}\mathcal{M}_I(\kappa,\lambda_+,\lambda_-)\Big(1+\Delta\alpha^{\mathrm{LL}}-\frac{c_{\mathrm{W}}^2}{s_{\mathrm{W}}^2}\Delta\rho\Big)\\ & +\mathcal{M}_Q(\kappa,\lambda_+,\lambda_-)\Big(1+\Delta\alpha^{\mathrm{LL}}\Big),\end{aligned} \tag{2.71}$$

with $\mathcal{M}_I$ and $\mathcal{M}_Q$ as given in (2.20). In addition also the phase-space factor β appearing in the cross-sections is taken into account. This procedure indeed improves the approximations by a factor of 2–3 for small and intermediate energies in those cases where the cross-section is sizeable, and brings the corresponding errors down to the level of 1% for $\sqrt{s} \gtrsim 500\,\mathrm{GeV}$.

The lowest-order cross-sections integrated over the angular region $-0.9 \leq \cos\theta \leq 0.9$ are listed in Tab. 7 for the non-suppressed polarizations at various energies. For the integrated luminosity of $10\,\mathrm{fb}^{-1}$ envisaged for a 500 GeV $\mathrm{e}^+\mathrm{e}^-$ collider, this corresponds to 22000 events for the total unpolarized cross-section σ_{U}, yielding a statistical accuracy of about 0.7%. As the luminosity at higher energies should be such as to compensate the drop in cross-section, we take 1% as a characteristic accuracy. Table 7 also shows the absolute virtual and soft-photonic $\mathcal{O}(\alpha)$ corrections as calculated from the exact formulae

$\sqrt{s}$/TeV	0.5	1	2	10
$\left(\sigma_{\text{exact}+\delta\sigma_{\text{app}}}^{\text{Born}+\delta\sigma_{\text{exact}}}\right)_{\text{U}}$/fb	2181^{+244}_{+229}	508^{+12}_{+12}	124^{-14}_{-14}	$4.94^{-2.96}_{-2.95}$
$\left(\sigma_{\text{exact}+\delta\sigma_{\text{app}}}^{\text{Born}+\delta\sigma_{\text{exact}}}\right)_{-,\text{T}}$/fb	7813^{+822}_{+784}	1895^{+30}_{+32}	470^{-57}_{-56}	$18.7^{-11.6}_{-11.6}$
$\left(\sigma_{\text{exact}+\delta\sigma_{\text{app}}}^{\text{Born}+\delta\sigma_{\text{exact}}}\right)_{-,\text{L}}$/fb	$340^{+52.0}_{+56.9}$	$86.3^{+8.8}_{+9.4}$	$21.7^{+0.5}_{+0.5}$	$0.872^{-0.230}_{-0.230}$
$\left(\sigma_{\text{exact}+\delta\sigma_{\text{app}}}^{\text{Born}+\delta\sigma_{\text{exact}}}\right)_{+,\text{L}}$/fb	$71.9^{+21.4}_{+20.8}$	$17.9^{+4.62}_{+4.60}$	$4.47^{+0.95}_{+0.95}$	$0.179^{+0.011}_{+0.011}$

Tab. 7: Lowest-order cross-sections integrated over $-0.9 \leq \cos\theta \leq 0.9$ together with the exact and approximated virtual and soft-photonic $\mathcal{O}(\alpha)$ corrections.

and from the approximation. Here and in the following figures we have chosen $\Delta E = E$ for the soft-photon cut-off, such that all cut-off-dependent terms drop out and do not influence the results. Note that the relative corrections in general grow with energy, e.g. for the unpolarized cross-section from 10% at 0.5 TeV to 60% at 10 TeV. Consequently the dominant $\mathcal{O}(\alpha^2)$ corrections should be evaluated in the future.

In the following we present the quality of the high-energy approximation as defined through

$$\Delta = \left|\frac{\delta\sigma_{\text{app}} - \delta\sigma_{\text{exact}}}{\sigma_{\text{exact}}^{\text{Born}}}\right| \qquad \text{or} \qquad \Delta' = \left|\frac{\delta\sigma_{\text{app}} - \delta\sigma_{\text{exact}}}{\sigma_{\text{app}}^{\text{Born}}}\right|, \tag{2.72}$$

where $\delta\sigma_{\text{exact}}$ is the full $\mathcal{O}(\alpha)$ correction, $\delta\sigma_{\text{app}}$ the corresponding high-energy approximation, $\sigma_{\text{exact}}^{\text{Born}}$ the exact lowest-order cross-section, and $\sigma_{\text{app}}^{\text{Born}}$ the high-energy approximation for the lowest-order cross-section as given in (2.26) including an additional phase-space factor β. The use of the approximated lowest-order cross-section for the normalization of the angular distributions is motivated by the fact that the exact one has a zero for longitudinal W bosons and left-handed electrons. Since for this polarization the t-channel pole drops out at high energies, but is sizeable at small and intermediate energies, the leading t-channel contribution is added and

$$\left(\frac{\mathrm{d}\sigma}{\mathrm{d}\Omega}\right)_{-,L}^{\text{app}} = \frac{\alpha^2}{4s}\beta\frac{\sin^2\theta}{16s_{\text{W}}^4 c_{\text{W}}^4}\left[1 + 16c_{\text{W}}^4\frac{M_{\text{W}}^4}{t^2}\right] \tag{2.73}$$

is used instead of (2.26) as normalization for $(-, L)$.

In Fig. 12 we show the quality of the approximation for the differential cross-sections and various polarizations. It improves, as expected, with increasing energy. For energies above 500 GeV the deviation of the approximation from the exact result is below $\sim 2\%$ for right-handed electrons at almost all scattering angles and below $\sim 1\%$ for $(-, L)$ at scattering angles around 90° (central region) as well as for $(-, T)$ and the unpolarized case in the forward hemisphere. Note that the approximation is in general best where the cross-sections are maximal, i.e. in the forward direction for transverse and unpolarized W bosons and in the central region for longitudinal W bosons.

In Fig. 13 we present the quality Δ of the approximations for the various polarized cross-sections integrated over $-0.9 \leq \cos\theta \leq 0.9$, using the exact lowest-order cross-section as normalization. For the unpolarized cross-section and the dominant polarization

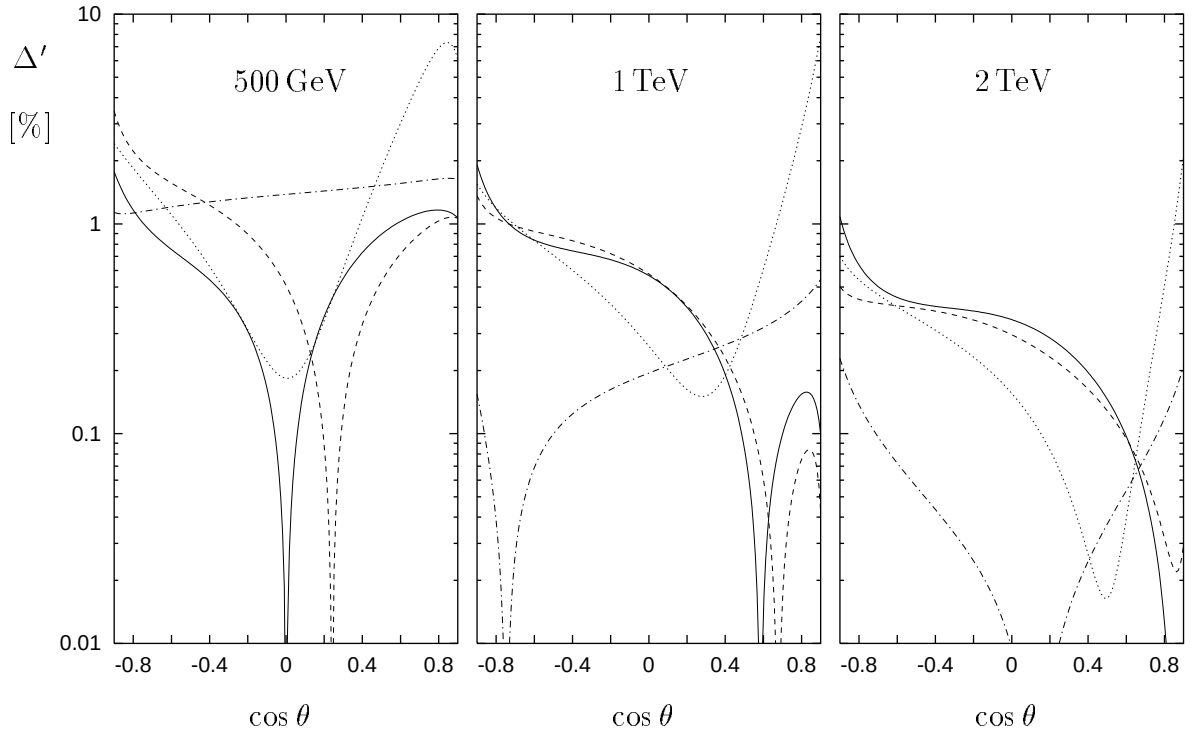

Fig. 12: Quality of the intermediate- and high-energy approximations for the differential cross-sections $(-,L)$: $(\cdots\cdots)$, $(+,L)$: $(-\cdot-\cdot)$, $(-,T)$: $(---)$, and (unpol.): (——).

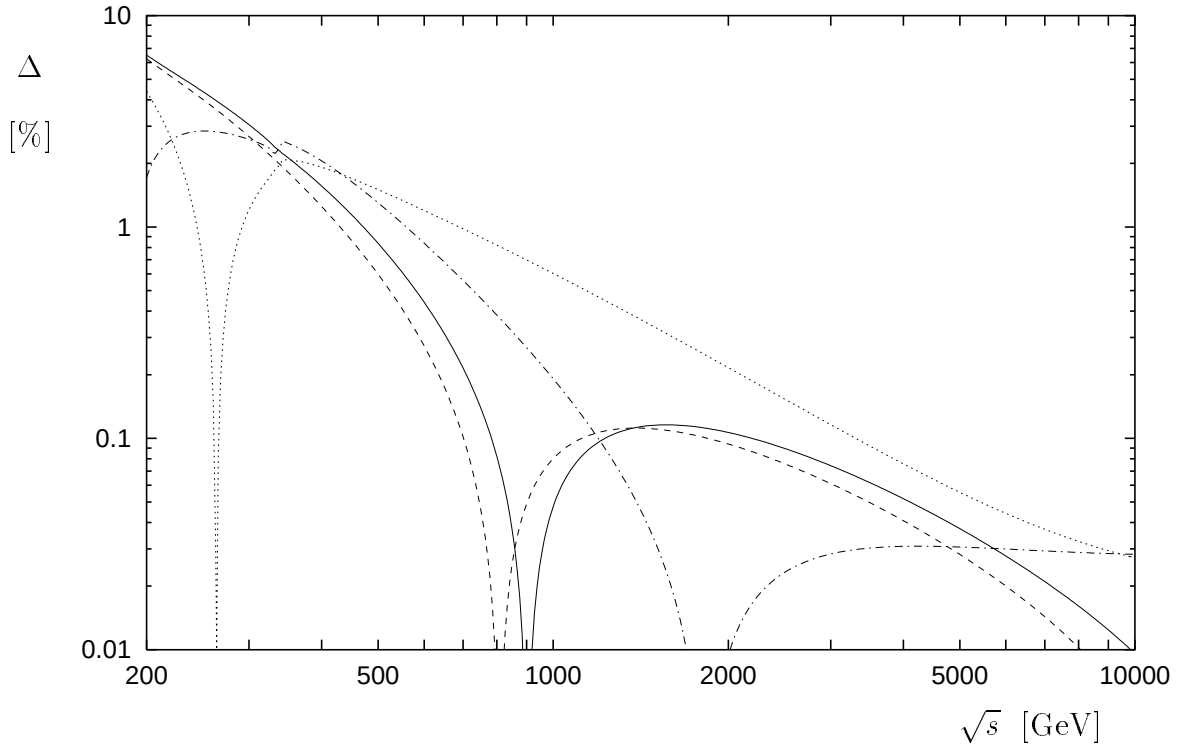

Fig. 13: Quality of the intermediate- and high-energy approximations for the integrated cross-sections ($-0.9 \leq \cos\theta \leq 0.9$): same signature as in Fig. 12.

$(-,T)$, the error is below 1% above 500 GeV, for the polarization $(+,L)$ this is the case above 600 GeV, and for the polarization $(-,L)$ above 700 GeV. Accordingly the accuracy of the high-energy approximation roughly matches the expected experimental precision at a future 500 GeV linear e^+e^- collider.

3 Off-Shell W-Pair Production

3.1 Lowest order

So far we have only considered stable W bosons. This is, however, only an approximation and in particular in the threshold region it is not sufficient. Therefore we have to take into account the finite-width effects, i.e. the decays of the W bosons.

To this end one has to consider the process

$$e^+ + e^- \to W^+ + W^- \to f_1 + \bar{f}_2 + f_3 + \bar{f}_4. \tag{3.1}$$

In lowest order this is represented by the three Feynman diagrams shown in Fig. 14. The corresponding matrix element can be written in the following form:

$$\begin{aligned}\widehat{\mathcal{M}}^{\kappa}_{\text{Born}} = &\left[\delta_{\kappa-}\frac{e^2}{2s_{\text{W}}^2}\mathcal{M}_I^{\kappa,\rho\sigma} + e^2\mathcal{M}_Q^{\kappa,\rho\sigma}\right] \\ &\times\frac{1}{k_+^2 - M_{\text{W}}^2}\times\frac{e}{\sqrt{2}s_{\text{W}}}\bar{u}_1\gamma_\rho\omega_- v_2\times\frac{1}{k_-^2 - M_{\text{W}}^2}\times\frac{e}{\sqrt{2}s_{\text{W}}}\bar{u}_3\gamma_\sigma\omega_- v_4,\end{aligned} \tag{3.2}$$

where

$$\begin{aligned}\mathcal{M}_Q^{\kappa,\rho\sigma} &= \frac{2M_Z^2}{s(s-M_Z^2)}\bar{v}_+\left[\not{k}_+ g^{\rho\sigma} - \gamma^\rho k_+^\sigma + \gamma^\sigma k_-^\rho\right]\omega_\kappa u_-, \\ \mathcal{M}_I^{\kappa,\rho\sigma} &= \frac{1}{t}\bar{v}_+\gamma^\rho(\not{k}_+ - \not{p}_+)\gamma^\sigma\omega_\kappa u_- - \frac{s}{M_{\text{Z}}^2}\mathcal{M}_Q^{\kappa,\rho\sigma}\end{aligned} \tag{3.3}$$

are directly related to the corresponding on-shell quantities $\mathcal{M}_I$ and $\mathcal{M}_Q$ (2.20). Here $k_\pm$ are the momenta of the $W^\pm$ bosons as reconstructed from the decay products and s and t the usual Mandelstam variables for $e^+e^- \to W^+W^-$. We have assumed that all

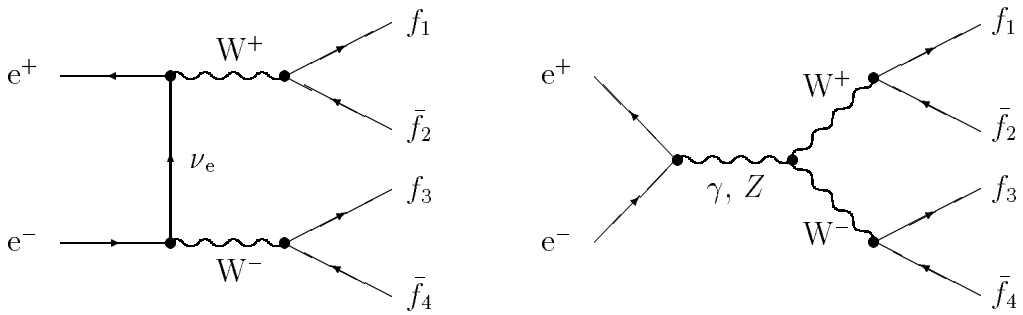

Fig. 14: Lowest-order diagrams for $e^+e^- \to W^+W^- \to 4f$

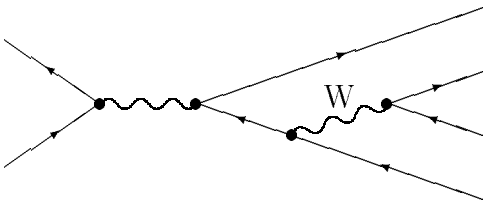

Fig. 15: Example of a singly-resonant diagram.

fermion masses are negligible. In a renormalizable gauge such as a R_ξ gauge one would otherwise have to consider in addition diagrams involving one or two unphysical charged Higgs bosons instead of the W bosons

Whereas for on-shell W bosons the contributions of $\mathcal{M}_I$ and $\mathcal{M}_Q$ are separately gauge-invariant, for off-shell W bosons not even $\widehat{\mathcal{M}}_{\rm Born}$ is gauge-invariant. This can be illustrated by considering the doubly-resonant diagrams in an axial gauge. To this end we replace the conventional 't Hooft–Feynman gauge-fixing term for the W boson by $-\lambda(n^\mu W^+_\mu)(n^\nu W^-_\nu)$. This modifies the W-boson propagators in the diagrams of Fig. 14 and, since this gauge-fixing term does not eliminate the mixing between the W-boson field and the corresponding unphysical Higgs field, leads to mixing propagators between those fields, giving rise to additional Feynman diagrams. Combining all relevant diagrams yields the following extra contribution to $\widehat{\mathcal{M}}^\kappa_{\rm Born}$ in the axial gauge:

$$\begin{aligned}\widehat{\mathcal{M}}^\kappa_{\rm Born}\Big|_{\text{axial gauge}} - \widehat{\mathcal{M}}^\kappa_{\rm Born}\Big|_{\text{'t Hooft–Feynman gauge}} &= e^2\left[\delta_{\kappa-}\frac{1}{2s^2_{\rm W}} - \frac{M^2_{\rm Z}}{s}\right]\frac{1}{s-M^2_{\rm Z}}\bar{v}_+\gamma_\mu\omega_\kappa u_- \\ &\times\left[\frac{g^{\mu\rho}n^\sigma}{(k^2_- - M^2_{\rm W})(n\cdot k_-)} - \frac{g^{\mu\sigma}n^\rho}{(k^2_+ - M^2_{\rm W})(n\cdot k_+)}\right] \\ &\times\frac{e}{\sqrt{2}s_{\rm W}}\bar{u}_1\gamma_\rho\omega_- v_2 \times \frac{e}{\sqrt{2}s_{\rm W}}\bar{u}_3\gamma_\sigma\omega_- v_4. \end{aligned} \tag{3.4}$$

Note that these gauge-dependent terms involve either a pole in $(k^2_+ - M^2_{\rm W})$ or $(k^2_- - M^2_{\rm W})$ but not both, i.e. they are only singly-resonant. These terms are exactly cancelled by the gauge-dependent contributions of four singly-resonant diagrams contributing to the same final state with the topology shown in Fig. 15.

The sum of the doubly-resonant diagrams and the singly-resonant ones with the topology shown in Fig. 15 is in general gauge-invariant. This follows directly from the fact that for final states with four different fermions and no electrons or positrons those diagrams are the only ones that contribute. As a consequence the non-resonant diagrams are not needed to cancel the gauge-dependent terms of the doubly-resonant diagrams. Among the other singly- and non-resonant diagrams further gauge-invariant subsets can be identified by considering different final-state fermions.

Thus in general all graphs that contribute to a given final state have to be taken into account and one is lead to consider the complete process $\mathrm{e^+e^-} \to 4f$, including all resonant and non-resonant graphs, in order to obtain a manifestly gauge-independent result.

This does, however, not solve the problem of gauge invariance completely. The resonant graphs involve poles at $k_\pm^2 = M_\mathrm{W}^2$.[h] These have to be cured by introducing the finite width via the substitution

$$\frac{1}{k_\pm^2 - M_\mathrm{W}^2} \to \frac{1}{k_\pm^2 - M_\mathrm{W}^2 + iM_\mathrm{W}\Gamma_\mathrm{W}}, \tag{3.5}$$

where Γ_W is the physical width of the W bosons[i]. As in general the resonant diagrams are not gauge-invariant by themselves, this substitution will again destroy gauge invariance if it is applied to the full resonant diagrams. Therefore one needs a consistent scheme to calculate gauge-invariant cross-sections.

One possibility is the so-called pole scheme. In this scheme one decomposes the complete amplitude, consisting of contributions from doubly-resonant diagrams R_{+-} (corresponding in lowest order to $\widehat{\mathcal{M}}_\mathrm{Born}$), singly-resonant diagrams R_+, R_-, and non-resonant diagrams N, according to their poles as follows:

$$\begin{aligned}
\mathcal{M} &= \frac{R_{+-}(k_+^2,k_-^2,\theta)}{(k_+^2-M_\mathrm{W}^2)(k_-^2-M_\mathrm{W}^2)} + \frac{R_+(k_+^2,k_-^2,\theta)}{k_+^2-M_\mathrm{W}^2} + \frac{R_-(k_+^2,k_-^2,\theta)}{k_-^2-M_\mathrm{W}^2} + N(k_+^2,k_-^2,\theta) \\
&= \frac{R_{+-}(M_\mathrm{W}^2,M_\mathrm{W}^2,\theta)}{(k_+^2-M_\mathrm{W}^2)(k_-^2-M_\mathrm{W}^2)} \\
&\quad + \frac{1}{k_+^2-M_\mathrm{W}^2}\left[\frac{R_{+-}(M_\mathrm{W}^2,k_-^2,\theta)-R_{+-}(M_\mathrm{W}^2,M_\mathrm{W}^2,\theta)}{k_-^2-M_\mathrm{W}^2} + R_+(M_\mathrm{W}^2,k_-^2,\theta)\right] \\
&\quad + \frac{1}{k_-^2-M_\mathrm{W}^2}\left[\frac{R_{+-}(k_+^2,M_\mathrm{W}^2,\theta)-R_{+-}(M_\mathrm{W}^2,M_\mathrm{W}^2,\theta)}{k_+^2-M_\mathrm{W}^2} + R_-(k_+^2,M_\mathrm{W}^2,\theta)\right] \\
&\quad + \Bigg[\frac{R_{+-}(k_+^2,k_-^2,\theta)+R_{+-}(M_\mathrm{W}^2,M_\mathrm{W}^2,\theta)-R_{+-}(M_\mathrm{W}^2,k_-^2,\theta)-R_{+-}(k_+^2,M_\mathrm{W}^2,\theta)}{(k_+^2-M_\mathrm{W}^2)(k_-^2-M_\mathrm{W}^2)} \\
&\quad + \frac{R_+(k_+^2,k_-^2,\theta)-R_+(M_\mathrm{W}^2,k_-^2,\theta)}{k_+^2-M_\mathrm{W}^2} \\
&\quad + \frac{R_-(k_+^2,k_-^2,\theta)-R_-(k_+^2,M_\mathrm{W}^2,\theta)}{k_-^2-M_\mathrm{W}^2} + N(k_+^2,k_-^2,\theta)\Bigg].
\end{aligned} \tag{3.6}$$

Here θ stands generically for all angular variables which should be defined in such a way that their integration boundaries are independent of k_+^2 and k_-^2. Otherwise these angular variables would introduce an additional dependence on k_+^2 and k_-^2, and the correct pole terms could only be extracted after the angular integrations had been performed. This would complicate the pole decomposition and, in particular, would not be suited for a Monte-Carlo generator. Appropriate variables are e.g. the angles in the $\mathrm{e^+e^-}$-CM system but not the Mandelstam variables. In (3.6) $\mathcal{M}$ is decomposed into gauge-invariant

[h] There are similar poles associated with diagrams containing internal Z propagators. These correspond to Z-pair production and are here considered as background to W-pair production.

[i] There is no unique prescription for the propagator including the finite width. Instead of the constant term $M_\mathrm{W}\Gamma_\mathrm{W}$ one can also use a width depending on the invariant mass $k_\pm^2$. This corresponds to different definitions of the (renormalized) W mass, which is fixed by the pole of the propagator. A popular choice is $k^2\Gamma_\mathrm{W}/M_\mathrm{W}$ which amounts to a shift in M_W by $\Gamma_\mathrm{W}^2/(2M_\mathrm{W}) \approx 26\,\mathrm{MeV}$ relative to the propagator with the constant-width term.

subsets originating from double-pole terms, single-pole terms and non-resonant terms (with repect to M_{W}). Introducing now the finite width only in the pole factors and not in the finite constant residues in brackets does not destroy gauge invariance. We note that different ways of introducing the finite width differ only by terms that are of higher-order and/or that are not doubly-resonant. The same holds for different choices of the angular variables θ.

Sufficiently far above the W-pair threshold the cross-section for off-shell W-pair production is dominated by (or may even by defined by) the doubly-resonant contributions $R_{+-}(M_{\mathrm{W}}^2, M_{\mathrm{W}}^2, \theta)$. At least at lowest order these may be related to on-shell W-pair production in the following way:

$$R_{+-}(M_{\mathrm{W}}^2, M_{\mathrm{W}}^2, \theta) = \sum_{\lambda_+,\lambda_-} \mathcal{M}^{\lambda_+,\lambda_-}_{\mathrm{e^+e^-}\to\mathrm{W^+W^-}} \times \mathcal{M}^{\lambda_+}_{\mathrm{W^+}\to f_1\bar{f}_2} \times \mathcal{M}^{\lambda_-}_{\mathrm{W^-}\to f_3\bar{f}_4} \tag{3.7}$$

where $\mathcal{M}_{\mathrm{e^+e^-}\to\mathrm{W^+W^-}}$, $\mathcal{M}_{\mathrm{W^+}\to f_1\bar{f}_2}$, $\mathcal{M}_{\mathrm{W^-}\to f_3\bar{f}_4}$ denote the matrix elements for the production of two on-shell W bosons and their subsequent decay into fermion–antifermion pairs. Integrating over the full phase space for $\mathrm{e^+e^-} \to 4f$ (phase-space element $\mathrm{d}PS_{\mathrm{e^+e^-}\to 4f}$) and summing over the W helicities and all possible final-state fermions yields the corresponding total cross-section:

$$\begin{aligned}\sigma(s) &= \frac{1}{2s}\int \mathrm{d}PS_{\mathrm{e^+e^-}\to 4f} \left| \frac{R_{+-}(M_{\mathrm{W}}^2, M_{\mathrm{W}}^2, \theta)}{(k_+^2 - M_{\mathrm{W}}^2 + iM_{\mathrm{W}}\Gamma_{\mathrm{W}})(k_-^2 - M_{\mathrm{W}}^2 + iM_{\mathrm{W}}\Gamma_{\mathrm{W}})} \right|^2 \\ &= \sigma(s, M_{\mathrm{W}}^2, M_{\mathrm{W}}^2) \int_0^s \mathrm{d}k_+^2 \int_0^{(\sqrt{s}-\sqrt{k_+^2})^2} \mathrm{d}k_-^2 C(s, k_+^2, k_-^2)\rho(k_+^2)\rho(k_-^2),\end{aligned} \tag{3.8}$$

where

$$\rho(k^2) = \frac{1}{\pi}\frac{M_{\mathrm{W}}\Gamma_{\mathrm{W}}}{(k^2 - M_{\mathrm{W}}^2)^2 + M_{\mathrm{W}}^2\Gamma_{\mathrm{W}}^2}, \tag{3.9}$$

and the correction factor

$$C(s, k_+^2, k_-^2) = \sqrt{\frac{s^2 - 2s(k_+^2 + k_-^2) + (k_+^2 - k_-^2)^2}{s(s - 4M_{\mathrm{W}}^2)}} \tag{3.10}$$

accounts for the off-shell phase space of W-pair production. A similar formula has been given in Ref. 65. However, since there also the complete resonant matrix elements were treated off shell, that formula is gauge-dependent.

By looking at (3.8) one can easily convince oneself that the finite-width effects do not vanish at very high energies. While for $s \to \infty$ the phase-space correction factor C approaches 1 and the upper limits of the integration goes to infinity, the lower integration limits stay at 0. Consequently part of the distributions $\rho(k_\pm^2)$ is cut out and one obtains

$$\sigma(s) \underset{s\to\infty}{\sim} \sigma(s, M_{\mathrm{W}}^2, M_{\mathrm{W}}^2)\left[1 - \frac{1}{\pi}\arctan\frac{\Gamma_{\mathrm{W}}}{M_{\mathrm{W}}}\right]^2 \tag{3.11}$$

for a constant width. This result differs from the on-shell one by terms of the order $\Gamma_{\mathrm{W}}/M_{\mathrm{W}}$, i.e. -1.7% to be precise. Additional deviations of the same order are obtained

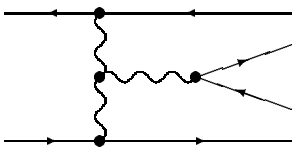

Fig. 16: W-fusion diagram.

by using an invariant-mass-dependent width. Replacing $M_{\mathrm{W}}\Gamma_{\mathrm{W}}$ by $k^2\Gamma_{\mathrm{W}}/M_{\mathrm{W}}$ in (3.9) results in

$$\sigma(s) \underset{s\to\infty}{\sim} \sigma(s, M_{\mathrm{W}}^2, M_{\mathrm{W}}^2)\left[1 - \frac{1}{\pi}\frac{\Gamma_{\mathrm{W}}}{M_{\mathrm{W}}}\left(1 - \log\frac{s}{M_{\mathrm{W}}^2}\right)\right]^2 \tag{3.12}$$

up to terms of order $(\Gamma_{\mathrm{W}}/M_{\mathrm{W}})^2$. In this order this result is only sensitive to the k^2 dependence in the numerator but not in the denominator. This effect is of the order of 6.8% at 1 TeV.

Simple estimates indicate that all non-doubly-resonant contributions are typically suppressed by a factor $\Gamma_{\mathrm{W}}/M_{\mathrm{W}} \approx 2.5\%$ on the cross-section level for each non-resonant W propagator. This is confirmed by explicit calculations[66–68] in the energy range from threshold to 1 TeV, at least for final states involving four different fermions and no electrons or electron neutrinos. A potentially large physical background is due to Z-pair production, which contributes to final states with two fermion–antifermion pairs. However, the corresponding cross-section is smaller by a factor of ~ 10 and can be further reduced by a small-enough cut on the invariant masses of the decay products

$$M_{\mathrm{W}} - \Delta < \sqrt{k_\pm^2} < M_{\mathrm{W}} + \Delta. \tag{3.13}$$

Such a cut typically suppresses a flat background[69] by an additional factor Δ/M_{W}. Nevertheless the non-doubly-resonant contributions have to be taken into account to reach a theoretical accuracy of better than 1%. We note that in particular the background to the lower-statistics final states including electrons will be larger than the above estimates in view of the t-channel W-fusion diagram (see Fig. 16), which is singly-resonant but contains an additional t-channel pole at high energies. Without an invariant-mass cut[68] it amounts to roughly 40% of the resonant contributions at $\sqrt{s} = 500\,\mathrm{GeV}$. By imposing invariant-mass cuts of the order of 10 GeV on both W-boson masses this background can be brought back to the level of 1%. At energies above 1 TeV the background will get larger, even after invariant-mass cuts, because W-pair production will not be the dominant contribution to $\mathrm{e^+e^-} \to 4f$ any more.

Below threshold the doubly-resonant contributions vanish and the singly-resonant ones dominate. This is reflected by the fact that $R_{+-}(M_{\mathrm{W}}^2, M_{\mathrm{W}}^2, \theta)$ becomes undefined because the momenta of the on-shell W bosons would have to be taken complex in order to satisfy energy–momentum conservation and the on-shell conditions. Therefore one is forced to use a different decomposition below threshold that does not involve $R_{+-}(M_{\mathrm{W}}^2, M_{\mathrm{W}}^2, \theta)$. As a consequence one encounters the original poles at $k_\pm^2 = M_{\mathrm{W}}^2$ when approaching the

threshold from below, as can be read off from (3.6) by setting $R_{+-}(M_W^2, M_W^2, \theta)$ equal to zero. Thus the accuracy of the pole scheme is doubtful around threshold.

Similar problems occur also for high energies at the level of the singly-resonant contributions. There exist regions in phase space where even far above threshold $R_+(M_W^2, k_-^2, \theta)$ or $R_-(k_+^2, M_W^2, \theta)$ becomes undefined and has to be put to zero. As a result one obtains poles in the non-resonant contributions. In contrast to the case above this does not imply a breakdown of the pole scheme because the leading doubly-resonant contributions are still well defined. However, putting the non-resonant contributions to zero in those regions, in order to avoid the poles, in general introduces errors of the order Γ_W^2/M_W^2, except of course in the threshold region where the pole scheme has problems anyhow.

A critical discussion of this and other schemes to include the finite-width effects has been given in Ref. 66. None of the presently known schemes is theoretically satisfactory. The advantages of the pole scheme are that it is gauge-invariant, well-defined sufficiently far above threshold, and that it is a natural starting point for the systematic evaluation of the higher-order corrections. Moreover an accurate experimental study of the threshold region at LEP200 seems not very likely.

3.2 Radiative corrections

So far no complete treatment for the $\mathcal{O}(\alpha)$ corrections to off-shell W-pair production has been published. Essentially only the initial-state photonic corrections have been treated so far. These are discussed in the following[j]. In addition we describe a general strategy for the calculation of higher-order corrections using the pole scheme, which is based on own investigations and a recent work of Aeppli, van Oldenborgh and Wyler[70].

3.2.1 Photonic corrections

All published calculations for corrections to off-shell W-pair production that have been done so far cover only part of the photonic corrections, mainly because these are easily treatable and constitute a large part of the radiative corrections. These calculations do not adopt the pole scheme but are, following the lowest-order calculations of Ref. 65, based on the complete resonant diagrams (Fig. 14). Although, as demonstrated above, this approach breaks gauge invariance, it involves the relevant doubly-resonant contributions and an explicit comparison of this treatment with gauge-invariant schemes has shown[66] that at least below 1 TeV the effect of breaking gauge invariance is not of numerical importance if the unitary gauge is used[k]. While this analysis was carried out at lowest order it applies as well to those photonic corrections which are discussed in the following, because these are essentially obtained as gauge-invariant correction factors to the lowest-order cross-section.

From the discussion of the on-shell process we know that initial-state radiation (ISR) yields large corrections originating from the leading collinear logarithms. As will be

[j] There also exists a calculation for the process $e^+e^- \to W^+W^- \to 4f\gamma$ for hard photons (see Sec. 3.2.2).

[k] For off-shell W-pair production and vanishing fermion masses this statement holds in an arbitrary R_ξ gauge, as in this case all ξ-dependent terms drop out.

discussed in Sec. 5 these can be easily obtained by applying the structure-function method. Just in the same way as in the on-shell case the corrections to the off-shell cross-section are calculated by convoluting the lowest-order cross-section with the appropriate structure functions. If one restricts oneself to the leading logarithms this procedure is trivially gauge-invariant if it is applied to a gauge-invariant cross-section. If applied to a gauge-dependent cross-section this gauge dependence should not be enhanced.

The initial-state leading logarithmic corrections are calculated by the Monte-Carlo event-generator WOPPER[71]. As in this program the evolution equations for the structure functions are solved numerically using techniques known from parton-shower algorithms, soft-photon exponentiation and resummation of the leading logarithms from multiple hard-photon emission are automatically taken into account. In Fig. 17 we show the effect of the ISR in the LL approximation on the differential cross-section $\mathrm{d}\sigma/\mathrm{d}\cos\theta^*$ including finite-width effects as obtained from this generator for $\sqrt{s} = 500\,\mathrm{GeV}$, $M_\mathrm{W} = 80.220\,\mathrm{GeV}$, and $\Gamma_\mathrm{W} = 2.084\,\mathrm{GeV}$. One of the W bosons is assumed to decay leptonically, and various schemes to reconstruct the lepton decay angle θ^* are investigated. For the production angle a cut $5^\circ < \theta < 175^\circ$ has been used. For reference Fig. 17 includes in each plot the lowest-order result and a plot where the kinematics of all particles (including the neutrino) are as generated by the Monte Carlo (MC $\rightarrow p_\nu$). The simplest determination of the decay angle θ^*, which was introduced in Ref. 72, makes only use of the energy of the charged lepton in the laboratory system E_Lepton:

$$\cos\theta^* = \left(\frac{2E_\mathrm{Lepton}}{E_\mathrm{Beam}} - 1\right) \Big/ \sqrt{1 - \left(\frac{M_\mathrm{W}}{E_\mathrm{Beam}}\right)^2}. \tag{3.14}$$

As this reconstruction of $\cos\theta^*$ assumes the absence of real-photon radiation, one observes sizeable ISR migration effects from the forward direction to the other angular regions as compared to the lowest-order distribution. As has been discussed in the context of on-shell W-pair production these large migration effects can be reduced by cuts on the hard-photon spectrum or by proper reconstruction. This can be achieved by measuring the missing energy and momentum and using $p_\nu^2 = 0$ and $(p_\nu + p_l)^2 = M_\mathrm{W}^2$.[l] The last condition introduces a small error, which can be controlled by the Monte Carlo. In Fig. 17 we show the result of this reconstruction method with and without an additional cut on the still missing momentum $|(p_\nu + p_\ell + p_X)^2/s - 1| < 0.1$. This cut removes events with hard photons or far off-shell W bosons. While the first case works reasonably well up to a beam-hole size of five degrees, it has problems with poorly reconstructed events for large decay angles at larger beam-hole sizes. These problems can be avoided with the additional cut, which removes only a small fraction of the events. It affects the decay distributions by a constant factor over almost the whole phase and parameter space with respect to the generated distributions[73].

The next step is to include the complete ISR. To this end one has to define it in a way that preserves the $U(1)$ electromagnetic gauge invariance. This is non-trivial because of the presence of the t-channel diagram which involves a non-conserved charge flow in

[l] This still allows in general for two solutions of the neutrino momentum. Out of these the one has been selected for which the square of the sum of all reconstructed final-state momenta is closest to s.

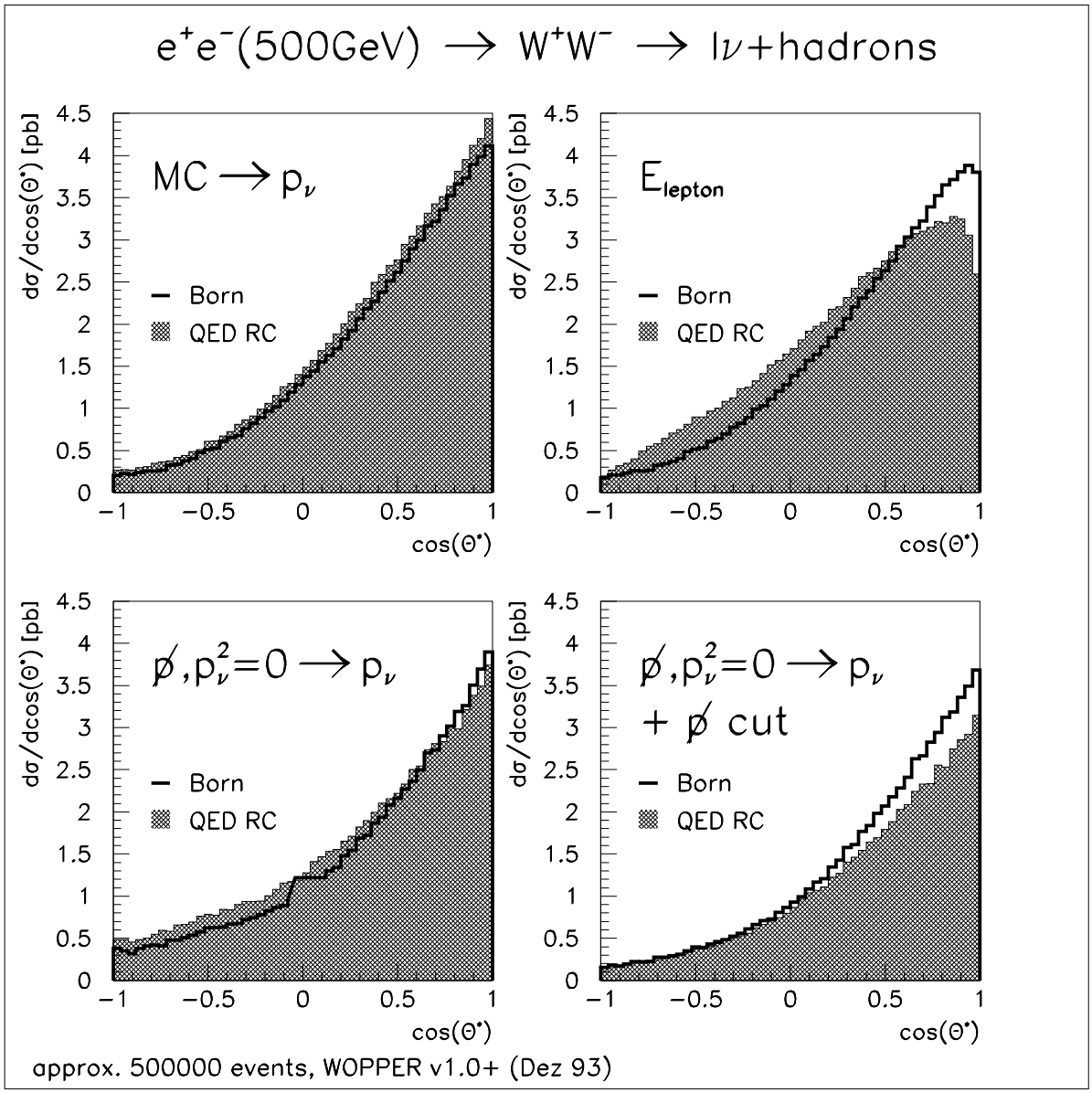

Fig. 17: Decay angular distribution for a W boson decaying leptonically for various reconstruction schemes.

the initial state. One technique to circumvent this problem is the so-called current-splitting technique[74], which amounts to splitting the electrically neutral neutrino in the t-channel diagram into two oppositely flowing leptons each with charge one. One of them is attributed to the initial state to build a continous flow of charge, the other is attributed to the final state to do the same there. The modified ν_e propagator leads to additional real and virtual initial-state photonic diagrams which render the ISR gauge-invariant.

In this way one obtains the usual universal s-channel ISR known from LEP1 plus additional non-universal contributions arising from the t-channel diagrams. The latter are non-factorizing with respect to the lowest-order cross-section, but are screened by a factor $k_+^2 k_-^2/s^2$ to guarantee a unitary behaviour at high energies. Moreover they turn out to be numerically small. The universal ISR contains all leading logarithms and can be supplemented by the known universal higher-order terms[75].

The ISR defined by the current-splitting technique has been implemented into the semi Monte-Carlo program GENTLE[74]. It generates distributions based on compact analytical formulae for $\mathrm{d}^3\sigma/(\mathrm{d}k_+^2\mathrm{d}k_-^2\mathrm{d}s')$ with $s' = s - 2\sqrt{s}E_\gamma$. The total cross-section for W-pair production as obtained from this program is shown in Fig. 18. The figure includes the cross-section for on-shell W bosons in lowest order, and for off-shell W bosons in lowest order and including the universal ISR for $M_\mathrm{W} = 80.220\,\mathrm{GeV}$ and $\Gamma_\mathrm{W} = 2.033\,\mathrm{GeV}$. The effects of the ISR are roughly the same as in the on-shell case. Figure 18 also confirms the before-mentioned fact that the finite-width effects do not vanish at high energies but are about 6.5% at $\sqrt{s} = 1\,\mathrm{TeV}$ for an k^2-dependent width, in agreement with the simple estimate (3.12). The effect of the non-universal initial-state corrections (which is not contained in the figure) is only +0.4%, +0.8% and +1.5% at $\sqrt{s} = 165\,\mathrm{GeV}$, $500\,\mathrm{GeV}$ and $1\,\mathrm{TeV}$, respectively.

In Fig. 19 we show the energy spectrum of the radiated initial-state photons as obtained by GENTLE which is of crucial importance for those determinations of the W mass at LEP200 that involve beam-energy constraints. As explained in the introduction the corresponding shift in the measured W mass is given by $\Delta M_\mathrm{W} \approx (M_\mathrm{W}/\sqrt{s})\langle E_\gamma\rangle$ and amounts to 890 MeV and 533 MeV for $\sqrt{s} = 190\,\mathrm{GeV}$ and $176\,\mathrm{GeV}$, respectively[74]. These numbers include higher-order corrections. The contribution of those higher-order corrections that are not covered by soft-photon exponentiation is 27 MeV and 14 MeV for $\sqrt{s} = 190\,\mathrm{GeV}$ and $176\,\mathrm{GeV}$, respectively, mainly caused by corrections of the leading-log type.

Another potentially large photonic correction is due to the Coulomb singularity in the threshold region, which has been discussed for off-shell W-pair production in Refs. 76 and 77. It originates from the IR limit and at one-loop it emerges from a single IR-singular scalar three-point function and a related IR-singular scalar four-point function, the IR-singular part of which is just a scaled version of the one contained in that three-point function (see Fig. 20). The gauge invariance of the coefficients of these two scalar functions allows us to include the width in a gauge-invariant way. Thus one obtaines a gauge-invariant correction factor to the lowest-order cross-section resulting from the doubly-resonant diagrams:

$$\sigma_\mathrm{Coul} = \sigma_\mathrm{Born}\,\frac{\alpha\pi}{2\bar{\beta}}\left[1 - \frac{2}{\pi}\arctan\left(\frac{|\beta_M + \Delta|^2 - \bar{\beta}^2}{2\bar{\beta}\,\mathrm{Im}\,\beta_M}\right)\right], \tag{3.15}$$

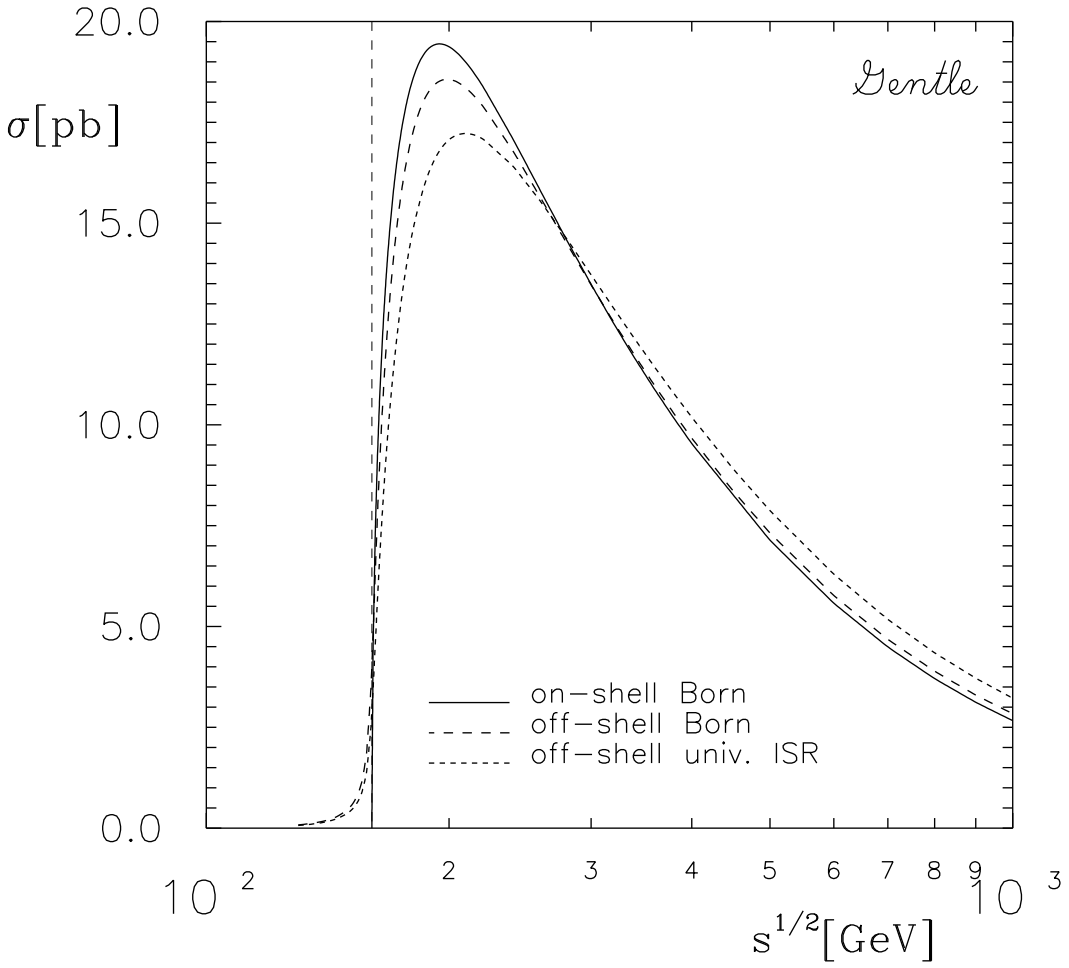

Fig. 18: Total cross-section for W-pair production in lowest order and including universal ISR corrections.

with

$$\begin{aligned}
\bar{\beta} &= \frac{1}{s}\sqrt{s^2 - 2s(k_+^2 + k_-^2) + (k_+^2 - k_-^2)^2}, \\
\beta_M &= \sqrt{1 - 4M^2/s}, \qquad M^2 = M_{\mathrm{W}}^2 - iM_{\mathrm{W}}\Gamma_{\mathrm{W}} - i\epsilon, \\
\Delta &= \frac{|k_+^2 - k_-^2|}{s},
\end{aligned} \tag{3.16}$$

and $-\pi/2 < \arctan y < \pi/2$. Here $\bar{\beta}$ is the average velocity of the W bosons in their centre-of-mass system. Equation (3.15) only refers to the Coulomb singularity; the finite remnants of the above mentioned three-point function, containing also the IR divergence, have been left out. From (3.15) we obtain the usual on-shell Coulomb singularity for stable W bosons and $\bar{\beta} \neq 0$ by first going on-shell, i.e. $\Delta = 0$ and $\bar{\beta}^2 = \mathrm{Re}\,\beta_M^2 = \beta^2$, and

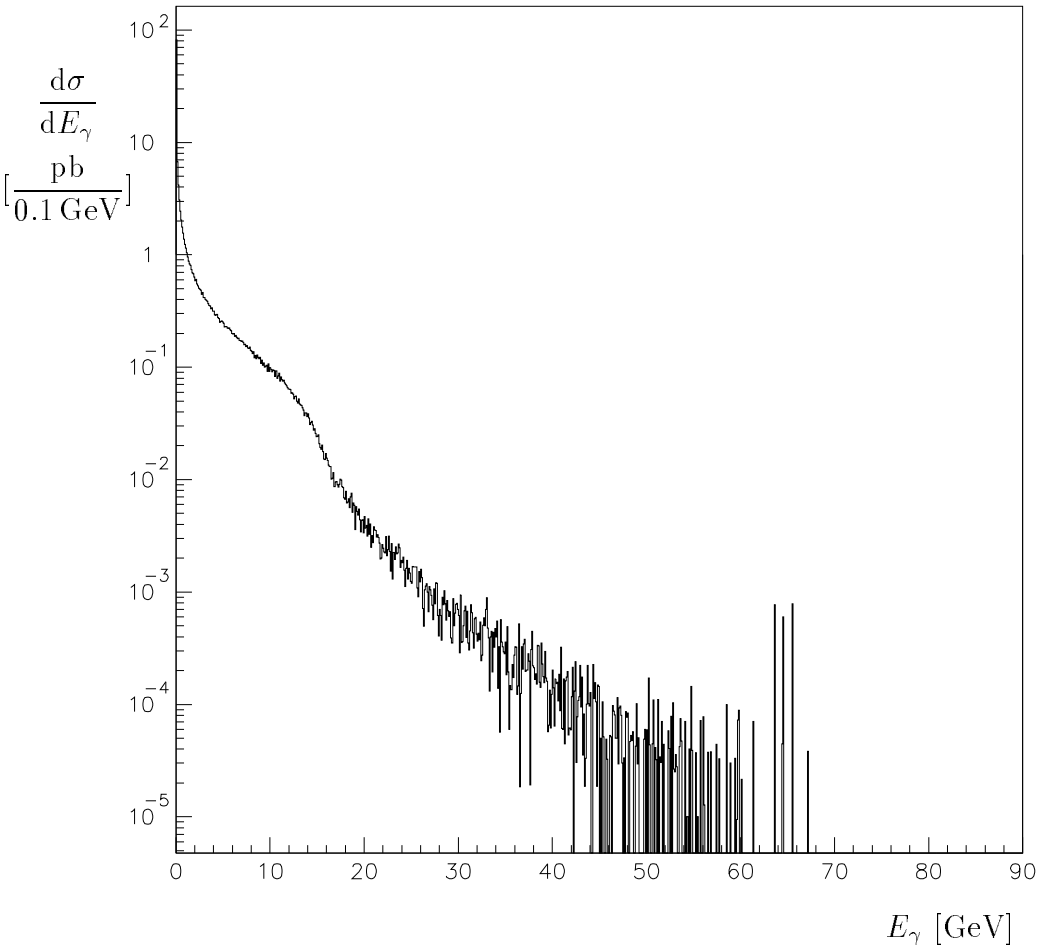

Fig. 19: Energy spectrum of initial-state photons for $\sqrt{s} = 176\,\mathrm{GeV}$.

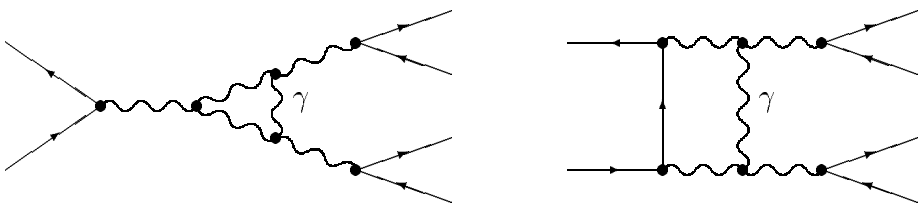

Fig. 20: Diagrams that contribute to the Coulomb singularity.

subsequently taking the limit $\Gamma_{\mathrm{W}} \to 0$. Note that in this limit the otherwise negligible $i\epsilon$ in M^2 becomes relevant.

In contrast to the on-shell case there are various effects present in (3.15) that effectively truncate the range of the Coulomb interaction. The presence of a Coulomb singularity requires that $\bar{\beta}$ be at least of the same order of magnitude as Δ and $|\beta_M|$, which is bounded by the W width according to $|\beta_M| \gtrsim \sqrt{\Gamma_{\mathrm{W}}/M_{\mathrm{W}}}$. This confirms the intuitive argument[76] that the Coulomb singularity is modified substantially by finite-width effects if the characteristic time of the Coulomb interaction ($t_{\mathrm{Coul}} \sim 1/[\bar{\beta}^2 M_{\mathrm{W}}]$) is of the same order as or larger than the typical decay time ($t_\tau \sim 1/\Gamma_{\mathrm{W}}$) of the W bosons. While the effect of the finite W width is contained in β_M, the off-shellness shows up in Δ and in the difference $|\beta_M^2 - \bar{\beta}^2|$, which effectively involves $|k_+^2 + k_-^2 - 2M_{\mathrm{W}}^2|/s$. This is in agreement with the argument[77] that the off-shellness of the virtual W bosons will affect the Coulomb singularity, if the typical times ($t_{\mathrm{OFS}}^{\pm} \sim 1/|k_{\pm,0} - \sqrt{M_{\mathrm{W}}^2 + \vec{k}_\pm^2}| \sim 1/|\sqrt{k_\pm^2} - M_{\mathrm{W}}|$) for which off-shell $\mathrm{W}^\pm$ bosons with virtualities $k_\pm^2$, energies $k_{\pm,0}$ and momenta $\vec{k}_\pm$ exist is of the same order as or smaller than t_{Coul}.

In the case of the total cross-section for the production of off-shell W bosons the Coulomb singularity gives rise to a correction factor which reaches its maximal value of $\sim 5.7\%$ at the nominal threshold and drops smoothly below and above threshold. While it amounts to 2.4% at $\sqrt{s} = 176\,\mathrm{GeV}$ it is only 1.8% at 190 GeV. The corresponding effect on the reconstructed W mass, resulting from the pronounced energy dependence, leads to a shift at the level of 5–10 MeV. Because of the fact that the Coulomb singularity is screened by the off-shell effects, the finite width of the W bosons and relativistic effects, higher-order corrections related to the Coulomb singularity are not important for off-shell W-pair production. Moreover, bound states of the two W bosons do not have the time to form because of the finite-width effects. The typical time scale needed for the formation of a bound state $t_{\mathrm{form}} \sim 1/(\alpha^2 M_{\mathrm{W}})$ is much larger than the typical decay time t_τ.

3.2.2 General approach to radiative corrections within the pole scheme

As discussed in Sec. 3.1, sufficiently far above threshold the doubly-resonant contributions dominate the cross-sections for W-pair production and all others are suppressed by $\Gamma_{\mathrm{W}}/M_{\mathrm{W}}$ at least[m] and thus formally of relative order α. While the suppressed contributions are certainly relevant at lowest order, they are in general negligible as far as the $\mathcal{O}(\alpha)$ corrections are concerned. Exceptions are enhanced corrections such as leading logarithms, which can usually be treated by renormalization group methods and which can thus simply be combined with the lowest-order cross-section.

Thus, as has been argued in Ref. 70, for an $\mathcal{O}(\alpha)$ calculation of the process $\mathrm{e}^+\mathrm{e}^- \to 4f$ one needs the following ingredients: the physical W-width to $\mathcal{O}(\alpha^2)$, the doubly-resonant contributions to $\mathcal{O}(\alpha)$, including the parts of the W self-energy that have not been resummed into the propagators, and the non-doubly-resonant contributions in lowest order. In the following we focus on the doubly-resonant $\mathcal{O}(\alpha)$ contributions. In higher orders there are two different sources of double-pole terms, the factorizable contributions and

[m] Beware of the fact that there might be enhanced contributions in exclusive channels as e.g. the W-fusion diagram for final-state electrons.

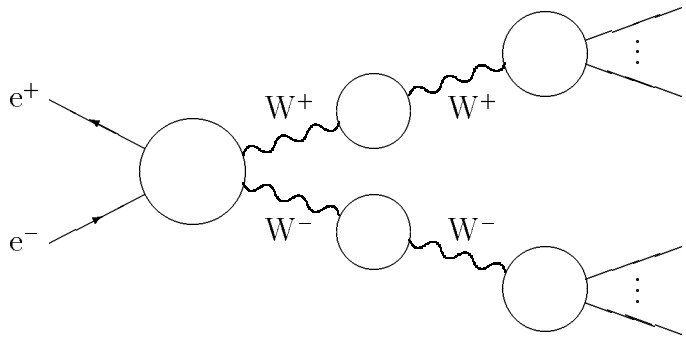

Fig. 21: General structure of factorizable diagrams.

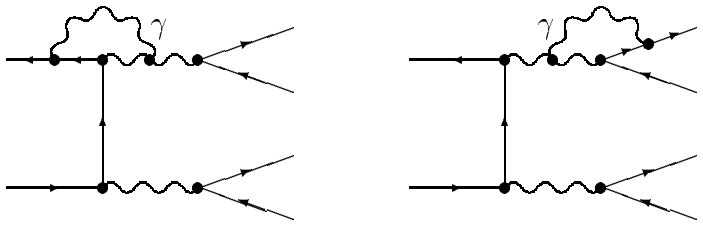

Fig. 22: Examples of factorizable IR-singular corrections.

the non-factorizable photonic corrections. The photonic corrections, i.e. those diagrams which result from attaching an additional virtual photon to the lowest-order diagrams, are not separately gauge-invariant. However, as the sum of photonic and non-photonic corrections is gauge-invariant one can treat both classes separately as long as one uses the same gauge for both of them.

The factorizable corrections consist of all those loop diagrams where the W-production and decay parts can be separated by cutting the two resonant W propagators, i.e. the ones that are reducible at both W lines (Fig. 21), and the corresponding real bremsstrahlung contributions. They contain the resonant W propagators explicitly and can be related to the on-shell matrix elements according to (3.7). At $\mathcal{O}(\alpha)$ they comprise the complete resonant non-photonic corrections, the most important resonant photonic corrections, in particular those involving leading logarithms, and the QCD corrections related to the decay of the W bosons. The factorizable corrections can be simply incorporated into the convolution formula (3.8).

The factorizable contributions involve amongst others diagrams where a photon is exchanged between a resonant W boson and one of the external fermions or between both resonant W bosons (see Figs. 22 and 20). These are IR-singular in the on-shell limit and give rise to terms proportional to $\log(k_\pm^2 - M_\mathrm{W}^2)/(k_\pm^2 - M_\mathrm{W}^2)$ in the off-shell case, which cause the residue to be undefined. However, these terms are completely contained in scalar 3-point functions involving one or two virtual W bosons and one virtual photon. As the contributions of these 3-point functions are gauge-invariant one can calculate them for complex W-boson masses without violating gauge invariance. For the IR-singular higher-

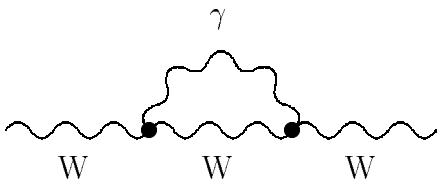

Fig. 23: Contribution to the W self-energy that gives rise to IR-singularities for on-shell W bosons.

point functions one simply subtracts the appropriate suitably-scaled IR-singular 3-point function and adds the same for complex W masses. For the remaining contributions that do not involve those 3-point functions one can still take the residue. Moreover, the prefactors of the IR-divergent scalar integrals can be calculated in the on-shell limit. Thus one obtains a well-defined gauge-invariant result. Note that the IR-singularities that are related to the W-bosons are now regulated by the off-shell momenta and the finite width of the W bosons. It is important that the same regularization is also used for the corresponding bremsstrahlung corrections, because otherwise spurious contributions might result from the mismatch of the different regularizations.

As discussed in Ref. 70, there are a couple of variants to the method just described. One is to use complex masses in the divergent logarithms only. In this way one would for instance miss the effects related to the Coulomb singularity discussed in the previous subsection. The Coulomb singularity also originates from the IR limit and is completely contained in the scalar integrals. As it is very sensitive to screening effects caused by the off-shellness and the decay of the W bosons it is important to take these effects into account. The same holds for all other corrections that do not behave smoothly when going from the off-shell to the on-shell cross-section.

The other extreme variant, which will not miss such effects, is to use a complex mass everywhere in the scalar functions. This introduces errors that are of higher order in α. As the contributions of individual scalar functions are separately gauge-invariant, one can even leave the momenta off-shell in the non-divergent parts, i.e. not take the residue. As long as there are no strong arguments for one of these variants one should consider the differences as some kind of estimate on the theoretical uncertainty of the off-shell calculations.

The factorizable contributions contain also W-self-energy insertions (see Fig. 21). As the finite W-width in the denominators of the propagators results from a resummation of parts of these self-energy insertions, these parts have to be subtracted in order to avoid double-counting. After W-mass renormalization these self-energy insertions result in correction factors of the form $[f(k_\pm^2)-f(M_\mathrm{W}^2)]/(k_\pm^2-M_\mathrm{W}^2)$, which are finite for $k_\pm^2 = M_\mathrm{W}^2$ apart from the IR-singular contribution of the photon to the W self-energy (see Fig. 23). This on-shell IR-singular term can be treated in the same way as the IR-singular 3-point functions above. The IR-singular combination of 2-point functions is just a special case of an IR-singular 3-point function:

$$C_0(k_\pm^2, 0, k_\pm^2, 0, M_\mathrm{W}, M_\mathrm{W}) = \frac{B_0(M_\mathrm{W}^2, M_\mathrm{W}, 0) - B_0(k_\pm^2, M_\mathrm{W}, 0)}{k_\pm^2 - M_\mathrm{W}^2}. \tag{3.17}$$

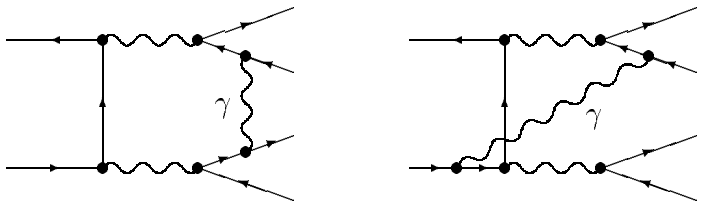

Fig. 24: Examples of non-factorizable resonant photonic corrections.

Feynman diagrams that are not reducible at both W lines do in general not yield doubly-resonant contributions. This does, however, not hold for non-factorizable contributions resulting from diagrams where a virtual photon is exchanged between the two decay parts, or between the production and a decay part of the diagram (see Fig. 24). The corresponding $\mathcal{O}(\alpha_s)$ diagrams involving gluons do not contribute owing to their colour structure. The non-factorizable diagrams contain resonant contributions related to the IR limit, i.e. to those parts of the integration region where both the energy and the momentum of the virtual photon are zero.

The resonant diagrams can be easily obtained through power counting. To this end one considers the loop integrals for the case that the W-momenta are on shell and determines the degree of the IR-singularity. This degree minus four yields the resonance behaviour of the integral, i.e. the integral is doubly-resonant if the degree of the IR divergence is six, it is singly resonant if the degree is five and it is nonresonant if the degree is four. Whereas the photon momenta can be safely neglected in the numerator and in those denominators that do not contribute to the IR singularity, they have to be kept in the other denominators, in particular also in those that correspond to resonant W bosons in the IR limit (cf. tail effects at LEP1).

The non-factorizable doubly-resonant diagrams do not just involve a product of two resonant W propagators, but also polynomials of k_+^2, k_-^2 and M_{W}^2 in the denominator with a double zero for $k_+^2 = k_-^2 = M_{\mathrm{W}}^2$. They also yield contributions of the form $\log(k_\pm^2 - M_{\mathrm{W}}^2)/(k_\pm^2 - M_{\mathrm{W}}^2)$, which have to be treated by evaluating the corresponding scalar integrals for complex W masses. As the non-factorizable doubly-resonant diagrams are associated with scalar functions that do not appear in the factorizable contributions, they are separately gauge-invariant. For the evaluation of these contributions essentially the same remarks apply as to the on-shell IR-singular contributions discussed above.

We now discuss the real bremsstrahlung corrections for off-shell W-pair production. As already mentioned above, the soft-bremsstrahlung contributions have to be regularized in the same way as the corresponding virtual photonic corrections. This can be most easily done on the level of squared diagrams as there is a one–to–one correspondence between squared bremsstrahlung diagrams and photonic loop-diagrams. Note that in this way a photon emitted from a resonant W-boson (Fig. 25) is counted as emitted from the production or decay part of the diagram if one considers its interference with a diagram where the photon is emitted from the production or the corresponding decay part, respectively. The resulting soft-bremsstrahlung integrals have the same resonance structure as the corresponding virtual integrals and can be treated analogously.

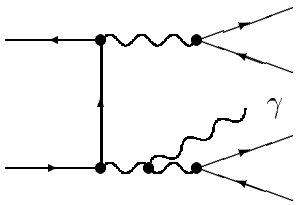

Fig. 25: Feynman diagram with a real photon attached to the W boson.

If the emitted photons are hard the diagrams where the photon is emitted from the resonant internal W bosons contain three W propagators (Fig. 25). The corresponding diagrams get doubly-resonant in two different regions of phase space and both contributions have to be extracted to get the double-pole terms[n].

The non-factorizable interference effects only yield doubly-resonant contributions for sufficiently-soft photons[78] $k_{\gamma 0} \lesssim \Gamma_{\mathrm{W}}$. This is caused by the fact that for hard photons the W bosons have resonances at different positions in the two interfering matrix elements. The interference contribution can be estimated to be proportional to $\Gamma_{\mathrm{W}}^2/(k_{\gamma 0}^2 + \Gamma_{\mathrm{W}}^2)$, i.e. the harder the photon is the stronger is the suppression. In other words, for $k_{\gamma 0} \gg \Gamma_{\mathrm{W}}$ the relative phases of the emission during production and decay are large, and when averaging over all decay times the interferences between those emissions will average to zero.

When combining the real and virtual corrections the doubly-resonant non-factorizable contributions cancel in fully inclusive cross-sections[78,79]. This can be viewed as a generalization of the cancellation of the IR-singularities. For differential distributions, however, this cancellation does not take place completely and the corresponding contributions have to be evaluated.

In Ref. 80 a different treatment of the diagrams involving the emission of a photon from an internal W-boson line has been introduced. By performing a partial-fraction decomposition of the product of the two W propagators separated by the photon

$$\begin{aligned}
&\frac{1}{(k_\pm^2 - M_{\mathrm{W}}^2 + iM_{\mathrm{W}}\Gamma_{\mathrm{W}})[(k_\pm - k_\gamma)^2 - M_{\mathrm{W}}^2 + iM_{\mathrm{W}}\Gamma_{\mathrm{W}}]} \\
&\quad = \frac{1}{2(k_\gamma \cdot k_\pm)}\left(\frac{1}{(k_\pm - k_\gamma)^2 - M_{\mathrm{W}}^2 + iM_{\mathrm{W}}\Gamma_{\mathrm{W}}} - \frac{1}{k_\pm^2 - M_{\mathrm{W}}^2 + iM_{\mathrm{W}}\Gamma_{\mathrm{W}}}\right), \qquad (3.18)
\end{aligned}$$

one obtains a sum of two resonant W propagators multiplied by an ordinary soft-photon denominator. Thus one obtains a gauge-invariant split-up of the matrix-element in a contribution where the photon is emitted from the production part, and another one where it is emitted from the decay part. The squares of the two contributions yield exactly the bremsstrahlung corrections to the on-shell production and decay processes, while the interference yields a non-factorizable contribution. The same split-up can be done for the corresponding virtual corrections. It has the advantage that one can directly reproduce the on-shell contributions. Compared to the above treatment it shifts part of the factorizable contributions to the non-factorizable ones and thus enlarges the number of different

[n] Owing to hard-photon radiation associated with the W-pair production, which can reduce the available energy for the $\mathrm{W^+W^-}$ system to or even below the corresponding threshold, the problems of the pole scheme at threshold become to a certain extent also relevant at higher energies.

contributions to be calculated. While in the pole-scheme treatment both propagators in the first line of (3.18) are kept exact and the on-shell condition for the resonant W boson is only used in the rest of the diagram, the treatment of Ref. 80 corresponds to splitting the diagram into two contributions, in each of which only one of the W propagators is kept exact and the on-shell condition is used in the other one. The difference is accounted for by extra interference contributions that are only present in the latter scheme.

The doubly-resonant hard-photonic corrections have been evaluated by calculating the complete resonant diagrams for $e^+e^- \to 4f\gamma$ via two W bosons using spinor techniques and performing the phase-space integrations with a Monte-Carlo integration program[67]. It turned out that for the total cross-section the results can be well described by the on-shell contributions if one takes into account the photon emission both during production and decay. This shows that the hierarchy introduced in the pole scheme works well for the total cross-section and, moreover, that in this case the interference contributions between production and decay are small.

4 The Width of the W Boson

As is evident from the discussion in the last chapter, the width of the W boson is a crucial ingredient for the W-pair production cross-section, especially in the threshold region. Moreover, the branching ratios enter the cross-sections for definite fermions in the final state.

But the total and partial W widths are not only needed as input parameters for the theoretical prediction and the experimental analysis, they can also serve to measure fundamental physical parameters. The leptonic partial widths allow a test on lepton universality, and the hadronic partial widths can serve to determine the quark-mixing-matrix elements[19]. The expected experimental error for Γ^{W} is about 7% for the total width[18] and at the few per-cent level for the branching ratios[81].

4.1 The W-boson width in lowest order

The W width is dominated by decays into fermion–antifermion pairs. In lowest order the partial width for the decay of a W boson into two fermions with masses m_{f_i} and $m_{f'_j}$ (i,j denote the generation index and f, f' stand for u, d or ν, l) is given by

$$\Gamma^{\mathrm{W}f_i f'_j}_{\mathrm{Born}} = N_{\mathrm{C}}^f \frac{\alpha}{6} \frac{M_{\mathrm{W}}}{2s_{\mathrm{W}}^2} |V_{ij}|^2 \left[1 - \frac{m_{f_i}^2 + m_{f'_j}^2}{2M_{\mathrm{W}}^2} - \frac{(m_{f_i}^2 - m_{f'_j}^2)^2}{2M_{\mathrm{W}}^4} \right] \times \frac{\sqrt{\left(M_{\mathrm{W}}^2 - (m_{f_i} + m_{f'_j})^2\right)\left(M_{\mathrm{W}}^2 - (m_{f_i} - m_{f'_j})^2\right)}}{M_{\mathrm{W}}^2}. \tag{4.1}$$

For leptonic decays the mixing matrix is diagonal ($V_{ij} = \delta_{ij}$) and the colour factor N_{C}^f equals one. For decays into quarks there is a non-trivial quark mixing matrix and $N_{\mathrm{C}}^f = 3$.

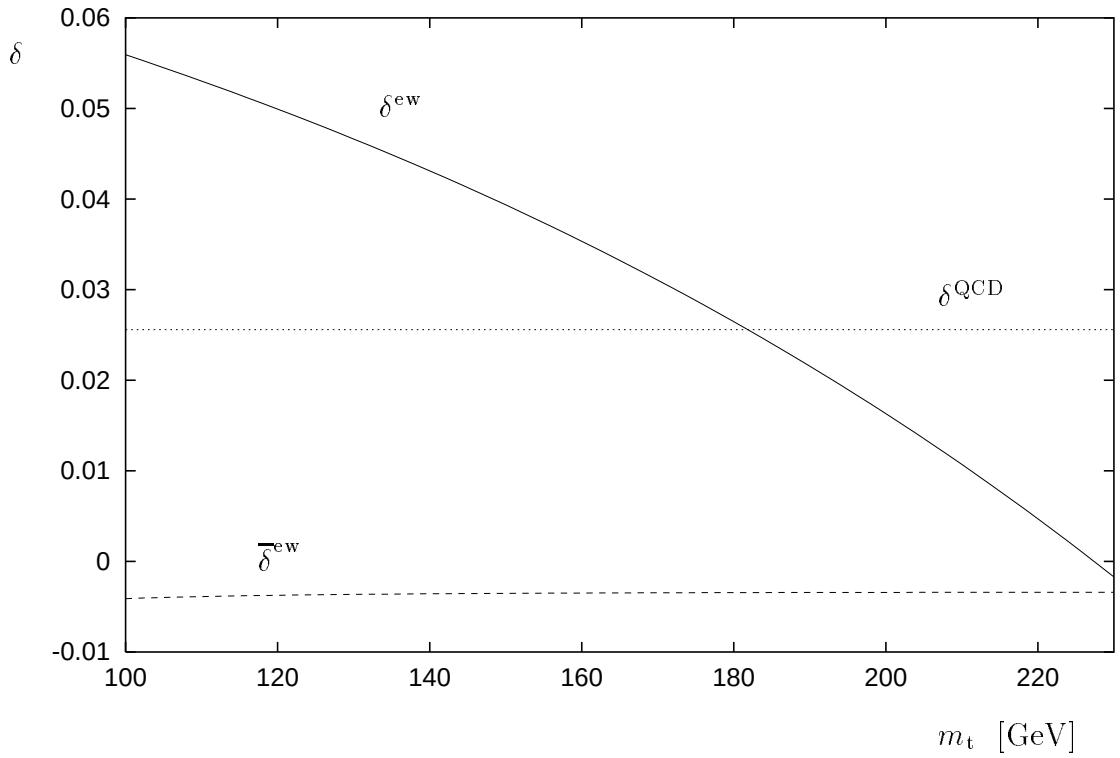

Fig. 26: Electroweak radiative corrections $\delta^{\rm ew}$ and $\bar{\delta}^{\rm ew}$ and QCD corrections $\delta^{\rm QCD}$ to the total W width $\Gamma^{\rm W}$ versus the top mass.

The total width is obtained as a sum over the partial fermionic decay widths with $m_{f_i} + m_{f'_j} < M_{\rm W}$

$$\Gamma^{\rm W}_{\rm Born} = \sum_{i,j} \Gamma^{{\rm W}{\rm u}_i{\rm d}_j}_{\rm Born} + \sum_i \Gamma^{{\rm W}\nu_i{\rm l}_i}_{\rm Born}. \tag{4.2}$$

quark masses are small compared to $M_{\rm W}$, the fermion-mass effects are small for the W decay. If we neglect them we obtain the simple formulae

$$\Gamma^{{\rm W}f_i f'_j}_{\rm Born} = N^f_{\rm C} \frac{\alpha}{6} \frac{M_{\rm W}}{2s^2_{\rm W}} |V_{ij}|^2, \qquad \Gamma^{\rm W}_{\rm Born} \approx \frac{3\alpha}{2} \frac{M_{\rm W}}{2s^2_{\rm W}}. \tag{4.3}$$

4.2 Higher-order corrections to $\Gamma^{\rm W}$

The electroweak and QCD radiative corrections for decays into massless fermions ($m_f \ll M_{\rm W}$) have been calculated in Refs. 82–84. The full one-loop electroweak and QCD corrections, together with the complete photonic and gluonic bremsstrahlung, were evaluated for arbitrary finite fermion masses in Ref. 85. The various calculations are in good agreement.

The relative corrections to the total W-boson decay width are shown in Fig. 26. The electroweak corrections in the on-shell scheme $\delta^{\rm ew} = \Gamma^{\rm W}/\Gamma^{\rm W}_{\rm Born} - 1$ are large and strongly $m_{\rm t}$ dependent. This behaviour arises from the fermionic contributions to the ρ parameter which contain terms $\propto \alpha\, m^2_{\rm t}/M^2_{\rm W}$. These and the large corrections associated with the running of α can be easily accounted for by parametrizing the lowest-order width in terms

of G_μ and $M_{\rm W}$ instead of α and $s_{\rm W}^2$. The width in this parametrization $\overline{\Gamma}^{\rm W}$ is related to the width in the on-shell parametrization $\Gamma^{\rm W}$ by

$$\overline{\Gamma}^{\rm W} = \Gamma^{\rm W}_{\rm Born} \frac{1+\delta^{\rm ew}-\Delta r^{\text{1-loop}}}{1-\Delta r} = \overline{\Gamma}^{\rm W}_{\rm Born}(1+\delta^{\rm ew}-\Delta r^{\text{1-loop}}) = \overline{\Gamma}^{\rm W}_{\rm Born}(1+\overline{\delta}^{\rm ew}). \tag{4.4}$$

In this way one automatically takes into account the leading higher-order corrections associated with the running of α and the ρ parameter (terms $\propto \alpha^2 m_{\rm t}^4/M_{\rm W}^4$). As can be seen from Fig. 26 the electroweak corrections with respect to the parametrization with G_μ, $\bar{\delta}^{\rm ew}$, depend only weakly on $m_{\rm t}$ and remain below 0.5% for the total width. The QCD corrections $\delta^{\rm QCD}$ are practically constant and equal to $2\alpha_s(M_{\rm W}^2)/(3\pi)$, their value for zero fermion masses. For the numerical evaluation we use $\alpha_s(M_{\rm W}^2) = 0.12$.

As a consequence we obtain the following improved Born approximation for the total and partial widths[86]

$$\begin{aligned}
\Gamma^{{\rm W}\nu_i{\rm l}_i} &\approx \overline{\Gamma}^{{\rm W}\nu_i{\rm l}_i}_{\rm Born} = \frac{G_\mu M_{\rm W}^3}{6\sqrt{2}\pi}, \\
\Gamma^{{\rm W u}_i{\rm d}_j} &\approx \overline{\Gamma}^{{\rm W u}_i{\rm d}_j}_{\rm Born}\left(1+\frac{\alpha_s(M_{\rm W}^2)}{\pi}\right) = \frac{G_\mu M_{\rm W}^3}{2\sqrt{2}\pi}|V_{ij}|^2\left(1+\frac{\alpha_s(M_{\rm W}^2)}{\pi}\right), \\
\Gamma^{\rm W} &\approx \overline{\Gamma}^{\rm W}_{\rm Born}\left(1+\frac{2\alpha_s(M_{\rm W}^2)}{3\pi}\right) = \frac{3G_\mu M_{\rm W}^3}{2\sqrt{2}\pi}\left(1+\frac{2\alpha_s(M_{\rm W}^2)}{3\pi}\right).
\end{aligned} \tag{4.5}$$

In Tab. 8 we compare the improved Born approximation (4.5) for the partial and total widths with the lowest-order widths, the widths including the complete first-order and leading higher-order corrections for finite fermion masses, and the same for vanishing fermion masses. The effects of the fermion masses, which are of the order $m_f^2/M_{\rm W}^2$, are below 0.3%. Consequently the exact numerical values for the masses of the external fermions are irrelevant. The improved Born approximation reproduces the exact results within 0.4% (0.6% for the decays into a b-quark). The branching ratios derived from (4.5), which depend only on α_s and V_{ij}, agree numerically within 0.1% with those obtained from the full one-loop results.

For α, G_F and M_Z fixed a variation of $m_{\rm t}$ between 120 and 210 GeV affects the total and partial widths by $\sim 2.5\%$, a variation of $M_{\rm H}$ between 60 and 1000 GeV by $\sim 0.8\%$. This is essentially due to the variation of $M_{\rm W}$, which is the only source of the $m_{\rm t}$ and $M_{\rm H}$ dependence of the improved Born approximation.

5 The Structure-Function Method for Calculating QED Corrections

As pointed out in the previous sections, the virtual and real corrections reveal the presence of large logarithmic QED effects of the form $\alpha L/\pi \equiv (\alpha/\pi)\log(Q^2/m_{\rm e}^2)$ with $Q^2 \gg m_{\rm e}^2$. They arise when photons or light fermions are radiated off in the direction of incoming or outgoing light particles[87,88], provided the momentum of the latter is kept fixed (exclusive)[88]. In a massless theory these large logarithms would show up as collinear divergences (like in QCD), but in the SM the masses of the particles act as natural cut-offs.

	Born $m_f \neq 0$	complete $m_f \neq 0$	complete $m_f = 0$	IBA ($m_f = 0$)	Branching ratio
$\Gamma(\mathrm{W} \to \mathrm{e}\nu_\mathrm{e})$	0.2265	0.2258	0.2258	0.2265	0.1084
$\Gamma(\mathrm{W} \to \mu\nu_\mu)$	0.2265	0.2258	0.2258	0.2265	0.1084
$\Gamma(\mathrm{W} \to \tau\nu_\tau)$	0.2264	0.2257	0.2258	0.2265	0.1083
$\Gamma(\mathrm{W} \to \mathrm{lep.})$	0.6795	0.6773	0.6775	0.6796	0.3251
$\Gamma(\mathrm{W} \to \mathrm{ud})$	0.6467	0.6691	0.6691	0.6714	0.3211
$\Gamma(\mathrm{W} \to \mathrm{us}) \times 10$	0.3289	0.3403	0.3403	0.3415	0.0163
$\Gamma(\mathrm{W} \to \mathrm{ub}) \times 10^4$	0.3315	0.3437	0.3445	0.3457	0.00002
$\Gamma(\mathrm{W} \to \mathrm{cd}) \times 10$	0.3290	0.3405	0.3406	0.3418	0.0163
$\Gamma(\mathrm{W} \to \mathrm{cs})$	0.6449	0.6675	0.6676	0.6699	0.3204
$\Gamma(\mathrm{W} \to \mathrm{cb}) \times 10^2$	0.1431	0.1484	0.1488	0.1493	0.0007
$\Gamma(\mathrm{W} \to \mathrm{had.})$	1.3589	1.4062	1.4063	1.4112	0.6749
$\Gamma(\mathrm{W} \to \mathrm{all})$	2.0384	2.0835	2.0837	2.0909	

Tab. 8: Partial and total W-decay widths Γ^W in different approximations given in GeV.

The fact that they can nevertheless give rise to sizeable corrections is due to the difference in scale between the mass of the radiating particle and its energy. This is illustrated by considering the propagator P of a light particle after photon emission

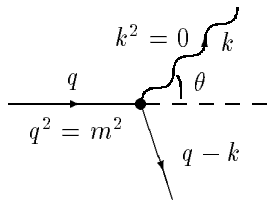

$$\longrightarrow \quad P = \frac{1}{(q-k)^2 - m^2} \overset{q_0 \gg m}{\sim} \frac{-1}{2q_0 k_0 \left[1 - (1 - m^2/2q_0^2)\cos\theta\right]}.$$

In the limit $m \to 0$ this propagator gives rise to a pole at $\cos\theta = 1$. For finite m it yields large logarithmic terms of the form $\log(q_0^2/m^2)$ when the photon momentum is integrated over (inclusive photon). A consequence of the direct relation between the large QED logarithms and collinear divergences is that they are controlled by renormalization group equations and that they are universal, i.e. they are process-independent. They can be calculated using the so-called structure-function method[60], taken over from QCD. This procedure also allows the inclusion of soft-photon effects to all orders by means of exponentiation.

The structure-function method is based on the mass-factorization theorem (see Fig. 27):

$$s^4 \frac{\mathrm{d}^4\sigma_{\mathrm{e^+e^-}\to\mathrm{W^+W^-}X}}{\mathrm{d}t_1\mathrm{d}u_1\mathrm{d}t_2\mathrm{d}u_2} = \int_0^1 \frac{\mathrm{d}x_+}{x_+^2}\int_0^1 \frac{\mathrm{d}x_-}{x_-^2}\Gamma_{i\mathrm{e^+}}(x_+,Q^2)\Gamma_{j\mathrm{e^-}}(x_-,Q^2)\hat{s}^4\frac{\mathrm{d}^4\hat{\sigma}_{ij\to\mathrm{W^+W^-}X'}}{\mathrm{d}\hat{t}_1\mathrm{d}\hat{u}_1\mathrm{d}\hat{t}_2\mathrm{d}\hat{u}_2}(Q^2), \tag{5.1}$$

which links the cross-section $\sigma_{\mathrm{e^+e^-}\to\mathrm{W^+W^-}X}$, where X indicates an arbitrary number of undetected particles, to the hard scattering cross-section $\hat{\sigma}_{ij\to\mathrm{W^+W^-}X'}$ which is free of the

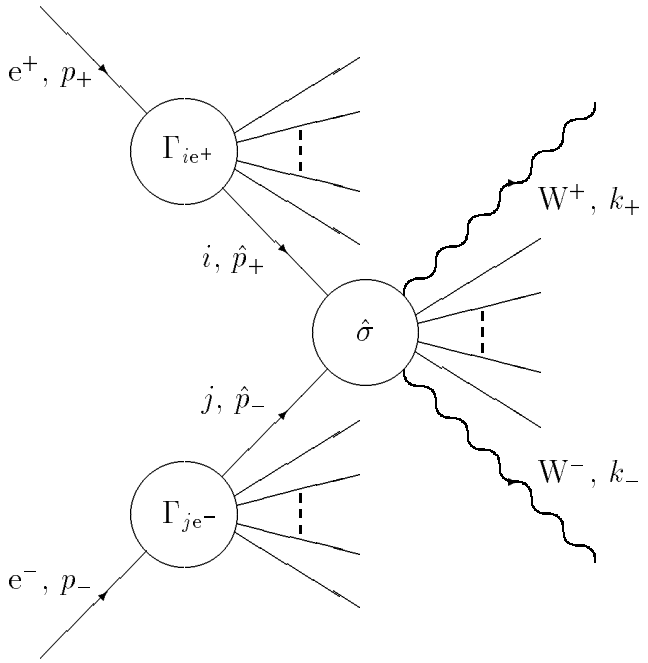

Fig. 27: Initial-state collinear radiation in $e^+e^- \to W^+W^-$. The unlabeled external lines represent an arbitrary number of undetected (inclusive) particles.

large collinear logarithms[o]. The indices i, j represent all light-particle transitions allowed by QED (e.g. $\gamma, e^\pm, \mu^\pm, \cdots$). Furthermore we have defined

$$\begin{aligned} t_1 &\equiv (p_- - k_-)^2 - M_W^2, & u_1 &\equiv (p_+ - k_-)^2 - M_W^2, \\ t_2 &\equiv (p_+ - k_+)^2 - M_W^2, & u_2 &\equiv (p_- - k_+)^2 - M_W^2. \end{aligned} \tag{5.2}$$

Analogously their hatted counterparts are given by the same expressions with $p_\pm$ replaced by $\hat{p}_\pm = x_\pm p_\pm$. It should be noted that (5.1) allows the implementation of various cuts on the energies and angles of the produced W bosons, and that it can be used to extract more commonly used distributions [like $\mathrm{d}\sigma/(\mathrm{d}\cos\theta_+)$] by supplying the appropriate Jacobians[61]. The splitting functions Γ_{ij} describe 'mass singular' initial-state collinear radiation and represent the probability of finding in the parent particle j at the scale Q^2 a particle i with fraction x of longitudinal momentum. So $(1-x)$ denotes the fraction of energy carried away by collinear radiation. All large collinear logarithms are contained in the splitting functions, which depend, just like the hard scattering cross-section, on the mass-

[o] If the final state consists of exclusively treated light particles (e.g. $e^+e^- \to 4f$), large collinear final-state QED logarithms appear. These large logs can be treated in a way similar to the initial-state ones, provided proper account is taken of the fact that now $\hat{p} = p/x$.

factorization scale Q^2. These splitting functions can be decomposed into a part containing the collinear logarithms and a non-log part according to

$$\begin{aligned}\Gamma_{ij}^{\log}(x,Q^2) &= \delta_{ij}\delta(1-x) + \sum_{n=1}^{\infty}\left(\frac{\alpha}{\pi}\right)^n \sum_{m=1}^{n} a_{mn}^{ij}(x) L^m, \\ \Gamma_{ij}^{\text{non-log}}(x,Q^2) &= \sum_{n=1}^{\infty}\left(\frac{\alpha}{\pi}\right)^n b_n^{ij}(x). \end{aligned} \tag{5.3}$$

Analogously the hard scattering cross-section can be decomposed into the scale-independent Born cross-section plus non-log higher-order terms

$$\mathrm{d}\hat{\sigma}_{ij}(Q^2) = \mathrm{d}\sigma_{ij}^{\text{Born}} + \sum_{n=1}^{\infty}\left(\frac{\alpha}{\pi}\right)^n c_n^{ij}(Q^2). \tag{5.4}$$

For convenience we have dropped the explicit dependence on $x_\pm$ in this decomposition. This dependence enters via the reduced momenta $\hat{p}_\pm$. The large-logarithmic part of the splitting functions can be expressed in terms of the Altarelli–Parisi functions[89] $P_{ij}^{(n)}(x)$ by solving the renormalization group equations perturbatively[p]:

$$\begin{aligned}\Gamma_{ij}^{\log}(x,Q^2) = \delta_{ij}\delta(1-x) + \frac{\alpha}{2\pi}P_{ij}^{(0)}(x)\,L + \frac{1}{2}\left(\frac{\alpha}{2\pi}\right)^2\left[\left(P_{ik}^{(0)}\otimes P_{kj}^{(0)}\right)(x)\,L^2 + P_{ij}^{(1)}(x)\,L\right] \\ + \text{higher-order terms,}\end{aligned} \tag{5.5}$$

with

$$(f\otimes g)(x) \equiv \int_0^1 \mathrm{d}x_1 \int_0^1 \mathrm{d}x_2\, f(x_1)\, g(x_2)\, \delta(x - x_1 x_2). \tag{5.6}$$

The Altarelli–Parisi functions have been calculated[90] up to $\mathcal{O}(\alpha^2)$. Here we will give the relevant $\mathcal{O}(\alpha)$ ones[89] for unpolarized particles:

$$\begin{aligned}P_{\mathrm{e}^+\mathrm{e}^+}^{(0)}(x) = P_{\mathrm{e}^-\mathrm{e}^-}^{(0)}(x) \equiv P_{\mathrm{ee}}^{(0)}(x) &= Q_e^2\left\{\delta(1-x)\left[\frac{3}{2} + 2\log(\varepsilon)\right] + \theta(1-x-\varepsilon)\frac{1+x^2}{1-x}\right\}, \\ P_{\mathrm{e}^+\gamma}^{(0)}(x) = P_{\mathrm{e}^-\gamma}^{(0)}(x) \equiv P_{\mathrm{e}\gamma}^{(0)}(x) &= Q_e^2[x^2 + (1-x)^2], \\ P_{\gamma\mathrm{e}^+}^{(0)}(x) = P_{\gamma\mathrm{e}^-}^{(0)}(x) \equiv P_{\gamma\mathrm{e}}^{(0)}(x) &= Q_e^2\left[\frac{1+(1-x)^2}{x}\right],\end{aligned} \tag{5.7}$$

and for polarized particles:

$$\begin{aligned}P_{\mathrm{e}_{\kappa_1}\mathrm{e}_{\kappa_2}}^{(0)}(x) &= \delta_{\kappa_2}^{\kappa_1}\, P_{\mathrm{ee}}^{(0)}(x), \\ P_{\mathrm{e}_\kappa\gamma_\lambda}^{(0)}(x) &= Q_e^2[\delta_\lambda^{2\kappa}\, x^2 + \delta_{-\lambda}^{2\kappa}\,(1-x)^2], \\ P_{\gamma_\lambda\mathrm{e}_\kappa}^{(0)}(x) &= \frac{Q_e^2}{x}\left[\delta_{2\kappa}^{\lambda} + \delta_{-2\kappa}^{\lambda}\,(1-x)^2\right],\end{aligned} \tag{5.8}$$

[p] Here we have left out the effects of the QED β-function in the renormalization group equations. We will come back to that point later on.

with Q_e the charge fraction of the electron, which will be set to -1 in the following, and κ, λ the helicities of the particles.

The so-called leading-log (LL) approximation consists in only taking along the terms $\propto (\alpha L/\pi)^n$, which automatically means that the hard scattering cross-section $\hat{\sigma}$ should be identical to the scale-independent Born cross-section. In addition this Born cross-section could be dressed by the leading corrections that are not of the LL type in order to improve the approximation. As these LL contributions constitute the most important higher-order QED effects, it is on most occasions sufficient to add the $\mathcal{O}(\alpha^2)$ LL contributions to the full $\mathcal{O}(\alpha)$ results and to exponentiate the soft-photon distribution. In this way the resulting cross-section becomes scale-dependent. In e^+e^- collisions the bulk of the QED corrections frequently originates from pure photon radiation, especially when the soft-photon contributions are dominant. In those cases the LL evaluation can be restricted to the diagonal Altarelli–Parisi functions $P_{ee}^{(0)}(x)$. The non-diagonal Altarelli–Parisi functions $P_{ij}^{(0)}(x)$ $(i \neq j)$ do not contain soft poles $\propto 1/(1-x)$ and are hence suppressed by lack of phase space in soft processes, like W-pair production near threshold or, if the hard-radiation boost effects are cut away, at large energies[q]. After these simplifications the relevant splitting function takes on the form[91]

$$\Gamma_{ee}^{\mathrm{LL,exp}}(x,Q^2) \equiv \phi(\alpha,x,Q^2) = \frac{\exp(-\zeta_\alpha\gamma_E + 3\alpha L/4\pi)}{\Gamma(1+\zeta_\alpha)}\zeta_\alpha(1-x)^{-1+\zeta_\alpha} - \frac{\alpha}{2\pi}(1+x)\,L$$
$$-\frac{1}{2}(\frac{\alpha}{2\pi})^2\left[\frac{1+3x^2}{1-x}\log(x) + 4(1+x)\log(1-x) + 5 + x\right]L^2, \qquad (5.9)$$

with

$$\zeta_\alpha = \frac{\alpha}{\pi}(L-1). \qquad (5.10)$$

Here γ_E is the Euler constant and $\Gamma(y)$ the Gamma function, which should not be confused with the splitting functions. Note that some non-leading terms are incorporated, taking into account the fact that the residue of the soft-photon pole is proportional to $L-1$ rather than L for the initial-state photon radiation. In terms of this splitting function the total W-pair production cross-section including exponentiated LL QED corrections can be written as

$$\sigma_{\mathrm{LL,exp}}(s,Q^2) = \int_{4M_W^2/s}^1 \mathrm{d}z\;\phi(2\alpha,z,Q^2)\,\hat{\sigma}_0(zs), \qquad (5.11)$$

where $\hat{\sigma}_0(zs)$ denotes the (possibly improved) Born cross-section at the reduced CM energy squared zs.

At this point we would like to note that the leading effects related to the production of undetected e^+e^- pairs from conversion of a virtual photon emitted from the initial state (+ corresponding loop corrections) can be accounted for by replacing α in $\phi(\alpha,x,Q^2)$ by $\alpha[1+\alpha L/(6\pi)]$. This takes into account the QED β-function contributions appearing in the renormalization group equations. Also other fermion pairs can be included, but care has to be taken with the fact that the real pair-production process requires the virtual photon to be sufficiently hard.

[q] If hard radiation does play a role, these non-diagonal effects can get large as $P_{\gamma e}^{(0)}(x)$ peaks for $x \to 0$.

Another important fact to note is that the scale Q^2 is a free parameter. Order by order the cross-sections are independent of Q^2. However, as soon as collinear logarithms are added to a cross-section without also including the corresponding remaining (non-log) QED corrections of the same order in α, the scale dependence enters the game. The choice of Q^2 is ruled by two considerations. First of all no 'alien' (unnatural) terms should enter a distribution via a scale choice. Which scales are natural and which ones are not can be judged on the basis of either physical grounds or explicit analytical evaluations. For instance, in the absence of a calculation of next-to-leading logarithmic corrections at $\mathcal{O}(\alpha^2)$ an explicit analytical calculation at $\mathcal{O}(\alpha)$ might help to set the scale for the higher-order LL corrections. Secondly, if a distribution is governed by more than one scale, the motivation of the scale choice is very often of numerical nature. The better for instance the $\mathcal{O}(\alpha)$ LL calculation approximates the full $\mathcal{O}(\alpha)$ QED corrections, the better in general the chosen scale will be. This should, however, not be overdone, as we would like Q^2 in the end to be appropriate for the approximation of the full $\mathcal{O}(\alpha^2)$ corrections rather than the $\mathcal{O}(\alpha)$ ones. Hence, making a scale choice physically plausible is, in our opinion, just as important as its numerical motivation. In the case of the near threshold example (2.59), the process is ruled by soft kinematics. In such a soft regime a well motivated scale choice would be $Q^2 = st_1/u_1$ for the angular distribution [see $\log(\varepsilon)$ part in (2.44)]. This takes into account the fact that the interference effects $\propto \log(\varepsilon)\log(t_1/u_1)$ exponentiate in a similar way as the $\log(\varepsilon)\log(s/m_e^2)$ terms. As near threshold the interference effects are suppressed as a result of lack of phase space, we end up with the scale choice $Q^2 = s$. This manifests itself in the fact that $t_1/u_1 \approx 1$ near threshold.

6 Summary

The production of W pairs in e^+e^- annihilation is very well suited for the exploration of so far untested sectors of the electroweak interaction, such as its non-abelian structure or the mass-generation mechanism. It allows a precise measurement of M_W, which will supplement the electroweak precision tests performed at LEP1/SLC and provide an improved indirect bound on m_t or even on M_H. By studying W-pair production at LEP200 one will approach the interesting area of direct tests of the triple couplings between electroweak gauge bosons; the errors will be such that, assuming the SM values for these couplings, their presence can be proved. At the NLC it will be possible to measure the non-Abelian gauge couplings at the per-cent level or even better. W-pair production also provides a new laboratory for CP tests and, in the event of a strongly interacting Higgs sector, for rescattering effects from vector resonances. In addition it might even allow, through the study of the hadronic decays of the W bosons, to learn more about hadronization.

With the expected number of about 8000 W pairs at LEP200 the experimental accuracy will typically be at the few per-cent level and even better for selected observables such as the W-boson mass. At a high-energy e^+e^- collider the yield of W pairs could be increased by about a factor 10, such that the experimental errors could be even below one per cent. Accordingly the theoretical predictions should have an accuracy of at least better than 1%. To this end one has to calculate the complete lowest-order pro-

cess $e^+e^- \to 4f$ including all non-resonant diagrams. Already at this level the leading corrections, like running couplings and leading collinear QED logarithms, should be implemented. For the remaining $\mathcal{O}(\alpha)$ corrections the complete doubly-resonant contributions have to be evaluated. These involve electroweak as well as QCD corrections. Of course all relevant higher-order effects should be taken into account. Finally everything must be implemented in a Monte-Carlo (MC) generator. To allow a systematic study of anomalous couplings their effects should be included.

In this review we have mainly focused on the radiative corrections. The doubly-resonant $\mathcal{O}(\alpha)$ contributions involve corrections to the W-pair production process, corrections to the W decay, and non-factorizable photonic corrections, i.e. corrections that result from the interference between the production and the decay, or between the decays of the two W bosons. For inclusive cross-sections the non-factorizable corrections vanish and the factorizable ones are essentially those for stable W bosons, with exception of the Coulomb singularity near the W-pair production threshold, which is very sensitive to screening effects resulting from the off-shellness and decay of the W bosons. Consequently the corrections to on-shell W-pair production are a fairly good approximation to the full corrections for inclusive quantities; for non-inclusive quantities they constitute at least a very important ingredient that already contains the most interesting physics.

Therefore we started out by considering on-shell W-pair production. The main features of this process are determined by the lowest-order matrix elements. We have discussed them and the corresponding differential and integrated cross-sections in detail. Moreover we have included a short discussion of anomalous couplings.

The $\mathcal{O}(\alpha)$ corrections to on-shell W-pair production are settled. For the virtual and soft-photonic corrections as well as for the hard-photonic corrections there exist several calculations that are in good agreement. The corrections are in general moderate when the cross-section is sizeable, even at high energies. There are large corrections close to threshold originating from soft-photon emission. At high energies the corrections get large exactly there where the cross-section is small and thus especially sensitive to deviations from the SM, i.e. in the backward direction or for polarizations that are not dominated by the t-channel pole. As these large corrections arise from hard-photonic boost effects, they can be removed by appropriate cuts or by reconstruction methods that take into account the photon radiation. If these boost effects are not cut out, the corresponding $\mathcal{O}(\alpha)$ contributions will dominate over the lowest-order cross-section and the $\mathcal{O}(\alpha^2)$ corrections would be needed to achieve a relative $\mathcal{O}(\alpha)$ accuracy.

In the absence of large boost effects the $\mathcal{O}(\alpha^2)$ and $\mathcal{O}(\alpha\alpha_s)$ corrections seem to be under control, at least at low and intermediate energies. The leading universal $\mathcal{O}(\alpha^2)$ and $\mathcal{O}(\alpha\alpha_s)$ corrections originating from renormalization and the leading logarithmic corrections arising from collinear photon radiation off the initial-state fermions are known. The $\mathcal{O}(\alpha^2)$ leading-log corrections are in general below 0.5%, apart from the region close to threshold, where exponentiation of soft-photon effects becomes relevant, and at very high energies. At high energies the full higher-order leading-log corrections are somewhat larger than this, i.e. $> 1\%$, owing to known higher-order corrections related to Δr. Accordingly the overall accuracy of the theoretical predictions for on-shell W-pair production are at the level of 0.5% or even better (assuming that the large boost effects have been removed).

There exists an improved Born approximation for on-shell W-pair production in the LEP200 energy region which roughly matches the expected experimental accuracy. In addition a high-energy approximation has been constructed by systematic expansion of the complete results. Its most important feature is the appearance of contributions of the form $(\alpha/\pi)\log^2(s/M_{\mathrm{W}}^2)$, which get rather large at very high energies. As a consequence one should either calculate the corresponding higher-order corrections or try to find a way to resum these terms.

The on-shell approximation is not sufficient to describe the expected experimental results and one has to consider off-shell W-pair production, i.e. one has to study the process $\mathrm{e}^+\mathrm{e}^- \to 4f$. The most important contributions arise from diagrams involving two resonant W bosons. For exclusive channels, however, there are other enhanced contributions arising from different peakings of the invariant matrix element. These can be removed by using invariant-mass cuts. Since one does not consider the full process $\mathrm{e}^+\mathrm{e}^- \to 4f$ but only its leading contributions and since one has to take into account the finite-width effects, one has to be careful not to violate gauge invariance. This can be ensured by making a decomposition of the complete matrix element according to its poles. After that the finite-width effects can be easily included in a gauge-invariant way. Extracting the double-pole terms provides a systematic framework for the calculation of gauge-invariant higher-order corrections. Since so far no complete calculation of the doubly-resonant corrections to $\mathrm{e}^+\mathrm{e}^- \to 4f$ has been published, we could only outline the general strategy. Complete calculations are, however, under way.

So far only some results for the most important corresponding QED corrections exist. These have in particular been evaluated in the leading-logarithmic approximation. Moreover, the complete initial-state QED corrections have been calculated by defining a gauge-invariant initial-state radiation through the so-called current-splitting technique. In addition the Coulomb singularity has been discussed for off-shell W bosons.

For the W width several complete calculations for the $\mathcal{O}(\alpha)$ corrections exist, which are in good agreement. Moreover, there is a very good improved Born approximation.

Finally we have given a general discussion of the structure-function method for calculating leading higher-order corrections associated with collinear radiation. This is not only useful for W-pair production but applies to other processes as well.

As already mentioned, there is not yet a complete calculation for off-shell W-pair production with the required accuracy of below 1%. However, many calculations are performed right now. A MC generator for the full lowest-order process $\mathrm{e}^+\mathrm{e}^- \to 4f$ should be available soon. A MC generator involving the full resonant $\mathcal{O}(\alpha)$ corrections to off-shell W-pair production is under development.

If these MCs are available there is still some work to be done. The calculations should be checked and different MCs should be compared. This will give an assessment of the quality of simple MCs, e.g. those containing only the leading corrections, as compared with the full ones. In particular the interference effects for non-inclusive quantities should be studied. Moreover, the anomalous couplings should be included in the full MC(s).

In conclusion, although many ingredients exist, there is still some work to be done to arrive at a completely satisfactory Monte-Carlo generator. Nevertheless this should be available before LEP200 will start to take data.

Acknowledgements

Various people have contributed directly or indirectly to this review. Many of the presented results were obtained in collaboration with F.A. Berends, D. Bardin, M. Böhm, S. Dittmaier, R. Mertig and T. Sack. We thank them as well as A. Aeppli, F. Jegerlehner, B.A. Kniehl, J.H. Kühn, W. van Neerven, G.J. van Oldenborgh, D. Schildknecht, F. Schrempp, T. Sjöstrand and P. Zerwas for many stimulating and clarifying discussions and/or reading the manuscript. Special mention goes to F. Boudjema for providing us with extensive information on anomalous couplings and for reading the corresponding sections of the review. For information on the experimental possibilities we are indebted to S. Katsanevas, N. Kjaer and R. Settles. The GENTLE plots were provided by D. Bardin, A. Olchevski and T. Riemann, the WOPPER plot by T. Ohl and A. Himmler. We thank R. Pittau for providing us with numbers from his lowest-order four-fermion Monte Carlo prior to publication.

Appendix A Explicit expressions for the basic matrix elements

In this appendix we list the explicit expressions for the non-vanishing basic matrix elements $\mathcal{M}_i^\kappa(\lambda_+,\lambda_-)$ for $i=1,\ldots,8$ and $\widetilde{\mathcal{M}}_i^\kappa(\lambda_+,\lambda_-)$ for $i=3,4,7,8,9$, as defined in (2.9), (2.11) and (2.41) in terms of the beam energy E, the scattering angle θ and the velocity of the W bosons β:

$$\begin{aligned}
\mathcal{M}_1^\kappa(\pm,\mp) &= 2E^2\sin\theta\,(\cos\theta\mp 2\kappa),\\
\mathcal{M}_4^\kappa(\pm,\mp) &= 2E^2\sin\theta\,(\cos\theta\mp 2\kappa),\\
\mathcal{M}_6^\kappa(\pm,\mp) &= \beta E^4\sin^3\theta,
\end{aligned} \tag{A.1}$$

$$\begin{aligned}
\mathcal{M}_1^\kappa(\pm,\pm) &= 2E^2\sin\theta\,(\cos\theta-\beta),\\
\mathcal{M}_2^\kappa(\pm,\pm) &= 2\beta E^2\sin\theta,\\
\mathcal{M}_4^\kappa(\pm,\pm) &= 2E^2\sin\theta\cos\theta,\\
\mathcal{M}_6^\kappa(\pm,\pm) &= \beta E^4\sin^3\theta,\\
\mathcal{M}_6^\kappa(\pm,\pm) &= \beta E^4\sin^3\theta,\\
\widetilde{\mathcal{M}}_4^\kappa(\pm,\pm) &= \mp 4\kappa E^2\sin\theta\ ,\\
\widetilde{\mathcal{M}}_8^\kappa(\pm,\pm) &= \mp 4E^2\sin\theta\ ,\\
\widetilde{\mathcal{M}}_9^\kappa(\pm,\pm) &= \mp 8\beta^2E^4\sin\theta\ ,
\end{aligned} \tag{A.2}$$

$$\begin{aligned}
\mathcal{M}_1^\kappa(\pm,0) &= \mathcal{M}_1^\kappa(0,\mp) = \frac{\sqrt{2}E}{M_{\mathrm{W}}}E^2(\cos\theta\mp 2\kappa)[2\beta-2\cos\theta\mp 2\kappa(1-\beta^2)],\\
\mathcal{M}_3^\kappa(\pm,0) &= \mathcal{M}_3^\kappa(0,\mp) = \frac{\sqrt{2}E}{M_{\mathrm{W}}}2\beta E^2(\cos\theta\mp 2\kappa),\\
\mathcal{M}_4^\kappa(\pm,0) &= \mathcal{M}_4^\kappa(0,\mp) = \frac{\sqrt{2}E}{M_{\mathrm{W}}}E^2(\cos\theta\mp 2\kappa)(\beta-2\cos\theta\mp 2\kappa),
\end{aligned}$$

$$
\begin{aligned}
\mathcal{M}_6^\kappa(\pm,0) &= \mathcal{M}_6^\kappa(0,\mp) = \frac{\sqrt{2}E}{M_{\rm W}}\beta E^4 \sin^2\theta\,(\beta-\cos\theta),\\
\mathcal{M}_7^\kappa(\pm,0) &= \mathcal{M}_7^\kappa(0,\mp) = \frac{\sqrt{2}E}{M_{\rm W}}2\beta^2 E^4 \sin^2\theta,\\
\mathcal{M}_8^\kappa(\pm,0) &= \mathcal{M}_8^\kappa(0,\mp) = \pm\frac{\sqrt{2}E}{M_{\rm W}}2\beta^2 E^2(\cos\theta\mp 2\kappa),\\
\widetilde{\mathcal{M}}_3^\kappa(\pm,0) &= -\widetilde{\mathcal{M}}_3^\kappa(0,\mp) = \frac{\sqrt{2}E}{M_{\rm W}}2\beta E^2(\cos\theta\mp 2\kappa),\\
\widetilde{\mathcal{M}}_4^\kappa(\pm,0) &= -\widetilde{\mathcal{M}}_4^\kappa(0,\mp) = \frac{\sqrt{2}E}{M_{\rm W}}E^2(\cos\theta\mp 2\kappa)(\beta\pm 2\kappa),\\
\widetilde{\mathcal{M}}_7^\kappa(\pm,0) &= -\widetilde{\mathcal{M}}_7^\kappa(0,\mp) = \frac{\sqrt{2}E}{M_{\rm W}}2\beta^2 E^4 \sin^2\theta,\\
\widetilde{\mathcal{M}}_8^\kappa(\pm,0) &= -\widetilde{\mathcal{M}}_8^\kappa(0,\mp) = \pm\frac{\sqrt{2}E}{M_{\rm W}}2E^2(\cos\theta\mp 2\kappa),
\end{aligned}
\tag{A.3}
$$

$$
\begin{aligned}
\mathcal{M}_1^\kappa(0,0) &= \frac{E^2}{M_{\rm W}^2}2E^2\sin\theta\,[3\beta-\beta^3-2\cos\theta],\\
\mathcal{M}_2^\kappa(0,0) &= \frac{E^2}{M_{\rm W}^2}2\beta E^2\sin\theta\,(1+\beta^2),\\
\mathcal{M}_3^\kappa(0,0) &= \frac{E^2}{M_{\rm W}^2}8\beta E^2\sin\theta,\\
\mathcal{M}_4^\kappa(0,0) &= \frac{E^2}{M_{\rm W}^2}4E^2\sin\theta\,(\beta-\cos\theta),\\
\mathcal{M}_5^\kappa(0,0) &= \frac{E^2}{M_{\rm W}^2}8\beta^3 E^4\sin\theta,\\
\mathcal{M}_6^\kappa(0,0) &= \frac{E^2}{M_{\rm W}^2}2\beta E^4\sin\theta\,(\beta-\cos\theta)^2,\\
\mathcal{M}_7^\kappa(0,0) &= \frac{E^2}{M_{\rm W}^2}8\beta^2 E^4\sin\theta\,(\beta-\cos\theta).
\end{aligned}
\tag{A.4}
$$

Appendix B Total cross-section for on-shell W-pair production

The polarized total cross-section for on-shell W-pair production can be obtained by squaring the helicity amplitude and integrating over the phase space. According to our representation for the helicity-matrix element (2.19) we write the cross-section in the following way

$$
\sigma_{\rm Born}(\kappa,\lambda_+,\lambda_-) = \frac{\pi\alpha^2}{s}\left(\frac{\delta_{\kappa-}}{4s_{\rm W}^4}\sigma_{II}(\kappa,\lambda_+,\lambda_-) + \frac{\delta_{\kappa-}}{2s_{\rm W}^2}\sigma_{IQ}(\kappa,\lambda_+,\lambda_-) + \sigma_{QQ}(\kappa,\lambda_+,\lambda_-)\right).
\tag{B.1}
$$

The explicit expressions are formulated in such a way that one can directly read off the high-energy limit. Owing to the symmetry relation[r]

$$\mathcal{M}_{I,Q}(\kappa,\lambda_+,\lambda_-) = \mathcal{M}_{I,Q}(-\kappa,-\lambda_+,-\lambda_-) \tag{B.2}$$

the following quantities are independent of κ ($w = 4M_{\mathrm{W}}^2/s$, $z = M_{\mathrm{Z}}^2/s$)

$$\begin{aligned}
\sigma_{\pm,\mathrm{T}}^{II} &= \frac{1}{6\beta^4(1-z)^2}\Big\{2\beta\Big[-32+32w-11w^2-w^3 \\
&\quad + z(64-66w+29w^2-3w^3) - 2z^2(14-11w+3w^2)\Big] \\
&\quad - 3(1-z)\Big[16-24w+14w^2-3w^3+w^4 \\
&\quad - 2z(8-12w+7w^2-w^3)\Big]\log\frac{w}{(1+\beta)^2}\Big\}, \\
\sigma_{\pm,\mathrm{T}}^{IQ} &= \frac{zw}{6\beta^2(1-z)^2}\Big\{2\beta\Big[(2-5w) - \frac{M_Z^2}{4M_{\mathrm{W}}^2}(4-w)(2-3w)\Big] \\
&\quad - 3w^2(1-z)\log\frac{w}{(1+\beta)^2}\Big\}, \\
\sigma_{\pm,\mathrm{T}}^{QQ} &= \frac{z^2}{3(1-z)^2}4\beta(1-w), \\
\sigma_{\pm,\mathrm{M}}^{II} &= \frac{w}{3\beta^4(1-z)^2}\Big\{4\beta\Big[(8-2w) - \frac{M_Z^2}{4M_{\mathrm{W}}^2}(10-w+3w^2) \\
&\quad + \Big(\frac{M_Z^2}{4M_{\mathrm{W}}^2}\Big)^2(4-w)(2-3w+3w^2)\Big] \\
&\quad + 6w(1-z)\Big[2(2-w) - \frac{M_Z^2}{4M_{\mathrm{W}}^2}(4-3w+w^2)\Big]\log\frac{w}{(1+\beta)^2}\Big\}, \\
\sigma_{\pm,\mathrm{M}}^{IQ} &= \frac{z}{3\beta^2(1-z)^2}\Big\{4\beta\Big[10-7w - \frac{M_Z^2}{4M_{\mathrm{W}}^2}(16-22w+9w^2)\Big] \\
&\quad + 6w(4-3w)(1-z)\log\frac{w}{(1+\beta)^2}\Big\}, \\
\sigma_{\pm,\mathrm{M}}^{QQ} &= \frac{M_Z^2}{4M_{\mathrm{W}}^2}\frac{z}{3(1-z)^2}32\beta(1-w), \\
\sigma_{\pm,\mathrm{L}}^{II} &= \frac{1}{6\beta^4(1-z)^2}\Big\{2\beta\Big[2-4w-11w^2+w^3 - \frac{M_Z^2}{4M_{\mathrm{W}}^2}(8-12w-8w^2-15w^3+3w^4)
\end{aligned}$$

[r] This relation for the basic matrix elements is a consequence of parity conservation. The parity violation is completely contained in the invariant functions.

$$+2\Big(\frac{M_Z^2}{4M_{\rm W}^2}\Big)^2(4-4w-6w^2+3w^3-3w^4)\Big]$$

$$-3w^2(1-z)\Big[4-w+w^2-2z(3-w)\Big]\log\frac{w}{(1+\beta)^2}\Big\},$$

$$\sigma_{\pm,\rm L}^{IQ} = \frac{M_Z^2}{4M_{\rm W}^2}\frac{2+w}{6\beta^2(1-z)^2}\Big\{2\beta\Big[4-6w-w^2-\frac{M_Z^2}{4M_{\rm W}^2}(8-8w-6w^2+3w^3)\Big]$$

$$-3w^3(1-z)\log\frac{w}{(1+\beta)^2}\Big\},$$

$$\sigma_{\pm,\rm L}^{QQ} = \Big(\frac{M_Z^2}{4M_{\rm W}^2}\Big)^2\frac{1}{3(1-z)^2}2\beta(1-w)(2+w)^2,$$

$$\sigma_{\pm,\rm U}^{II} = \frac{1}{3(1-z)^2}\Big\{2\beta\Big[-15-\frac{M_Z^2}{4M_{\rm W}^2}(4-10w+3w^2)+4\Big(\frac{M_Z^2}{4M_{\rm W}^2}\Big)^2(1+5w-3w^2)\Big]$$

$$-3(1-z)\Big[8+4w+w^2-4z(2-w)\Big]\log\frac{w}{(1+\beta)^2}\Big\},$$

$$\sigma_{\pm,\rm U}^{IQ} = \frac{M_Z^2}{4M_{\rm W}^2}\frac{1}{3(1-z)^2}\Big\{2\beta(4+20w+3w^2)\Big[1-\frac{M_Z^2}{4M_{\rm W}^2}(2-w)\Big]$$

$$+3w^2(8+w)(1-z)\log\frac{w}{(1+\beta)^2}\Big\},$$

$$\sigma_{\pm,\rm U}^{QQ} = \Big(\frac{M_Z^2}{4M_{\rm W}^2}\Big)^2\frac{1}{3(1-z)^2}2\beta(1-w)(4+20w+3w^2). \qquad \text{(B.3)}$$

References

1. Particle Data Group, *Phys. Rev.* **D45** (1992) S1.

2. W. Hollik, MPI-Ph/93-83, to appear in *Proceedings of the XVI International Symposium on Lepton-Photon Interactions*, Cornell University, Ithaca, New York, 10–15 August 1993;
   G. Altarelli, CERN-TH.7045/93, to appear in *Proceedings of the Europhysics Conference on High Energy Physics*, Marseille, France, 22–28 July 1993;
   J. Lefrancois, Orsay preprint LAL-93-64, to appear in *Proceedings of the Europhysics Conference on High Energy Physics*, Marseille, France, 22–28 July 1993.

3. A. Schwarz, MPI-PHE-93-24, to appear in *Proceedings of the XVI International Symposium on Lepton-Photon Interactions*, Cornell University, Ithaca, New York, 10–15 August 1993.

4. The LEP Collaborations, CERN/PPE/93-157, to appear in *Proceedings of the Europhysics Conference on High Energy Physics*, Marseille, France, 22–28 July 1993 and

in *Proceedings of the XVI International Symposium on Lepton-Photon Interactions*, Cornell University, Ithaca, New York, 10–15 August 1993.

5. S.L. Glashow, *Nucl. Phys.* **22** (1961) 579;
S. Weinberg, *Phys. Rev. Lett.* **19** (1967) 1264;
A. Salam, in *Elementary Particle Theory*, ed. N. Svartholm (Almqvist and Wiksells, Stockholm, 1968), p. 367;
S.L. Glashow, J. Iliopoulos and L. Maiani, *Phys. Rev.* **D2** (1970) 1285.

6. CDF Collaboration, F. Abe et al., *Phys. Rev.* **D43** (1991) 2070;
UA2 Collaboration, J. Alitti et al., *Phys. Lett.* **B276** (1992) 354.

7. L. Camilleri, talk given at the LEPC meeting, CERN, November 1992.

8. S. Katsanevas et al., internal DELPHI report DELPHI 92-166 PHYS 250.

9. R. Eichler, talk given at the LEPC meeting, CERN, November 1992.

10. M. Bilenky, J.L. Kneur, F.M. Renard and D. Schildknecht, *Nucl. Phys.* **B409** (1993) 22.

11. T. Barklow, in Ref. 25, Vol. I, p. 423;
The JLC Group, *JLC-I*, KEK report 92-16;
M. Bilenky, J.L. Kneur, F.M. Renard and D. Schildknecht, Bielefeld preprint BI-TP 93/47, to appear in *Nucl. Phys.* **B**;
A. Miyamoto, in Ref. 26, Vol. I, p. 141.

12. T. Appelquist and J. Carazzone, *Phys. Rev.* **D11** (1975) 2856;
Y. Kazama and Y.P. Yao, *Phys. Rev.* **D25** (1982) 1605.

13. T. Han, in Ref. 26, Vol. I, p. 270.

14. W. Bernreuther and T. Schröder, DESY 93-163.

15. A. Bilal, E. Massó and A. de Rújula, *Nucl. Phys.* **B355** (1991) 549.

16. K. Hagiwara, R. D. Peccei, D. Zeppenfeld and K. Hikasa, *Nucl. Phys.* **B282** (1987) 253.

17. G.J. Gounaris, F.M. Renard and D. Schildknecht, *Phys. Lett.* **B263** (1991) 291.

18. P. Roudeau et al., in Ref. 23, p. 49;
N. Kjaer, private communication.

19. E. Longo et al., in Ref. 23, p. 85.

20. G. Gustafson, U. Pettersson and P.M. Zerwas, *Phys. Lett.* **B209** (1988) 90.

21. T. Sjöstrand and V.A. Khoze, CERN-TH.7011/93 and CERN-TH.7043/93.

22. J. Ellis and R. Peccei (eds.), *Physics at LEP* (CERN-86-02, Geneva, 1986), Vols. 1 and 2.

23. A. Böhm and W. Hoogland (eds.), *ECFA Workshop on LEP200* (CERN-87-08, Geneva, 1987), Vol. 1.

24. P.M. Zerwas (ed.), e^+e^- *Collisions at 500 GeV: The Physics Potential* (DESY 92-123, Hamburg, 1992), parts A and B.

25. R. Orava, P. Eerola and M. Nordberg (eds.), *Physics and Experiments with Linear Colliders* (World Scientific, Singapore, 1992), Vols. I and II.

26. F.A. Harris, S.L. Olsen, S. Pakvasa and X. Tata (eds.), *Physics and Experiments with Linear* e^+e^- *Colliders* (World Scientific, Singapore, 1993), Vols. I and II.

27. P.M. Zerwas (ed.), e^+e^- *Collisions at 500 GeV: The Physics Potential* (DESY 93-123C, Hamburg, 1993), part C.

28. F. Jegerlehner, in *Proc. 1990 Theoretical Advanced Study Institute in Elementary Particle Physics*, eds. M. Cvetič and P. Langacker (World Scientific, Singapore, 1991), p. 476.

29. W.J. Marciano, *Phys. Rev.* **D29** (1984) 580.

30. K. Hagiwara and D. Zeppenfeld, *Phys. Lett.* **B196** (1987) 97.

31. B. Grzadkowski, Z. Hioki and J.H. Kühn, *Phys. Lett.* **B205** (1988) 388;
Z. Hioki, *Nucl. Phys.* **B316** (1989) 1.

32. G.J. Gounaris and F.M. Renard, *Z. Phys.* **C59** (1993) 133;
C.P. Burgess and D. London, *Phys. Rev. Lett.* **69** (1992) 3428, *Phys. Rev.* **D48** (1993) 4337 and Montréal preprint McGill-92-04;
C. Grosse-Knetter, I. Kuss and D. Schildknecht, *Z. Phys.* **C60** (1993) 375.

33. F. Boudjema, in Ref. 26, Vol. II, p. 712.

34. W. Buchmüller and D. Wyler, *Nucl. Phys.* **B268** (1986) 621.

35. K. Hagiwara, S. Ishihara, R. Szalapski and D. Zeppenfeld, *Phys. Rev.* **D48** (1993) 2182.

36. S. Weinberg, *Phys. Rev. Lett.* **17** (1966) 616;
M.S. Chanowitz, M. Golden and H. Georgi, *Phys. Rev. Lett.* **57** (1986) 2344 and *Phys. Rev.* **D36** (1987) 1490.

37. G.J. Gounaris, J.L. Kneur, J. Layssac, G. Moultaka, F.M. Renard and D. Schildknecht, in Ref. 24, part B, p. 735 and references therein.

38. A. de Rújula, M.B. Gavela, P. Hernandez and E. Massó, *Nucl. Phys.* **B384** (1992) 3.

39. M. Lemoine and M. Veltman, *Nucl. Phys.* **B164** (1980) 445.

40. R. Philippe, *Phys. Rev.* **D26** (1982) 1588.

41. M. Böhm, A. Denner, T. Sack, W. Beenakker, F.A. Berends and H. Kuijf, *Nucl. Phys.* **B304** (1988) 463.

42. J. Fleischer, F. Jegerlehner and M. Zrałek, *Z. Phys.* **C42** (1989) 409.

43. A. Sommerfeld, *Atombau und Spektrallinien*, (Vieweg, Braunschweig, 1939), Bd. 2; A.D. Sakharov, *JETP* **18** (1948) 631.

44. C. Ahn, B.W. Lynn, M. Peskin and S. Selipsky, *Nucl. Phys.* **B309** (1988) 221.

45. W. Beenakker, A. Denner, S. Dittmaier, R. Mertig and T. Sack, *Nucl. Phys.* **B410** (1993) 245;
W. Beenakker, A. Denner, S. Dittmaier and R. Mertig, *Phys. Lett.* **B317** (1993) 622 and in Ref. 27, p. 153.

46. F. Jegerlehner, in *Radiative Corrections for* e^+e^- *Collisions*, ed. J.H. Kühn (Springer, Berlin Heidelberg, 1989), p. 208.

47. V. Barger, T. Han and R.J.N. Phillips, *Phys. Rev.* **D39** (1989) 146.

48. W. Beenakker, K. Kołodziej and T. Sack, *Phys. Lett.* **B258** (1991) 469;
W. Beenakker, F.A. Berends and T. Sack, *Nucl. Phys.* **B367** (1991) 287.

49. K. Kołodziej and M. Zrałek, *Phys. Rev.* **D43** (1991) 3619;
J. Fleischer, F. Jegerlehner and K. Kołodziej, *Phys. Rev.* **D47** (1993) 830.

50. H. Tanaka, T. Kaneko and Y. Shimizu, *Comp. Phys. Commun.* **64** (1991) 149.

51. E.N. Argyres, O. Korakiantis, C.G. Papadopoulos and W.J. Stirling, *Phys. Lett.* **B259** (1991) 195.

52. W. Beenakker, F.A. Berends and A. Denner, in Ref. 24, part A, p. 151.

53. T. Sack, in Ref. 24, part A, p. 171.

54. M. Martinez, in Ref. 24, part A, p. 165.

55. J.J. van der Bij and F. Hoogeveen, *Nucl. Phys.* **B283** (1987) 477;
M. Consoli, W. Hollik and F. Jegerlehner, *Phys. Lett.* **B227** (1989) 167;
S. Fanchiotti, B.A. Kniehl and A. Sirlin, *Phys. Rev.* **D48** (1993) 307 and references therein.

56. A. Djouadi and C. Verzegnassi, *Phys. Lett.* **B195** (1987) 265;
A. Djouadi, *Nuovo Cimento* **100A** (1988) 357;
B.A. Kniehl, *Nucl. Phys.* **B347** (1990) 86.

57. A. Sirlin, *Phys. Rev.* **D22** (1980) 971;
G. Burgers and F. Jegerlehner, in Z *physics at LEP 1*, eds. G. Altarelli, R. Kleiss and C. Verzegnassi, (CERN 89-08, Genève, 1989) p. 55.

58. W. Beenakker, in Ref. 24, part A, p. 195.

59. B.A. Kniehl and A. Sirlin, *Phys. Rev.* **D47** (1993) 883.

60. E.A. Kuraev and V.S. Fadin, *Sov. J. Nucl. Phys.* **41** (1985) 466;
G. Altarelli and G. Martinelli, in Ref. 22, Vol. 1, p. 47.

61. W. Beenakker, F.A. Berends and W.L. van Neerven, in *Radiative Corrections for* e^+e^- *Collisions*, ed. J.H. Kühn (Springer, Berlin Heidelberg, 1989), p. 3.

62. M. Cacciari, A. Deandrea, G. Montagna and O. Nicrosini, *Z. Phys.* **C52** (1991) 421.

63. S. Dittmaier, M. Böhm and A. Denner, *Nucl. Phys.* **B376** (1992) 29; E: **B391** (1993) 483.

64. J. Fleischer, J.L. Kneur, K. Kołodziej, M. Kuroda and D. Schildknecht, *Nucl. Phys.* **B378** (1992) 443.

65. T. Muta, R. Najima and S. Wakaizumi, *Mod. Phys. Lett.* **A1** (1986) 203.

66. A. Aeppli, F. Cuypers and G.J. van Oldenborgh, *Phys. Lett.* **B314** (1993) 413.

67. A. Aeppli and D. Wyler, *Phys. Lett.* **B262** (1991) 125.

68. F.A. Berends, R. Kleiss and R. Pittau, in preparation.

69. A. Aeppli, in Ref. 24, part A, p. 203.

70. A. Aeppli, G.J. van Oldenborgh and D. Wyler, preprint PSI-PR-93-22.

71. H. Anlauf, H.D. Dahmen, A. Himmler, P. Manakos and T. Mannel, in Ref. 26, Vol. II, p. 708.
H. Anlauf, H.D. Dahmen, P. Manakos and T. Mannel, in Ref. 27, p. 165;
H. Anlauf, J. Biebel, H.D. Dahmen, A. Himmler, P. Manakos, T. Mannel, W. Schoenau, Darmstadt/Siegen preprint IKDA 93/3, SI-93-6, to appear in *Comp. Phys. Commun.*

72. M. Davier et al., in Ref. 23, p. 120.

73. T. Ohl, private communication.

74. D. Bardin, M. Bilenky, A. Olshevsky and T. Riemann, *Phys. Lett.* **B308** (1993) 403.

75. F.A. Berends, G. Burgers and W.L. van Neerven, *Phys. Lett.* **B185** (1987) 395; *Nucl. Phys.* **B297** (1988) 429; E: **B304** (1988) 921.

76. V.S. Fadin, V.A. Khoze and A.D. Martin, *Phys. Lett.* **B311** (1993) 311.

77. D.Yu. Bardin, W. Beenakker and A. Denner, *Phys. Lett.* **B317** (1993) 213.

78. V.S. Fadin, V.A. Khoze and A.D. Martin, University of Durham preprint DTP/93/18, 1993.

79. K. Melnikov and O. Yakovlev, Novosibirsk preprint BUDKERINP 93-18;
V.S. Fadin, V.A. Khoze and A.D. Martin, *Phys. Lett.* **B320** (1994) 141.

80. F.A. Berends and R. Kleiss, *Z. Phys.* **C27** (1985) 365.

81. R. Settles, private communication.

82. W.J. Marciano and D. Wyler, *Z. Phys.* **C3** (1979) 181;
D. Albert, W.J. Marciano, D. Wyler and Z. Parsa, *Nucl. Phys.* **B166** (1980) 460;
K. Inoue, A. Kakuto, H. Komatsu and S. Takeshita, *Prog. Theo. Phys.* **64** (1980) 1008;
T.H. Chang, K.J.F. Gaemers and W.L. van Neerven, *Nucl. Phys.* **B202** (1982) 407.

83. F. Jegerlehner, *Z. Phys.* **C32** (1986) 425 and in *Proc. of the 11th International School of Theoretical Physics 'Testing of the Standard Model'*, Szczyrk-Bila (Poland) 1987, eds. M. Zralek and R. Manka (World Scientific, Singapore, 1988), p. 127.

84. D.Yu. Bardin, S. Riemann and T. Riemann, *Z. Phys.* **C32** (1986) 121.

85. A. Denner and T. Sack, *Z. Phys.* **C46** (1990) 653.

86. A. Denner, *Fortschr. Phys.* **41** (1993) 307.

87. N. Nakanishi, *Prog. Theo. Phys.* **19** (1958) 159.

88. T. Kinoshita, *J. Math. Phys.* **3** (1962) 650;
T.D. Lee and M. Nauenberg, *Phys. Rev.* **133** (1964) B1549.

89. V.N. Gribov and L.N. Lipatov, *Sov. J. Nucl. Phys.* **15** (1972) 438, 675;
G. Altarelli and G. Parisi, *Nucl. Phys.* **B126** (1977) 298.

90. E.G. Floratos, D.A. Ross and C.T. Sachrajda, *Nucl. Phys.* **B129** (1977) 66, E: **B139** (1978) 545;
A. González-Arroyo, C. López and F.J. Yndurain, *Nucl. Phys.* **B153** (1979) 161;
A. González-Arroyo and C. López, *Nucl. Phys.* **B166** (1980) 429;
E.G. Floratos, C. Kounnas and R. Lacaze, *Phys. Lett.* **B98** (1981) 89, 285.

91. F.A. Berends et al., in Z *physics at LEP 1*, eds. G. Altarelli, R. Kleiss and C. Verzegnassi (CERN 89-08, Genève, 1989), p. 89.